



**FACULTY OF SCIENCE AND TECHNOLOGY**  
**BACHELOR'S THESIS**

Study programme / specialisation:  Mechanical Engineering	The <i>spring</i> semester, 2023  Open
Author:  Minh Jimmy Le Patrick Kyorra	
Supervisor at UiS:  Ove Mikkelsen	
External supervisor(s):  Kristoffer Helliesen Ueland Erlend Halvorsen Simon Hus	
Thesis title:  Optimizing of Rack and Pinion System for Valve Intervention Tool	
Credits (ECTS): 20	
Keywords: Izomax, AOGV, Mechanical Isolation Tool, High pressure, Rack and Pinion, Autodesk Inventor	Pages: 52 + appendix: 31  Stavanger, 15.05.2023

---

## Abstract

This thesis looks at improvements in the rack and pinion system that is used to insert an intervention tool between two flanges to perform maintenance in process systems by using Izomax's mechanical isolation tool, Add On Gate Valve (AOGV). The ambition is to find a new solution to get the rack and pinion system more robust, eliminate leakage paths and make it more functional.

After conducting meetings and reviewing documentation, it was revealed that the current design had challenges with the sealing. A spring-energized seal was used as the sealing method, but during testing and pressurization, difficulties with the sealing ability were identified. The system had design errors that were discovered. Incorrect dimensions and surface specifications led to sealing challenges and cold welding of parts. To increase reliability and improve functionality, improvements to the design, sealing method, and materials are necessary.

This report is based on the 2 in (") 1500 lbs class (#) AOGV operating under ambient temperature conditions, at a design pressure of 173 bar, a test pressure of 248 bar as defined in Pressure Equipment Directive (PED) European Standard (EN) 13445, and with hydrocarbons as the system medium.

The project was initiated by identifying the scope of the issue through meetings with project managers, project engineers and mechanics. The emphasis was on gathering insights from both field operations and documentation. There were physical inspections in the workshop to gain an understanding to both installation and maintenance procedures of the current system. What proceeded was an extensive literature review, focused on sealing high pressure systems and finding relevant documentation for the design process. With the information gathered, the design process started by using the existing drawings of the AOGV provided by Izomax. It was clearly defined that the dimensions of the housing should not be changed to avoid over-dimensioning the rack and pinion housing and to maintain the geometry of the AOGV. Changes were made only inside the housing and external components underwent a redesign and were then assembled into the housing. Calculations were done to the main components to make sure the new design could be certified according to EN 13445 and Det Norske Veritas (DNV), where DNV has been designated as the notified body to assess the conformity of the AOGV.

From the documentation and meetings three designs were created and presented. Design 3 was deemed the most suitable due to its use of a seal hub with O-rings and corresponding back-up rings for sealing. With blending one side of the housing, one potential leakage passage was effectively eliminated from the existing design. To ensure the new design was sufficient and compliant with the EN 13445-3 standard for designing unfired pressure vessels, the choice of material was inspected and calculations were performed for shaft bending, bolt strength, and O-rings. This design was found to be the most sufficient in terms of being robust, functional and reliable. This is a design that was created as an improvement to the original system and can be considered as a suggestion to Izomax. This report presents the 3D models, calculations, and theory supporting the design. However, to validate the functionality and reliability of the design, it is imperative to conduct testing.

---

## Sammendrag

Hensikten med denne oppgaven er å se på forbedringer av rack- og pinion systemet som brukes i Izomax's isolasjonsverktøy Add On Gate Valve (AOGV). Dette systemet blir brukt til å sette inn en blindspade mellom to flenser for å utføre vedlikehold i rørledninger. Målet er å finne en ny løsning for å gjøre rack- og pinionsystemet mer robust, eliminere lekkasjeveier og gjøre det mer praktisk å håndtere.

Etter å ha gjennomført møter og gjennomgått dokumentasjon, viste det seg at det nåværende designet manglet tilstrekkelig tetning. En fjærbelastet tetning ble brukt som tetningsmetode, men under testing og trykksetting ble det identifisert problemer med tetningsevnen. Systemet hadde også designfeil som ble oppdaget. Feil dimensjoner og overflate spesifikasjoner førte til tetningsproblemer og kald sveising av deler. For å øke påliteligheten og for å gjøre systemet mer brukervennlig er forbedringer i designet, tetningsmetoden og materialene nødvendig.

Denne rapporten er basert på 2 in (") 1500 lbs class (#) AOGV som opererer under omgivelsestemperatur på 20°C, ved et designtrykk på 173 bar, et testtrykk på 248 bar som definert i direktivet for trykksatt utstyr (PED) Europeisk Standard (EN) 13445, og med hydrokarboner som mediet i rørledningene.

Arbeidet begynte med å identifisere omfanget av problemet gjennom møter med prosjektledere, prosjektingeniører og mekanikere. Fokuset var på å samle innsikt fra både feltoperasjoner og dokumentasjon. Det ble gjennomført fysiske inspeksjoner på verkstedet for å forstå både installasjons- og vedlikeholdsprosedyrer for det nåværende systemet. Det som fulgte var et omfattende litteratursøk, fokusert på tetting av høytrykksystemer og å finne relevant dokumentasjon for design prosessen. Med informasjonen som ble samlet inn, startet design prosessen ved å bruke de eksisterende tegningene av AOGVen som ble gjort disponible av Izomax. Endringer ble kun gjort inni huset for å beholde den opprinnelige ytre geometrien, mens de eksterne komponentene gjennomgikk et redesign slik at et nytt design kunne lages. Beregninger ble gjort for hovedkomponentene for å sikre at det nye designet vil kunne bli godkjent av Det Norske Veritas (DNV) og designet etter EN 13445.

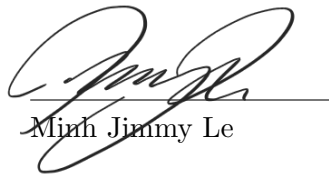
Med all dokumentasjon og møtene som ble utført ble det laget og presentert tre ulike design. Design 3 ble ansett som mest egnet for formålet. Dette designet består av en flens med O-ringer, inkludert støtteringer for å forsikre tetningen av systemet. Den ene åpne enden av huset ble blendet. Dette ble gjort for å effektivt eliminere en potensiell lekkasjevei fra det eksisterende design. For å sikre at det nye designet blir godkjent og er i samsvar med EN 13445-3, standarden for trykkbeholdere uten egen varmeenhet, ble valget av materiale inspisert og beregninger av komponentene utført. Dette designet anses av oss til å være best egnet for systemet i AOGVen når det gjelder å være robust, praktisk å håndtere og påliteligheten. Dette er et design som ble laget av oss som en forbedring av det opprinnelige systemet og kan betraktes som et forslag til Izomax. Denne rapporten presenterer 3D-modeller, beregninger og teori som støtter dette designet. Alt tatt i betraktning er det avgjørende å gjennomføre testing for å konstatere effektiviteten og påliteligheten til designet.

---

## Preface

This thesis has been written in cooperation with Izomax AS and is being submitted to fulfill our Bachelor's degree in Mechanical Engineering at the University of Stavanger. We want to express our gratitude to associate Professor Ove Mikkelsen, our internal supervisor, for his guidance, advice, feedback and helpful critique on our project. We are also grateful and wish to thank Izomax for giving us this opportunity to write our thesis in collaboration with the company, and for providing us with a highly inspiring workplace at their facilities. We extend a special thanks to our external supervisors and project managers at Izomax, namely Kristoffer Helliesen Ueland, Erlend Halvorsen and Simon Hus, for their invaluable support during the design and writing of our project. Additionally, we appreciate the helpfulness of the project engineers who assisted us throughout our journey.

Stavanger May 15.



Minh Jimmy Le



Patrick Kyorfa

---

# Contents

<b>Abstract</b>	<b>i</b>
<b>Sammendrag</b>	<b>ii</b>
<b>Preface</b>	<b>iii</b>
<b>List of Figures</b>	<b>vii</b>
<b>List of Tables</b>	<b>viii</b>
<b>List of Symbols</b>	<b>ix</b>
<b>Abbreviations</b>	<b>xiii</b>
<b>1 Introduction</b>	<b>1</b>
<b>2 Theory</b>	<b>2</b>
2.1 AOGV . . . . .	2
2.2 Design code and Standard . . . . .	4
2.3 Rack and Pinion . . . . .	4
2.4 Materials . . . . .	5
2.4.1 Elastic deformation . . . . .	5
2.4.2 Plastic deformation . . . . .	7
2.4.3 Stainless steel . . . . .	7
2.4.4 European steels for pressure purposes (P) . . . . .	9
2.4.5 American Iron and Steel Institute (AISI) 4140 . . . . .	9
2.4.6 American Society for Testing and Materials (ASTM) A320 Grade L7 bolts . . . . .	10
2.4.7 Structural steel (S) . . . . .	10
2.4.8 Nitrile Butadiene Rubber (NBR) and Polytetrafluoroethylene (PTFE) . . . . .	10
2.4.9 Surface finish . . . . .	11
2.5 Seals . . . . .	12
2.5.1 Spring-energized seal . . . . .	12
2.5.2 O-ring . . . . .	13
2.6 Bolted connections . . . . .	15

---

2.6.1	Fastener stiffness and geometry . . . . .	17
2.6.2	Member stiffness . . . . .	18
2.6.3	Bolt Strength Assessment . . . . .	20
2.6.4	Safety factors . . . . .	21
2.6.5	Using EN 13445-3 to verify bolt size . . . . .	22
2.7	Shaft . . . . .	23
2.7.1	Shaft design . . . . .	23
2.8	Bearings . . . . .	26
2.8.1	Iglidur X plain bearings . . . . .	26
2.9	Key and keyway . . . . .	27
<b>3</b>	<b>Methodology</b>	<b>28</b>
3.1	Autodesk Inventor . . . . .	28
3.2	Design review . . . . .	28
3.3	Literature review . . . . .	29
<b>4</b>	<b>A Comprehensive Review of the weaknesses in the Current Design</b>	<b>30</b>
<b>5</b>	<b>Results</b>	<b>33</b>
5.1	Design 1 . . . . .	33
5.2	Design 2 . . . . .	35
5.3	Design 3 . . . . .	36
5.3.1	Shaft calculations and design . . . . .	37
5.3.2	Bolt calculations . . . . .	39
5.3.3	O-rings and Back-up Rings . . . . .	41
<b>6</b>	<b>Discussion</b>	<b>42</b>
6.1	Design 1 . . . . .	42
6.2	Design 2 . . . . .	43
6.3	Design 3 . . . . .	44
<b>7</b>	<b>Conclusion</b>	<b>49</b>
	<b>References</b>	<b>50</b>

---

---

<b>Appendix</b>	<b>53</b>
<b>A Shaft Calculations</b>	<b>53</b>
<b>B Bolt calculations</b>	<b>58</b>
<b>C Seals calculations</b>	<b>63</b>
<b>D Inventor calculations</b>	<b>67</b>
<b>E Inventor drawings</b>	<b>72</b>
<b>F Standard parts</b>	<b>78</b>

---

## List of Figures

1	Brief illustration of the assembly process of an AOGV operation . . . . .	3
2	Involute Tooth profile . . . . .	5
3	Stress-strain curve . . . . .	6
4	Stress-strain curve showing 0.2 % offset Yield Strength . . . . .	7
5	Layer profile of steel and stainless steel . . . . .	8
6	Nickel and chromium content in stainless steel . . . . .	8
7	Average Roughness (Ra) . . . . .	11
8	Spring-energized seal . . . . .	12
9	Use of O-ring without back-up ring (left) and with back-up ring (right) . . . . .	13
10	Geometry of O-ring . . . . .	14
11	Illustration of geometry for piston- and rod sealing . . . . .	14
12	View of bolted joint (a) and a screw joint (b) . . . . .	16
13	Illustration of the different lengths in a bolted connection made in Inventor . . . . .	18
14	Stress Frustum . . . . .	19
15	Illustration of an Iglidur X plain bearing . . . . .	26
16	Illustration of a keyed joint . . . . .	27
17	Feather key according to DIN 6885 made in Inventor . . . . .	27
18	Illustration of the original design of the rack and pinion system designed by Izomax . . . . .	30
19	Sealing shim with elastomer, Photo by Izomax . . . . .	31
20	Welding damages on shaft and sealing shim, Photo by Izomax . . . . .	31
21	Disc with notches for counting revolutions, Photo by Izomax . . . . .	32
22	Illustration of design 1 made in Inventor . . . . .	33
23	Shaft configuration made in Inventor . . . . .	34
24	Assembly of bushing and Iglidur X plain bearing made in Inventor . . . . .	34
25	Half section view of design 2 with the different components made in Inventor . . . . .	35
26	Half section view of design 3 with the different components made in Inventor . . . . .	36
27	Free body diagram of shaft made in Inventor . . . . .	37
28	Mounted Iglidur X plain bearing in seal hub made in Inventor . . . . .	38
29	Illustration of A320 Grade L7 M10x1.5 bolt taken from Inventor . . . . .	39
A1	Free body diagram of the shaft with corresponding lengths made in Inventor . . . . .	53
A2	Shear force diagram made in Inventor . . . . .	54



---

A3	Moment diagram made in Inventor . . . . .	54
A4	$\frac{M}{EI}$ diagram made in Inventor . . . . .	55
A5	Elastic curve figure made in Inventor . . . . .	56
B1	The stress frustum with dimensions made in Inventor . . . . .	60
C1	Results from ERIKS calculator for O-rings for static application . . . . .	65
C2	Results from ERIKS calculator for O-rings for dynamic application . . . . .	66

## List of Tables

1	Extract of table for Pressure-Temperature Ratings for American Society for Testing and Materials (ASTM) Group 2-1.1 Materials Working pressure by Classes . . . . .	4
2	Mechanical properties of S32750/EN 1.4410 . . . . .	9
3	Mechanical properties of ASTM A320 Grade L7 screws . . . . .	10
A1	Area and centroid in tableform . . . . .	56

---

## List of Symbols

$A$	Area
$a$	Acceleration
$A_0$	Initial cross-section area
$A_B$	Effective bolt area
$A_{backupring}$	Cross-sectional area of back-up ring
$A_{gland}$	Area of the gland
$A_{oring}$	Cross-sectional area of O-ring
$A_s$	Tensile Stress area
$A_{shaft}$	Cross-sectional area of shaft
$A_t$	Tensile Stress area
$C$	Joint constant
$D$	Diameter
$d$	Diameter
$d_1$	Inner O-ring diameter
$d_2$	Cross-sectional diameter of O-ring
$d_3$	Inner gland diameter
$d_5$	Shaft diameter
$d_s$	Nominal diameter
$E$	Modulus of Elasticity
$F$	Force
$F_{axial}$	Axial Force
$F_B$	Load per bolt

---

$F_{thrust}$	Thrustforce
$F_b$	Tensile force in bolt
$f_d$	Nominal design stress
$F_i$	Preload
$F_p$	Proof load
$h$	Thickness of flange and washer
$I$	Moment of Inertia
$k$	Axial stiffness
$k$	Friction coefficient
$k_b$	Fastener stiffness
$k_m$	Member stiffness
$L$	Fastener length
$l$	Effective grip length
$L_T$	Thread length
$M$	Moment
$M_t$	Torque
$n_0$	Safety factor against joint separation
$n_L$	Load factor of safety
$n_p$	Yielding factor of safety
$n_{yielding}$	Safety factor against yielding
$P$	Pressure
$P_{surface}$	Surface pressure

---

---

$r$	Radius
$R_{0-3\%}$	Reduction in cross-sectional area between 0%-3%
$R$	Distance to centroid
$R_{3-25\%}$	Reduction in cross-sectional area between 3%-25%
$Ra$	Roughness average
$R_m$	Tensile Strength
$R_{p0.2}$	Offset Yield Strength
$S$	Stretch
$S_p$	Proof Strength
$t$	Member thickness
$t_{max}$	Maximum width on Back-up rings
$V$	Shear force
$V_a$	Tangential deviation line
$x$	Distance
$\Delta L$	Difference in length
$\delta$	Deflection
$\epsilon$	Strain
$\mu$	Friction coefficient
$\sigma$	Stress
$\sigma_b$	Bending stress
$\sigma_{bolt}$	Tensile stress in bolt
$\sigma_e$	Von Mises stress
$\sigma_i$	Preload stress in bolt
$\sigma_n$	Normal stress

---

---

$\tau$	Torsional shear stress
$\tau_i$	Shear stress in bolt
$\alpha$	Angle
$\Phi$	Bolt load ratio
$\phi$	Angle
#	lbs class
"	Inch

---

## Abbreviations

AISI	American Iron and Steel Institute
AOGV	Add On Gate Valve
ASME	American Society of Mechanical Engineers
ASTM	American Society for Testing and Materials
BOE/D	Barrels Of Oil Equivalent Per Day
CAD	Computer Aided Design
CE	Conformitè Européenne
DIN	Deutsches Institut für Normung
DNV	Det Norske Veritas
EEA	European economic area
EN	European standard
EU	European union
HB	Brinell Hardness
HBNR	Hydrogenated acrylonitrile butadiene rubber
HRC	Hardness Rockwell C
IC	Integrity Clamp
MUSD	Million United States dollars
NBR	Nitrile Butadiene Rubber
PED	Pressure Equipment Directive
PTFE	Polytetrafluoroethylene

---

# 1 Introduction

Izomax established an IK-Group subsidiary in early 2023, a company specializing in pipe and pipeline repair and maintenance services both topside and subsea. Izomax has developed the AOGV for topside operations, which allows for safe isolation by inserting an isolation spade on a live flange connection, eliminating the need for conventional extensive isolation procedures. The top priority when working with high-pressure systems is safety for both employees and the environment. This is why the AOGV is designed in accordance with design codes and standards to guarantee its safe use [1].

As of now the AOGV has been designed for sizes 1"-36" and up to 2500 lbs, but there is no upper limit. To insert an isolation spade, they use a rack and pinion system in some of the AOGV's. The current design employs spring-energized seals, which are reliable but pose challenges. The seals must be fitted onto a rotating shaft with a smooth surface and free from contaminant and scratches, otherwise a leakage-free path cannot be guaranteed. Also the material of the shaft is of importance when fitting seals on to it. The conditions in where the AOGV is used are harsh and til now it was not possible to use the spring-energized seal for what it is designed for. Currently Izomax uses elastomers which perform adequately but increase friction and makes assembling the sealing shims with the Igus bearings more challenging. An illustration of the design is given in figure 18.

To be able to continue its work in the most efficient and safe way, Izomax requires research into a more effective method to use the rack and pinion system. This thesis will be based on the 2" 1500# AOGV in operating temperature and the objective is to examine the existing rack and pinion system and explore opportunities for enhancement through:

- Reducing and eliminating potential leak paths
- Exploring new assembly methods and make it more robust
- Analyzing materials and seals and finding optimal combinations

This thesis consists of 7 chapters and 6 appendices. Chapter 1 gives an introduction to the problem and chapter 2 reviews the related literature. Chapter 3 details the methods used for analyzing and collecting of data in the study. A comprehensive review of the weaknesses in the current design are presented in chapter 4. The new designs with relevant calculations and figures are presented in chapter 5, followed by the discussion of results in chapter 6. Finally, chapter 7 concludes the whole thesis work.

---

## 2 Theory

### 2.1 AOGV

The AOGV is a patented tool developed by Izomax for safe isolation and maintenance of pipes and equipment in process plants, refineries, and Oil & Gas facilities. The prototype was created in 2016, with the first successful operation in 2017. It is designed to enable safe isolation and eliminating the need for extensive isolation activities, by inserting an isolation spade on a live flange connection. By reducing the need for drainage, venting, purging, and flushing, the tool reduces downtime for operators, saving up to 30,000 Barrels Of Oil Equivalent Per Day (BOE/D) or 20 Million United States dollars (MUSD). The savings are mainly due to increased production up time [1][2].

Typical applications of the AOGV may include replacement of valves and piping, isolate heat exchangers for chemical cleaning or replacing leaking flange gaskets with new gaskets and bolts. As a full or partial system shutdown is no longer necessary, there is normally no release of dangerous hydrocarbons into the environment [1][2].

Izomax has been focusing on the American Society of Mechanical Engineers (ASME) class 150 & 300 but have tools that can handle sizes up to 36" ASME up to class 2500. More information about the different classes in section 2.2.



---

The operation of the AOGV is complex and needs to be done by trained mechanics of Izomax. A short explanation of the operation steps is listed below. This list is taken out from the Izomax website [3]. See figure 1 for a brief illustration of the assembly process of an AOGV operation.

- Fits on any standard ASME flange
- Leave pipe medium in place
- Clamp on the AOGV and suspend its weight
- Transfer the compression force from the flange bolts to the AOGV & unbolt the flange using standard tools
- Plug the flange bolt holes
- Separate the pipe flanges and remove the gasket
- Insert a blind spade and compress the flanges to seal
- Perform the required work
- Release and retract the blind spade
- Insert new gasket and compress flanges to sea
- Install flange bolts and torque up flanges to reinstate the system

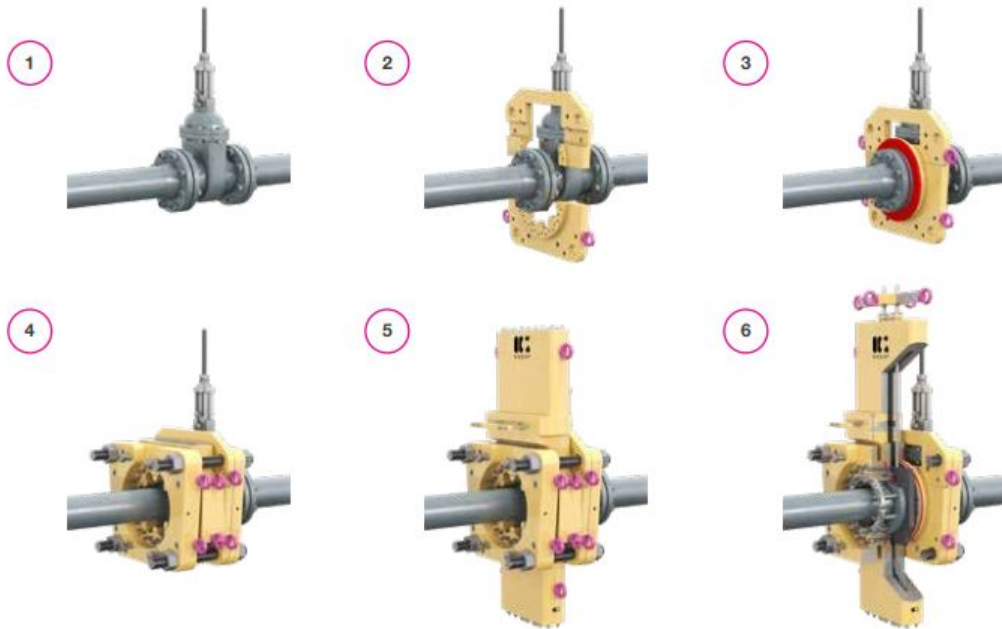


**Figure 1:** Brief illustration of the assembly process of an AOGV operation [3]

The AOGV is designed after EN 13445 for "Unfired pressure vessels". This standard specifies the requirements for the material, design, fabrication, inspection and testing of the AOGV [4].

---

## 2.2 Design code and Standard

PED 2014/68/EU is a European standard directive that establishes safety requirements for the design, manufacture, and conformity assessment of pressure equipment. The PED applies to equipment that operates at a pressure greater than 0.5 bar and includes items such as boilers, pipelines, and pressurized tools. Manufacturers are required to carry out a conformity assessment procedure and affix the Conformitè Européenne (CE) marking to their products before placing them on the market. This includes a formal design examination, a production quality assurance, and a random testing of the product [5].

Standard EN 13445 is a European standard that provides technical requirements and guidelines for the design, fabrication, inspection, non-destructive examination, overpressure protection and testing of unfired pressure vessels [4]. This standard is harmonized with the PED and is widely used in the European union (EU) and other countries as a reference. The list below specifies the topics covered in each chapter of the standard.

- EN 13445-1 - General
- EN 13445-2 - Materials
- EN 13445-3 - Design
- EN 13445-4 - Fabrication
- EN 13445-5 - Inspection and testing

Flanges are classified by their pressure rating, which is given by the class. The pressure that a flange can withstand is affected by the temperature it is exposed to. As the temperature increases, the pressure rating decreases. Additionally, the material group also influences the Pressure-Temperature Ratings. The extract of table 1 provides further details on the various ASME classes and pressures at different temperatures for group 2-1.1 materials [6].

**Table 1:** Extract of table for Pressure-Temperature Ratings for ASTM Group 2-1.1 Materials Working pressure by Classes [6]

Working pressure (bar)					
Temperature (°C)	Class 150	Class 300	...	Class 1500	Class 2500
-29 - 38	19.6	51.1	...	255.3	425.5
50	19.2	50.1	...	250.6	417.7
100	17.7	46.6	...	233	388.3
150	15.8	45.1	...	225.4	375.6
200	13.8	43.8	...	219	365
...	...	...	...	...	...
538	1.4	5.9	...	29.5	49.2

## 2.3 Rack and Pinion

The rack and pinion system is a simple mechanism that is widely used to convert rotational motion into linear motion. The system consists of a linear gear (rack) and a circular gear (pinion), which mesh together to transmit power and motion. The rack is typically a flat piece of metal with teeth cut into it, while the pinion is a circular gear that meshes with the teeth of the rack.

The geometry of the gears in a rack and pinion system plays a critical role in its performance and efficiency. One key aspect of this geometry is the pressure angle, which is the angle between the line of contact between the gear teeth and the normal line to the pitch circle. This angle is typically set at  $20^\circ$  for rack and pinion gears. Another important factor is the pitch, which is the distance between the gear teeth and measured at the point of contact. Other important parameters include the base circle, addendum, and dedendum, which provide reference points for the gear tooth profile. The addendum is the height of the tooth above the base circle, and the dedendum is the depth of the tooth below the base circle, as shown in figure 2. The involute gear profile is commonly used as it can transmit motion smoothly and efficiently, as the gear teeth are in contact at the pitch circle without slipping [7].

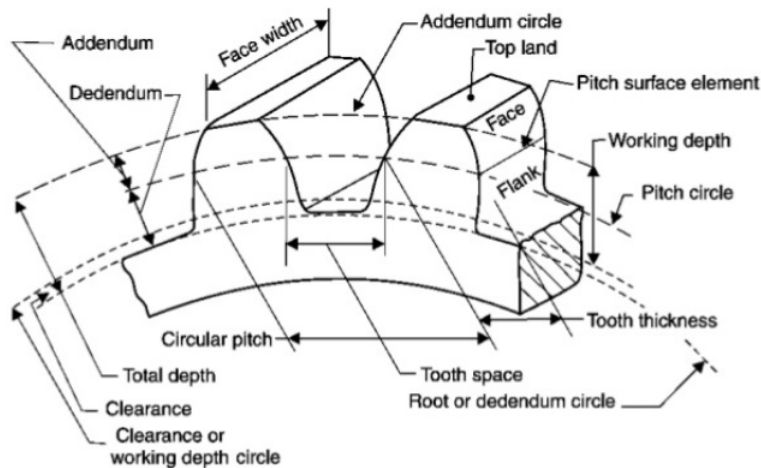


**Figure 2:** Involute Tooth profile [8]

## 2.4 Materials

When external forces are exerted on materials, their shape and size may be changed, but whether the resulting deformation is elastic or plastic depends on the material's mechanical properties. These properties, including strength, hardness, toughness, ductility, and stiffness, play a crucial role in determining a material's response to axial stress, which is the external force acting over the cross-sectional area of an object, and its resulting strain, which is the measure of the deformation. The mathematical formulas are defined in eq. 1 for stress and eq. 2 for strain. This understanding is essential for designing any machine or structure [9].

$$\sigma = \frac{F}{A_0} \quad (1)$$

$$\epsilon = \frac{\Delta L}{L_0} \quad (2)$$

### 2.4.1 Elastic deformation

When a force is applied to a material, it can undergo elastic deformation, which is a non permanent, reversible process. This means that the material will return to its original shape once the force is removed. By examining a stress-strain diagram as shown in figure 3, one can determine important

characteristics of the material, such as its yield strength, tensile strength, Young's Modulus ( $E$ ), and fracture point. The elastic region of the diagram is represented by the slope from zero to the yield strength, which is also known as the Young's Modulus ( $E$ ). The greater the modulus of elasticity, the stiffer the material. This modulus is an essential design parameter for the calculations of elastic deflection. The typical Modulus of Elasticity for steel at room temperature lies between 200 GPa and 210 GPa and the Poisson's ratio of 0.30. Any deformation that occurs up to the yield strength is elastic, meaning that the material will return to its original form after the load is removed. The elastic region is governed by Hooke's law, shown in eq. 3 [9][10].

$$\sigma = E\epsilon \tag{3}$$

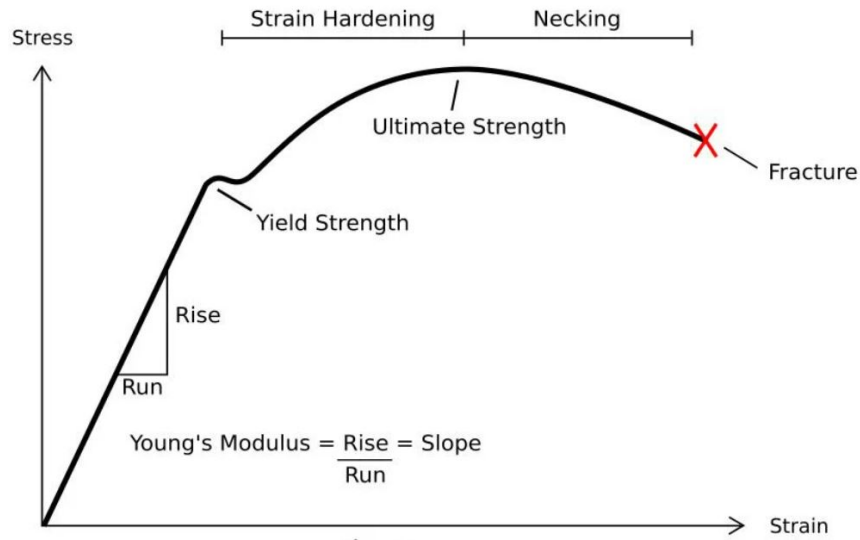


**Figure 3:** Stress-strain curve [11].

---

### 2.4.2 Plastic deformation

Plastic deformation occurs when a material is deformed beyond the yield strength of the material. This deformation is permanent and it stays deformed even after the force applied is removed. It is of very importance to identify when a material goes from elastic to plastic deformation. This point is difficult to measure precisely, and that is why a convention has been set to construct a parallel line to the elastic line with a strain offset of 0.2 %. This method is defined as the stress value corresponding to the 0.2 % plastic strain and is represented by  $R_{p0,2}$ , see figure 4. For some materials the transition between plastic-elastic deformation is well defined and called the Yield Point phenomenon. After the plastic deformation the strain continues until it reaches the tensile strength  $R_m$ , as illustrated in figure 3 where it shows where the stress decreases and finally fracture occur [10].

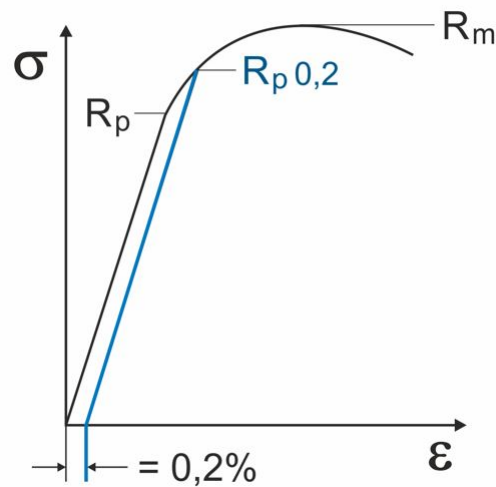


**Figure 4:** Stress-strain curve showing 0.2 % offset Yield Strength [12]

### 2.4.3 Stainless steel

Stainless steel is a type of metal that consists of iron, chromium and in some cases nickel and other elements, making it resistant to corrosion. Stainless steel has superior mechanical properties, including its combination of ductility, elasticity, and hardness. To meet the criteria of being classified as stainless steel, the steel must contain a minimum of 10.5 % chromium and no more than 1.2 % carbon and other elements. Adding other alloying elements such as nickel can further improve the corrosion resistance and mechanical properties. The steel's chromium oxide layer on its surface, formed by the natural reaction of chromium with air or water, gives it corrosion resistance as it can regenerate the surface when scratched. Unlike regular steel which forms a iron oxide layer which is know as rust. Figure 5 presents an illustration of the layers and composition of steel and stainless steel in a oxidizing environment such as air [13].

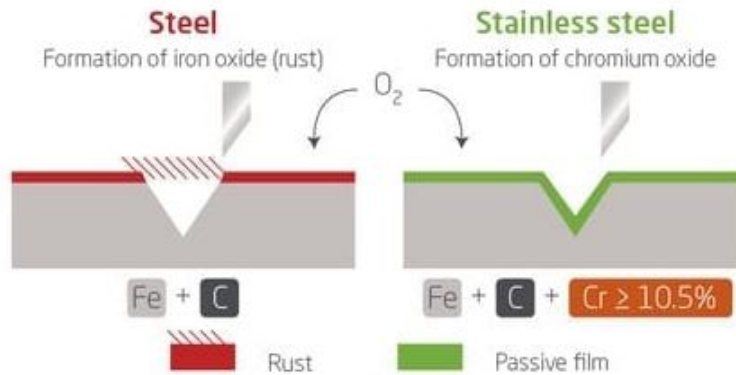


**Figure 5:** Layer profile of steel and stainless steel [13]

Stainless steel consists of five categories: ferritic, martensitic, austenitic, duplex and precipitation-harden. These designations are based on the steel's crystal structure and influence its metallurgical characteristics. Super Duplex (S32750/EN 1.4410) has a austenitic/ferritic crystal structure which gives this stainless steel its hardness of about 33 Hardness Rockwell C (HRC) and mechanical strength by adding elements such as nickel. See figure 6 for a diagram of nickel and chromium content in the five categories of stainless steel [13][14].

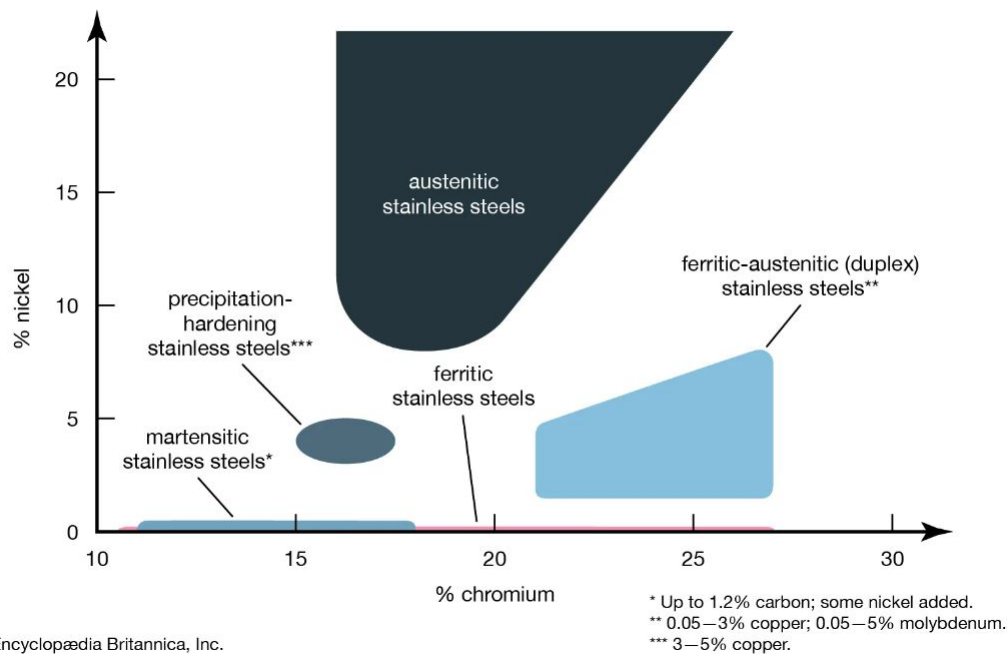


**Figure 6:** Nickel and chromium content in stainless steel [15]

---

Super duplex has a minimum guaranteed yield strength of 550 MPa, a modulus of elasticity of 200 GPa and its common area of use is in aggressive chloride-containing environments. This material has solid mechanical properties that are used often within oil & gas, hydro power and pressure vessels. Table 2 shows the mechanical properties [14].

**Table 2:** Mechanical properties of S32750/EN 1.4410 [14]

<b>Yield strength <math>R_{p0,2}</math> (MPa)</b>	<b>Tensile strength <math>R_m</math> (MPa)</b>	<b>Elongation (%)</b>	<b>Brinell Hardness (HB)</b>
$\geq 550$	$\geq 750$	$\geq 25$	$\leq 310$

#### 2.4.4 European steels for pressure purposes (P)

European steels for pressure purposes refer to steel grades utilized in the production of pressure vessels in Europe. Every design and manufacture of pressure vessels for storing raw materials at higher pressure than 0.5 bar is strictly regulated by the guidelines in the Standard EN 13445 for unfired pressure vessels. The "P" in the designation stand for pressure [16].

Two of those steels for pressure purposes are P355 and P460 NL2. P355 is a low-alloy steel grade that is used for the manufacture of pressure vessel tanks for storage of pressurized gases and is classified under EN 10028-2 for pressure vessel steel. It is known for its good weldability and toughness. 355 refers to the minimum yield strength in MPa. Like P355, P460 NL2 is also classified under EN 10028. The NL indicates that this steel is ideal for especially low temperature applications. This pressure vessel steel has a minimum yield strength of 430 MPa and is used in boiler and pressure vessel fabrication [17][18].

#### 2.4.5 American Iron and Steel Institute (AISI) 4140

AISI 4140 is a high tensile steel and contains significant amounts of manganese, molybdenum, and chromium elements. AISI 4140 is commonly used for making high-tensile tools and products, such as bolts, nuts and screws, that are exposed to heavy strain. Through annealing, hardening, and tempering, its physical and mechanical properties are enhanced [19][20].

---

#### 2.4.6 American Society for Testing and Materials (ASTM) A320 Grade L7 bolts

ASTM A320 Grade L7 is a material specification used for manufacturing of bolts, studs, stud bolts and other fasteners for bolting pressure vessels, valves and flanges in low temperatures and high pressure applications. The L7 indicates that the material is composed of AISI 4140. Screws made using this material are extremely resistant to corrosion and a varied range of environmental conditions. To ensure reliable performance, ASTM A320 Grade L7 Socket Head Cap Screws are manufactured to the ASME B18.3.1M standard for metric fasteners. This standard specifies the dimensional and mechanical requirements for metric socket head cap screws, including the head diameter, thread pitch, and overall length. Table 3 shows the mechanical properties for this type of bolt material [21][22][23].

**Table 3:** Mechanical properties of ASTM A320 Grade L7 bolts [21]

Yield strength $R_{p0.2}$ (MPa)	Tensile strength $R_m$ (MPa)	Elongation in 50mm (%)	Hardness (HB)
$\geq 725$	$\geq 860$	$\geq 16$	$\leq 321$

#### 2.4.7 Structural steel (S)

Structural steel is made from specific types of steel with standardized shapes. It is created with specific chemical and mechanical properties for specific applications. The standards and specifications of steel grades in the United States are established by the ASTM, while structural steel in Europe must comply with the EN 10025. One of the most common and popular is the structural steel S355 with a min yield strength of 355 MPa [24][25].

#### 2.4.8 Nitrile Butadiene Rubber (NBR) and Polytetrafluoroethylene (PTFE)

Elastomer covers a group of linear polymers that have a large range of elastic deformation when a force is applied. When the force is released and not greater than the maximum strain allowed, they will return to their original shape. Polymers that can do so are called elastomers, also known as rubber. All other polymers are termed as plastics. The Shore Hardness scale, using either the Shore A or Shore D scale, is the preferred method for measuring the hardness of rubbers and thermoplastic elastomers [26][27].

NBR is an elastomer and known as Nitrile Butadiene Rubber. It is a synthetic rubber and is usually the ideal choice for any product that requires oil or gas resistance at low pressure. For high pressure applications hydrogenated acrylonitrile butadiene rubber (HNBR) is used. One typical application is for O-rings with a typical Shore A hardness of 70-90 [27].

Polytetrafluoroethylene, also known as PTFE, is distinguished by its slippery surface, high melting point, and resistance to almost all chemicals [28].



---

### 2.4.9 Surface finish

The importance of surface finish goes beyond its aesthetic appeal as it can significantly affect the performance and durability of a part in its designated environment. A rough surface finish is more prone to wear and tear. However, if a fine surface finish is not necessary, opting for a rougher finish can be cheaper and more convenient, as it can also hide imperfections and scratches on the part. Surface finish comprises three elements: roughness, lay, and waviness, with surface roughness being the most common way to describe it. Roughness  $R_a$  refers to small irregularities on the surface, and is calculated as the mean deviation of the surface profile from its average line, measured over a specific distance, see figure 7 for an illustration. Achieving a fine surface finish is a more costly and time-consuming process, but it is often necessary when special seals are used in machinery. The next subsections will go further into the theory of seals and the importance of surface finish [29].

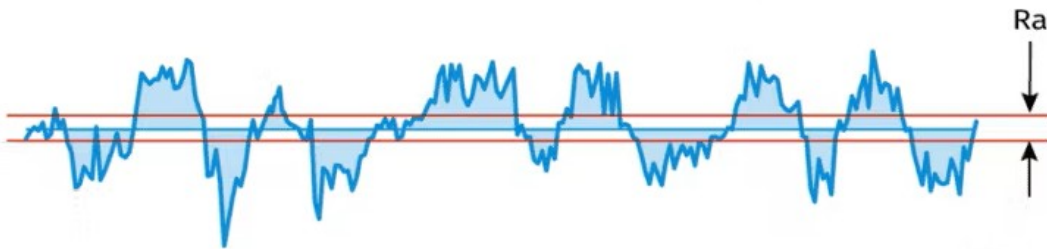


**Figure 7:** Average Roughness ( $R_a$ ) [29]

---

## 2.5 Seals

Seals play a vital role in ensuring the integrity of liquids and gases and protecting equipment from contamination. These are widely used across industries like automotive and oil and gas. The choice of material and design affects the longevity and performance of the seals, with rubber seals, made of materials like silicone and nitrile butadiene, being the most common [30]. To make the right choice of seals, one must consider factors like pressure, temperature, fluid, size, etc [31]. Regular inspections and maintenance are necessary to keep seals in good condition, and advancements in materials and technology have led to seals that are high-performing, durable, and cost-effective.

Dynamic seals are designed for mechanical systems with continuous motion such as rotating, reciprocating, or oscillating shafts. Factors to consider when selecting seals include sealing orientation, design, environment, and mating surface [31][32]. It must maintain its sealing performance despite various forces, including pressure and temperature changes. The most commonly used dynamic seals are O-ring seals, lip seals, and grease seals, and the choice of material depends on the application requirements and compatibility with the fluid or gas being sealed [31][32].

### 2.5.1 Spring-energized seal

Spring-energized seal is a type of lip seal that utilizes a spring to reinforce the contact pressure on the shaft. The presence of a spring enables this sealing method to function effectively in high pressure environments. As such, it is ideal for dynamic applications, including both rotary and reciprocating motion. When the spring-energized seal is pressurized, it forces the lips against the housing and shaft, resulting in improved sealing performance [33]. The spring-energized seal is applied in many applications. Similar to O-rings, it also requires a smooth shaft surface. For dynamic application with gas as the fluid medium, the surface roughness is  $Ra\ 0.15 - 0.40\ \mu m$  [34].



**Figure 8:** Spring-energized seal [34]

---

### 2.5.2 O-ring

O-rings are a widely used sealing method in many industries due to their versatility and cost-effectiveness. These seals are typically made of elastomers, which are materials that can be compressed and deformed to create a tight seal. O-rings are double-acting seals, meaning they can prevent leaks from both directions. They are easy to install and replace, and their simple shape makes them suitable for a wide range of applications. However, O-rings may not be suitable for high-pressure applications or environments with extreme temperatures or harsh chemicals. The choice of elastomer material for O-rings is crucial, as it determines the seal's properties such as temperature resistance, chemical compatibility, and durability [35].

Although the O-ring is a versatile and cost-effective sealing method for both static and dynamic applications, it has several limitations regarding rotary seals applications that designers must take into consideration. In a dynamic application, the groove should be on the stationary part, as it tends to extrude and develop high levels of rubbing wear when the groove is on the rotating part. However, if designed correctly, additional stress on the O-ring surface can be avoided. The other limitation is the concentricity of the shaft. If the concentricity is more than 0.127 mm off-center [35], achieving a leak-proof design could be challenging. Furthermore, the use of O-rings in high-pressure or high temperature applications may not be feasible due to the limitations of elastomeric materials. But this issue could be solved by installing back-up rings in the gland, the back-up ring should be of a material harder than the O-ring itself. It should always be installed furthest from pressure in the gland, as shown in figure 9. Previous research has shown that the use of alternative materials, such as thermoplastic elastomers, could improve the performance of O-rings in dynamic applications [36]. By conducting further research on O-ring design and material selection, one could gain a better understanding of the limitations and potential applications of this versatile sealing method [35].



**Figure 9:** Use of O-ring without back-up ring (left) and with back-up ring (right) [37]

To select the appropriate O-ring for both static and dynamic seals, several factors must be considered. The gland fill should be between 65 % to 85 % to allow for thermal expansion and volume swell when pressure is applied [38]. The gland fill can be calculated using the following equation

$$Gland\ fill = \frac{A_{oring}}{A_{gland}} \cdot 100 \quad (4)$$

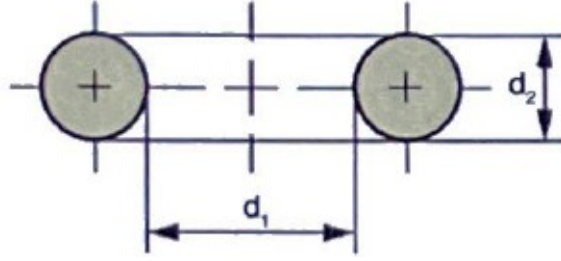


**Figure 10:** Geometry of O-ring [38]

The initial stretching of an O-ring during installation should not exceed 50 % of its original size. For shafts with a diameter greater than or equal to 20 mm, the recommended stretch range is between 2 % and 8 % for static applications, and between 2 % and 5 % for dynamic applications. However, achieving this level of stretch may not always be possible for shafts with diameters smaller than 20 mm. One possible solution to this issue is to minimize the tolerances of the housing diameter. When an O-ring is stretched, its cross-sectional area will naturally decrease, with a maximum allowed reduction of 3 %. The stretch for piston sealing can be calculated by using eq. 5 [38].

$$S = \frac{d_3 - d_1}{d_1} \cdot 100 \% \quad (5)$$

The stretch for rod sealing can be calculated using the following equation.

$$S = \frac{d_5 - d_1}{d_1} \cdot 100 \% \quad (6)$$

The different geometries that are needed for both calculations are illustrated in figure 11.

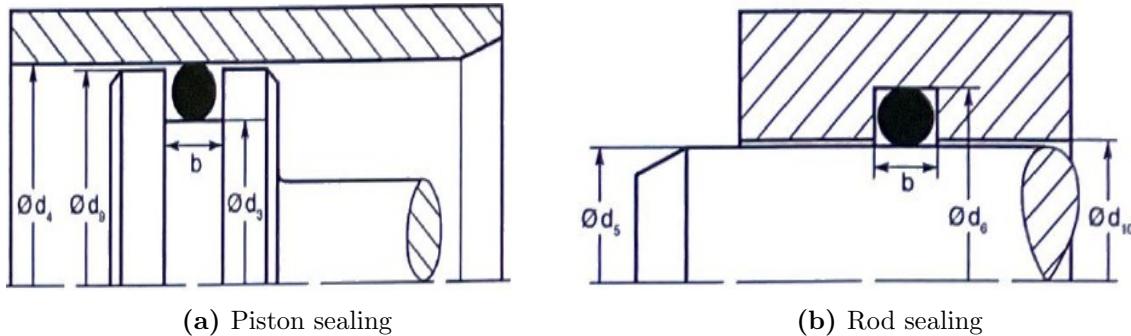


**Figure 11:** Illustration of geometry for piston- and rod sealing [38]

The reduction in cross-sectional area for O-rings stretched between 0 % and 3 % of their original size is given by eq. 7 [38].

$$R_{0-3 \%} = 0.01 + 1.06 \cdot S - 0.1 \cdot S^2 \quad (7)$$

Ensuring the correct compression of an O-ring is essential to achieve optimal sealing performance.

---

Insufficient compression can compromise the effectiveness of the seal, leading to potential leaks or inadequate sealing of the components. It is important to carefully consider the compression rate during the design and assembly process to guarantee a proper sealing. By providing adequate compression, the O-ring can effectively conform to the mating surfaces, creating a reliable and leak-free sealing barrier. The compression should be between 10% to 25% [38]. It can be determined by the following equation. Where  $d_{2min}$  is the cross-sectional diameter of the O-ring and  $t_{max}$  is the maximum gland height.

$$Compression = \frac{d_{2min} - t_{max}}{d_{2min}} \quad (8)$$

It is recommended a shore A hardness between 70 and 80 for sealing gases [38]. Surface roughness is a critical factor in the sealing ability of an O-ring, particularly in applications where sealing gases are involved. For dynamic applications, the following surface roughness standards should be met [38].

- Sealing surface: Ra 0.40  $\mu m$
- Groove surface: Ra 0.80  $\mu m$

For static applications, both the mating surface and groove diameter should have a minimum roughness of Ra 1.52  $\mu m$ . For static piston sealing the following surface roughness is recommended.

- Sealing surface: Ra 0.40  $\mu m$
- Groove surface: Ra 1.52  $\mu m$

The diametrical clearance, denoted as E, is an essential parameter that influences the achievement of sealing effectiveness. It plays a significant role in determining the compression ratio, which directly impacts the sealing performance. The recommended value for the diametrical clearance can be found in Parker's handbook, providing valuable guidance for designing and selecting the appropriate clearance for optimal sealing results [38].

## 2.6 Bolted connections

Bolted connections are widely used in the industrial world as fasteners to join structural components. They create mechanically locked and pretensioned connections, making them one of the most common types of connections. The usual configuration for these connections includes a bolt, nut, and washer. Washers should always be used to prevent stress concentrations and should always be of hardened steel. When the bolt and nut apply pressure to the components in between, the bolt stretches and generates a clamping load. Assuming the nut stays secure, this tension in the bolt remains as the preload or clamping force. The recommended preload for non permanent connections is given by eq. 9, where  $F_p$  is the proof load and given by eq. 10, where  $S_p$  is the proof strength [7].

$$F_i = 0.75F_p \quad (9)$$

$$F_p = A_t S_p \quad (10)$$

Due to varying conditions, frictions and other factors, one can not be sure of obtaining the exactly preload desired. Increasing the preload carries a higher risk of bolt breakage. The theoretical equation for torque when tightening is given by eq. 11, where  $k$  is the friction coefficient and can be considered as 0.20 in the most common cases [39].

$$M_t = kF_i d_s \quad (11)$$

where the diameter corresponding to the tension area  $d_s$  is defined as

$$d_s = \sqrt{\frac{4A_s}{\pi}} \quad (12)$$

Various types of bolts are used for different applications. Due to their characteristics, Socket Head Cap Screws are often used in various industries, particularly for secure and fasten heavy components and for applications that involve large force on the screw. Head Cap Screws are tapered fasteners that mate with an existing thread, but can also be used with a nut [7]. In figure 12 one can see a bolt fastened with a nut and a tapered fastener [40].

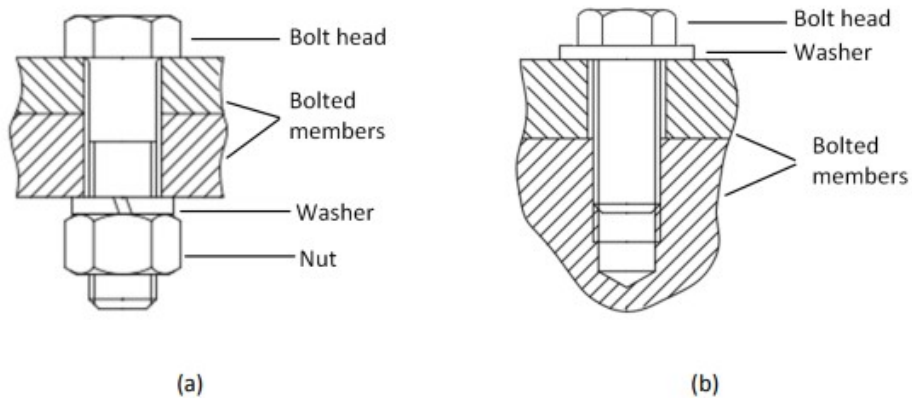


**Figure 12:** View of bolted joint (a) and a threaded tapered joint (b) [40]

---

### 2.6.1 Fastener stiffness and geometry

Various factors need to be considered when working with bolted connections. Bolted connections act as stiff springs exposed to tensile loading. To find the stiffness of a fastener in any bolted connection, the general definition for the spring stiffness eq. 13 is to be considered. The fasteners stiffness is equivalent to stiffness of two springs in series where it is necessary to consider the threaded and unthreaded portions of the bolt in the clamped zone [7].

$$k = \frac{AE}{l} \quad (13)$$

When a fastener is short and it is used a threaded tapped joint without a nut, the unthreaded area is small and it can be considered that the bolt is threaded all the way [7]. The effective grip length in this type of connection is given by

$$l = \begin{cases} h + \frac{t_2}{2}, & t_2 < d \\ h + \frac{d}{2}, & t_2 \geq d \end{cases} \quad (14)$$

With the effective grip length and the equation for the spring constant, the effective stiffness of the bolt  $k_b$  can be determined by eq. 15 when using a short fastener where the unthreaded area is small and not considered [7].

$$k_b = \frac{A_t E}{l} \quad (15)$$

Further for the design of those connections the fastener length and the threaded length of the bolt must be determined. To find a standard fastener it is recommended to round up the result for the fastener length from eq. 16 by using ISO's adopted Renard series. Thread length of the bolt is calculated with eq. 17 [7].

$$L > h + 1.5d \quad (16)$$

$$L_T = 2d + 6 \text{ mm}, \quad L \leq 125 \text{ mm}, d \leq 48 \text{ mm} \quad (17)$$

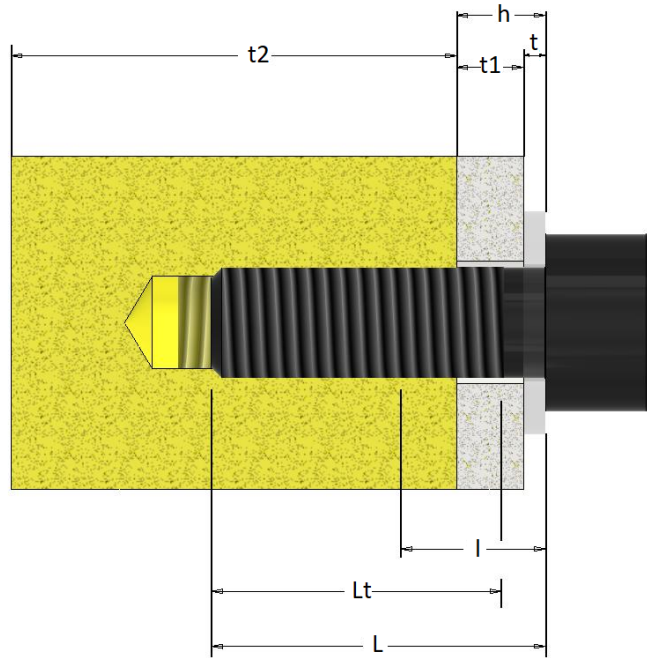


**Figure 13:** Illustration of the different lengths in a bolted connection made in Inventor [7]

### 2.6.2 Member stiffness

Along with the stiffness of the bolts, the stiffness of the members in the clamped zone are very important. It is necessary to know these values to understand the behavior of bolted connections under external tensile loading. All members that are included in the grip of the fastener act like compressive springs in series, and therefore the total spring rate of the members is given by

$$\frac{1}{k_m} = \frac{1}{k_1} + \frac{1}{k_2} + \frac{1}{k_3} + \dots + \frac{1}{k_i} \quad (18)$$



The individual stiffnesses must be determined for every member in the clamped zone to obtain the total member stiffness  $k_m$ . The methodology used here is the Shigley's Frustum Approach, see figure 14. This method sees the stress field like a frustum of a hollow cone and in this way the stiffness in a layer is obtained. By assuming axial compression and a half-apex angle of  $\alpha = 30^\circ$  for each frustum in compression the stiffness of an individual member is given by eq. 19 [7].

$$k_{m_i} = \frac{\pi E d t \tan \alpha}{\ln \left( \frac{(2l \tan \alpha + D - d)(D + d)}{(2l \tan \alpha + D + d)(D - d)} \right)} \quad (19)$$

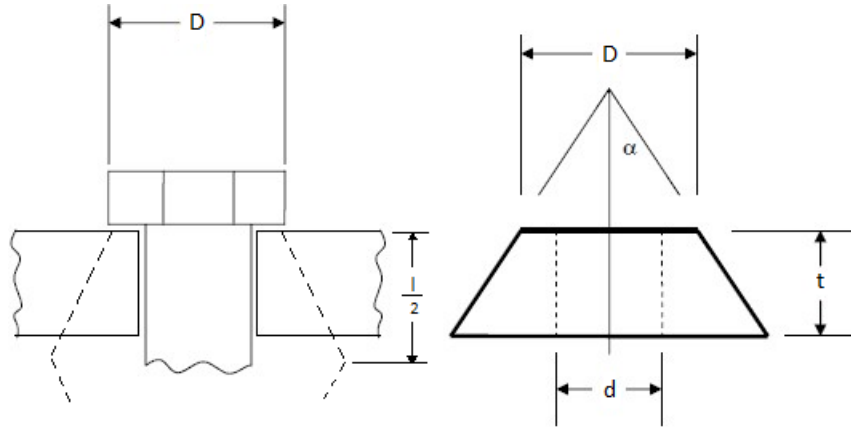


**Figure 14:** Stress Frustum [41]

The individual stiffnesses from eq. 19 are assembled to obtain  $k_m$  by using eq. 18. The resulting stiffnesses of the fastener and members are so used to find the stiffness constant of the joint  $C$  by eq. 20. This joint constant indicates how much of the external tensile load is carried by the bolt and how much by the members. It shows the ratio of external force and force of the bolt and is dependent on the relative stiffness of the bolt and the clamped parts. When the material of the fastener and members is steel, a typical value for the constant is 0.26. In most cases the members take over 80 % of the external load [7][39].

$$C = \frac{k_b}{k_b + k_m} \quad (20)$$

---

### 2.6.3 Bolt Strength Assessment

To determine the stresses acting on bolts in a connection, several factors need to be considered. Once an external force is applied, it is transferred to various components in the connection. According to the von Mises hypothesis, yielding occurs for the uniaxial state of stress when the equivalent stress is larger than the yielding strength  $R_p$  [39]. The von Mises stress is calculated by

$$\sigma_e = \sqrt{\sigma_{bolt}^2 + 3\tau_i^2} \geq R_p \quad (21)$$

The increasing tensile force in a bolt can be determined using eq. 22. With the increase of the tensile force in the bolt, the compressive force in the member decreases simultaneously.

$$F_b = C F_{thrust} = \frac{k_{b_{total}}}{k_{b_{total}} k_m} \cdot F_{thrust} \quad (22)$$

The total tensile stress occurring in the bolt after an external force is applied to it can be found by

$$\sigma_{bolt} = \frac{F_i + F_b}{A_t} \quad (23)$$

and the normal stress that occurs when preloading a bolt is given by the preload stress eq. 24.

$$\sigma_i = \frac{F_i}{A_t} \quad (24)$$

Also a shear stress will be present in a bolted connection. This shear stress is caused by torsion and together with the normal stress of the preload, the shear stress is given by

$$\tau_i \cong 0.5\sigma_i \quad (25)$$

---

#### 2.6.4 Safety factors

There are several safety factors that should be taking into account when designing bolted connections. With the previously identified parameters in this chapter, the safety factors can be determined and it can be concluded whether the bolts have been appropriately designed for their intended use.

The yielding factor of safety is the traditional factor of safety. It compares the maximum bolt stress to the proof strength and is not often much greater than 1, because its common to load a bolt to its proof strength. It is given by

$$n_p = \frac{S_p A_t}{C F_{thrust} + F_i} \quad (26)$$

Another approach to get the yielding factor of safety is by using the von Mises stress. Using von Mises the safety factor will be given by

$$n_{yielding} = \frac{R_{p0.2}}{\sigma_e} \quad (27)$$

Another factor of safety that comes into play with yielding is the load factor. The load factor of bolts is a measure of the amount of load that a bolt can safely withstand without exceeding the proof strength [7]. The load factor of safety is calculated with

$$n_L = \frac{S_p A_t - F_i}{C F_{thrust}} \quad (28)$$

To provide a safe joint, the external load must be smaller than the load that can cause the joint to separate. If the joint will separate, the bolt would take the entire load. The safety factor against joint separation is found by using eq. 29.

$$n_0 = \frac{F_i}{F_{thrust}(1 - C)} \quad (29)$$

By referring to all the calculations shown in this chapter, it can be ascertained whether the bolts were selected appropriately for statically applications.

---

### 2.6.5 Using EN 13445-3 to verify bolt size

When using the standard EN13445-3 for design of unfired pressure vessels, the procedure can be slightly different from the ones described in the previous sections. For steels other than austenitic steels, with a minimum rupture elongation below 30 %, the nominal design stress for normal operating load cases  $f$  shall not exceed  $f_d$  and is calculated by eq. 30.<sup>1</sup> With a yielding factor of safety of 1.5 and a tensile factor of safety of 2.4 at 20 °C [4].<sup>2</sup>

$$f_d = \min\left(\frac{R_{p0.2}}{1.5}, \frac{R_m}{2.4}\right) \quad (30)$$

From the EN13445-3 standard one can find the bolt load ratio. This ratio should not go below 0.3, if so, the bolts are underutilized or too thick [4].<sup>3</sup> This bolt load ratio is given by

$$\Phi_B = \frac{F_B}{A_B f_d} \cdot \sqrt{1 + (C \cdot 3.2 \cdot \mu)^2} \quad (31)$$

Where the term C takes account of the torque in bolting up. The value of C is 4/3 if strictly elastic behaviour of the bolts is required, which is recommended for not sufficient ductile bolt material.<sup>3</sup>  $F_B$  is the load taken of each bolt and  $A_B$  is the effective bolt area, which is found by using eqs. 32 and 33. The friction coefficient  $\mu$  for the threads lies between 0.10 - 0.15 for smooth, lubricated surfaces [4].

$$D_{effectiveBoltDia} = d - \frac{3}{4} \cdot \sqrt{3} \cdot Pitch \quad (32)$$

$$A_B = \frac{\pi \cdot D_{effectiveBoltDia}^2}{4} \quad (33)$$

---

<sup>1</sup>Tabell 6-1 "Maximum allowed values of the nominal design stress for pressure parts other than bolts" fra NS-EN 13445-3:2021 Ikke-fyrte trykkbeholdere — Del 3: Konstruksjon er gjengitt av Minh Jimmy Le og Patrick Kyorra til bruk i oppgaven "Optimizing of Rack and Pinion System for Valve Intervention Tool" med tillatelse fra Standard Online AS i (april 2023). Standard Online er ikke ansvarlig for eventuelle feil i gjengitt materiale. Se [www.standard.no](http://www.standard.no).

<sup>2</sup>Kapittel 6.2.1 "Normal operating load cases" fra NS-EN 13445-3:2021 Ikke-fyrte trykkbeholdere — Del 3: Konstruksjon er gjengitt av Minh Jimmy Le og Patrick Kyorra til bruk i oppgaven "Optimizing of Rack and Pinion System for Valve Intervention Tool" med tillatelse fra Standard Online AS i (april 2023). Standard Online er ikke ansvarlig for eventuelle feil i gjengitt materiale. Se [www.standard.no](http://www.standard.no).

<sup>3</sup>Annex G - G.7.2 "Bolts" fra NS-EN 13445-3:2021 Ikke-fyrte trykkbeholdere — Del 3: Konstruksjon er gjengitt av Minh Jimmy Le og Patrick Kyorra til bruk i oppgaven "Optimizing of Rack and Pinion System for Valve Intervention Tool" med tillatelse fra Standard Online AS i (april 2023). Standard Online er ikke ansvarlig for eventuelle feil i gjengitt materiale. Se [www.standard.no](http://www.standard.no).

---

## 2.7 Shaft

A shaft is an important mechanical component that is commonly used to transmit power and rotary motion between different parts of a mechanical system. This component is subjected to a variety of loads and forces during operation, including radial and axial loads, among others. Due to its critical role, it is essential to identify the specific forces that a shaft is likely to experience. An extended analysis will set minimum dimensions required according to material type chosen. In engineering design, a safety factor is typically set based on industry standards or common design safety factors which are based on experience. This helps to ensure that the shaft can withstand the loads and forces it will encounter, and that the mechanical system operates safely and reliably over its intended lifespan [42].

### 2.7.1 Shaft design

Typically, when designing a shaft, many of the restrictions are given by the applications the shaft would be applied. For a shaft in high pressure environment with sealing requirements, the diameter and material of the shaft must be carefully selected to withstand the forces and stresses that it will encounter. The design must also take into account factors such as the shaft's speed, deflection, the type and magnitude of the loads, the material properties, and the operating environment.

When designing a shaft, it is also important to consider factors such as the required tolerances, surface finish, and manufacturing methods. The design must be optimized to ensure that the shaft can be manufactured and assembled with the required precision and accuracy.

Overall, shaft design is a complex process that requires careful consideration of many different factors.

There are many methods to calculate deflection on a shaft. A common method is called moment-area theorem. This is an efficient way to calculating displacement in shaft when series of loads, or segments with different moment of inertia ( $I$ ) are existent.

Analysis procedure for moment-area theorem:

1. Determine reaction forces
2. Draw shear force-, moment-, and  $\frac{M}{EI}$  diagrams
3. Draw a representative drawing of the deflection curves
4. Draw tangent lines based from key locations based on the deflection curves

---

Reaction forces can be determined by applying fundamental formulas from statics eqs. 34 and 35 [9].

Recall Newton's second law where  $a = 0$

$$\sum F = 0 \quad (34)$$

Which gives sum of moment equals to 0

$$\sum M = 0 \quad (35)$$

Description to draw shear force-, moment-, and  $\frac{M}{EI}$  diagrams for calculating deflection is listed below [9].

1. Shear Force Diagram: Calculate and plot the shear force at each section of the shaft using a free body diagram. The shear force diagram shows the variation of shear forces along the shaft.
2. Bending Moment Diagram: Calculate and plot the bending moment at each section of the shaft by summing the moments due to external forces. The bending moment diagram shows the variation of bending moments along the shaft.
3.  $\frac{M}{EI}$  Diagram: Divide the bending moment at each section of the shaft by the modulus of elasticity and moment of inertia at that section. Plot these ratios on the diagram. The  $\frac{M}{EI}$  diagram shows the variation of this ratio along the shaft, indicating the deflection.

The deflection curve is a graphical representation of the vertical displacement of a shaft under a load. The vertical axis represents the amount of displacement at each point along the shaft, while the horizontal axis represents the length of the shaft. The deflection curve is an exaggerated view of the actual elastic curve, which represents the shape of the shaft when it is subjected to a load. The deflection curve shows the maximum deflection of the shaft at the point of interest and the points at which the deflection is zero. The deflection is always zero at fixed supports.

The tangential deviation line  $V_a$  can be found by using second moment-area theorem which is the sum of all area sections in the  $\frac{M}{EI}$  diagram multiplied by the centroid of each section. The second moment-area theorem states that the area of the moment diagram is proportional to the curvature of the deflection curve.  $V_a$  can be found by using eq. 36 [39].

$$V_a = \sum A_i R_i \quad (36)$$

The centroid for a rectangle is at the center of rectangle, and the centroid for a triangle is  $\frac{1}{3}$  of a triangle measured from the smallest end, and  $\frac{2}{3}$  from the largest end.

The slope of the tangent line represents the angle  $\phi$  of rotation at that point, and can be found by using eq. 37 [39].

$$\phi = \frac{V_a}{L} \quad (37)$$

---

While the deflection is represented by the distance between the tangent line and the original position of the shaft, and can be found as the product of the angle and length at rotation point [39].

$$\delta = \phi L \tag{38}$$

Eq. 39 can be used to calculate the moment of inertia of a solid circular shaft with radius  $r$  [9].

$$I = \frac{1}{4}\pi r^4 \tag{39}$$

---

## 2.8 Bearings

Bearings are machine elements that enable linear and rotating movements inside machinery. They reduce friction between two moving parts, improve efficiency in systems and help to save energy. Bearings are often hidden inside machinery where they perform on a high level in tough environments. There are several different types of bearings such as ball and roller bearings, linear bearing and plain bearings [43].

### 2.8.1 Iglidur X plain bearings

Iglidur X plain bearings from Igus, which is a manufacturer of high-performance polymers for movement, are designed to be press-fit into housings with H7/h9 standard holes and has a inside tolerance of F10. Figure 15 shows this type of bearing. With no lubrication and maintenance work needed the service life is increased. These bearings possess exceptional properties, including high temperature resistance, high compressive strength and excellent chemical resistance. They can operate effectively within a temperature range of  $-100\text{ }^{\circ}\text{C}$  to  $+250\text{ }^{\circ}\text{C}$  and have a maximal recommended surface pressure of 150 MPa. For optimal performance, it is recommended to use a shaft with a surface finish of  $R_a = 0.6 - 0.8\text{ }\mu\text{m}$  [44].



**Figure 15:** Illustration of an Iglidur X plain bearing [44]



---

## 2.9 Key and keyway

A keyed joint is a method used to securely transmit rotational motion without slipping, such as between a shaft and a sprocket. This is achieved by machining a keyseat on the shaft, creating a slot for the key to be inserted, and a keyway on the hub. The two parts are then slid together axially, with the key fitting snugly into both keyways. Keys are a popular and inexpensive method for connecting machine elements, with standardized keys readily available for use. Making it a popular choice for many applications. Additionally, the use of a key eliminates the need for complicated alignment procedures during assembly, simplifying the process. Disassembly is also straight forward, requiring only the removal of the key from the keyway [45].

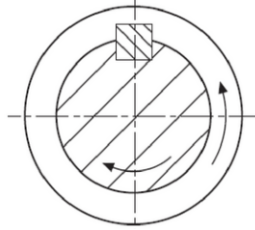


**Figure 16:** Illustration of a keyed joint [45]

A feather key according to Deutsches Institut für Normung (DIN) 6885 is a type of parallel sunk key that is commonly used in machinery for transmitting torque between rotating components. It has a rectangular shape with a half-circle or rounded shape at each end, see figure 17 for illustration. This rounded shape is designed to reduce stress concentrations at the corners of the keyway and to make it easier to install and remove the key. Feather keys are typically made of steel or other high-strength materials and come in a range of sizes to fit different shaft and hub diameters [46].

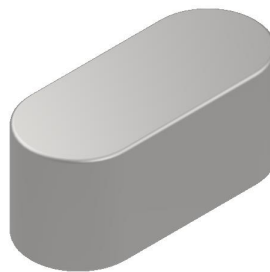


**Figure 17:** Feather key according to DIN 6885 made in Inventor

---

## 3 Methodology

The following section will describe the process by which information and data were collected to find and to design a solution that optimizes the rack and pinion system of Izomax's 2" 1500# AOGV. The issue Izomax faced were discussed, and detailed information was given before the start of this project. When a problem is to be clarified, there are various methodological approaches that can be employed. In this thesis, the Computer Aided Design (CAD) software for designing was Autodesk Inventor. Additionally, three design reviews were conducted to ensure that the new design would meet expectations. Relevant information for research were provided by Izomax and found in literature. Section 5 provides a detailed explanation and illustrations of all the designs that were created using the methods described in the methodology. In section 6 the various designs will be discussed.

### 3.1 Autodesk Inventor

The software used for designing the rack and pinion system was Autodesk Inventor. The University of Stavanger provides students with an educational license for their study period. The existing drawings of the AOGV were provided by Izomax. External components underwent a redesign and were then assembled into the housing. Websites such as SKF and Igus were used to download 3D part files of their bearings. The calculation tool for bolted connections was used to verify the calculations made by hand, with the understanding that there may be errors in the program. All the necessary specifications for performing the calculations, such as the material type, were located and entered into the settings of the Inventor program used for the calculations. The different designs that were made in Inventor are shown in section 5.

### 3.2 Design review

A design review is a process to evaluate and critique current design work and is often held in an early stage of a development process, this to allow changing the design if necessary [47]. A design review in this case was a technical meeting with individuals involved in the development process. Here the participants took a deeper look into technical content. These design reviews were found to be highly relevant in achieving a solution for the problem.

For each of the designs developed, a design review was completed. To minimize time wastage, meetings were arranged as soon as a new design was created. Under these meetings, the designs were presented, what resulted in constructive discussions.

The first design review was held on February 13. where design 1 was presented. This design was developed after receiving detailed information about the challenges Izomax faces. Interviewing engineers and mechanics and the own experience as former CNC-operator and industrial fitter helped to understand the problem and to kick off the project.

After the start of the project and the first design review conducted, the constructive feedback from the participants in those meetings led to the exploration and development of alternative solutions. This is why these design review were found to be highly relevant to the project.

From the beginning, requirements were to minimize potential leakage paths and to make the rack and pinion system more functional, but still to be robust and to be trusted. It was clearly defined that the dimensions of the housing should not be changed to avoid over-dimensioning the rack and pinion housing and to maintain the geometry of the AOGV. So the design of the housing was only

---

changed internally. External parts that should be fitted inside the housing underwent a thorough redesign.

The participants in the these design reviews had following job titles:

- Project manager, Izomax AS
- Project engineer, Izomax AS

### **3.3 Literature review**

A significant amount of time was spent on extensive literature search to investigate possible and alternative solutions to the current design, finding technologies and products that could be linked to the solution of the problem. The research was a precise and extensive process. The current design of the AOGV and the weaknesses of the rack and pinion system could be used as a reference point for exploring alternative and more effective solutions. Sealing of pressure vessels is a common practice in the industrial world. However, when dealing with high pressure systems like those in which the AOGV operates, the sealing process becomes more complex. It's crucial to conduct a accurate research on this topic to ensure the safety of such operations.

To gather relevant information and design recommendations of sealings, handbooks from Parker were used [38]. All changes and new designs had to be done according to the NS-EN 13345 Standard for unfired pressure vessels. Izomax provided the necessary standard, 3D models and analysis reports from Kiwa (a company specialized in providing inspection services for calculations to ensure they comply with established standards and laws) to achieve a solid result. The project also benefitted from the extensive experience of the project managers, project engineers, and mechanics.

---

## 4 A Comprehensive Review of the weaknesses in the Current Design

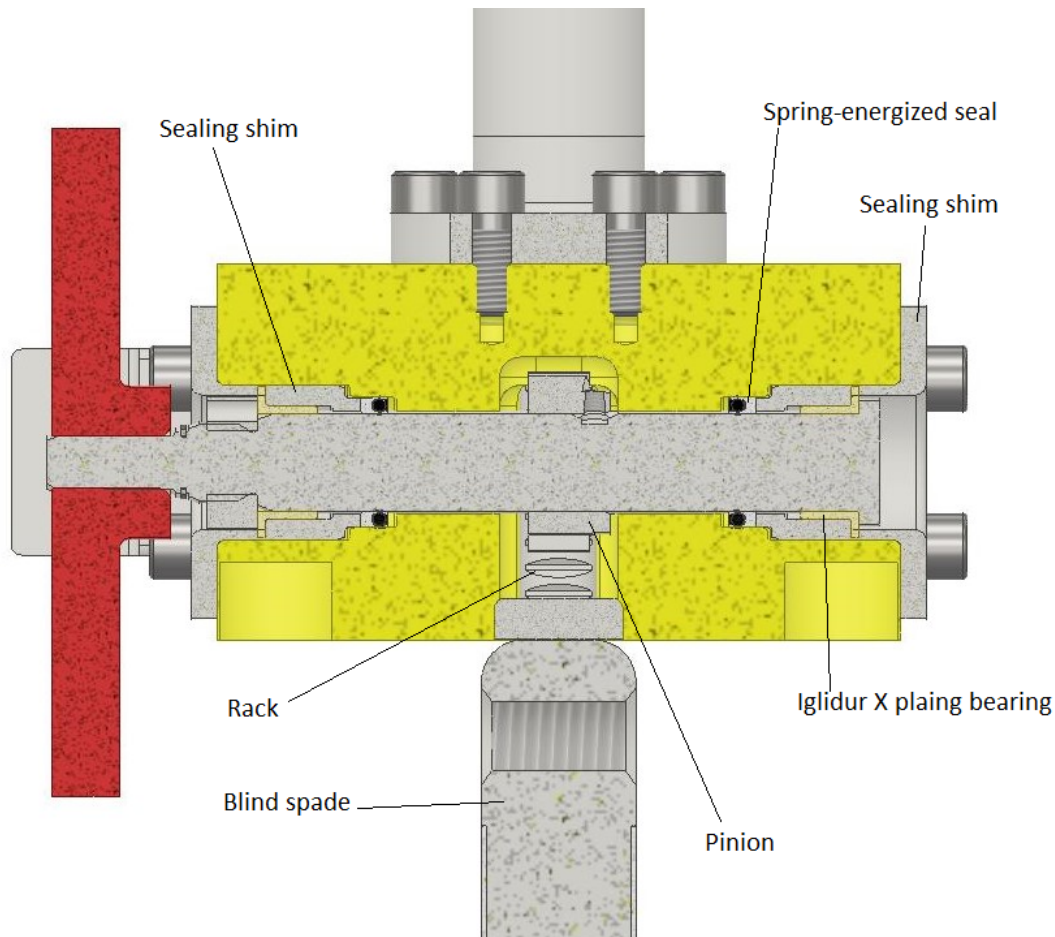


**Figure 18:** Illustration of the original design of the rack and pinion system designed by Izomax

The rack and pinion system was designed in-house by Izomax and verified by DNV. The concept features open ends on both sides of the housing, which expose the shaft to the environment. This allows for a balanced design that eliminates thrust forces on the shaft and considerably reduces the risk of shaft ejection. However, a notable disadvantage of this design is the additional leak passage it creates. A spring-energized seal like described in section 2.5.1 was selected as the sealing method to keep the system sealed. During testing and pressurization, challenges were identified with the sealing ability. It was difficult to keep the shaft leak-proof, and so a decision was made to replace the spring-energized seal with an elastomer as shown in figure 19. The elastomer was more effective at preventing leaks, but it created considerably more resistance when operated due to increased friction.



**Figure 19:** Sealing shim with elastomer, Photo by Izomax

The rack and pinion system had design challenges that were discovered later. The insufficient surface roughness has contributed to difficulties with sealing. In addition, the dimensions of the sealing shim and the shaft were identical, causing problems when the system was operated.

During an AOGV operation cycle, there was an incident where the blind spade became jammed inside the AOGV body, but the operators were unaware of this. The operators attempted to rotate the turning wheel in both directions several times, but were unable to avoid the position where the blind spade had become jammed. However, the resistance became too high for them to rotate the wheel, which led to using a torque wrench after calculations were done and material capabilities were identified from KIWA and Izomax's engineers. Unfortunately, this caused the shaft and the sealing shim to weld together due to friction, as shown in figure 20.



(a) Shaft



(b) Sealing shim

**Figure 20:** Welding damages on shaft and sealing shim, Photo by Izomax

---

It is hypothesized that the high torque applied on the wheel caused the shaft to slightly bend, which resulted in it rubbing against the sealing shim. To address this issue, Izomax increased the inside diameter of the sealing shim to 21 mm. As a result, similar incidents have not occurred since the redesign.

With the current design, it has shown to be challenging to identify the position of the blind spade while operating the rack and pinion system. During operation, this is done by counting the number of revolutions the turning wheel is turned, which can lead to high inaccuracies in identifying the current position of the blind spade. To address this issue, a disc with notches was designed to help with the counting process, which allowed for a higher degree of accuracy, as illustrated in Figure 21. However, this method is still not ideal as it is not completely accurate.



**Figure 21:** Disc with notches for counting revolutions, Photo by Izomax

The pinion is mounted on the shaft using set screws as constrain method. This method is taking all the forces acting on the pinion. This could be seen as a disadvantage as the set screws could break.

---

## 5 Results

The following chapter delivers all the results obtained in this thesis. The results for design 1 and 2 will be presented in a textual format, along with the corresponding 3D models that illustrate the solutions, as there were no calculations performed for these designs. Based on the current design and conducting 3 design reviews, design 3 was developed. This particular design include calculations for the various main components, which will be reflected in the final result. Technical drawings and extensive calculations will be given in the appendices attached to this document.

### 5.1 Design 1

The first design was intended to address Izomax’s requirements and solve existing challenges related to sealing. Also one potential leakage passage was eliminated from the current design. The concept aimed to provide an easy assembly and offer the option to adjust the sealing pressure. To achieve this, an open rack and pinion housing was designed, as illustrated in figure 22.

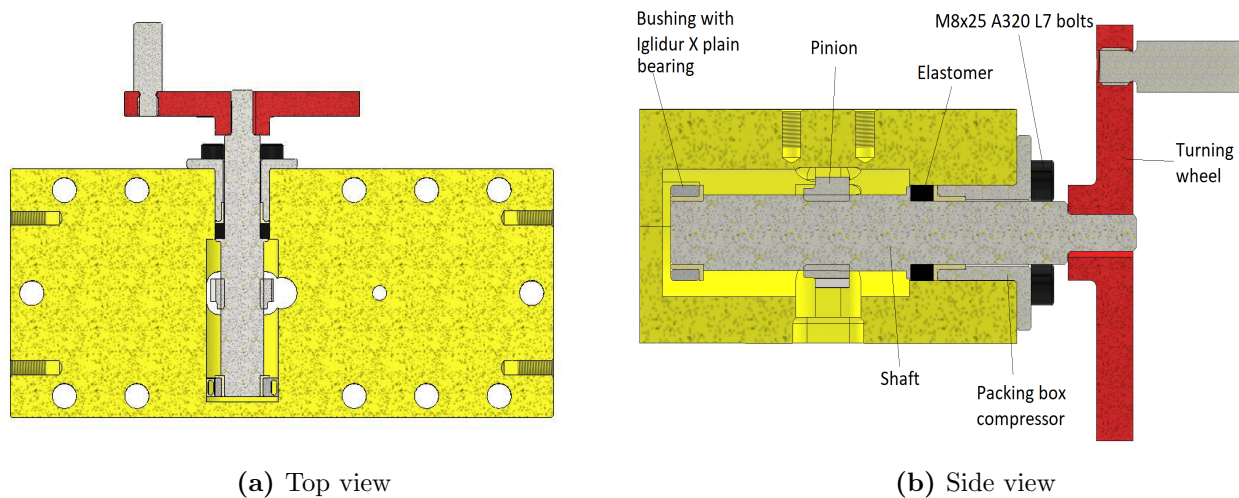


**Figure 22:** Illustration of design 1 made in Inventor

The most notable difference between the existing design and design 1 is the rack and pinion housing being split into two parts. This would allow personnel to assemble the shaft and its components, such as bearings, bushings, and seals, outside of the rack and pinion housing before installing the sealing shim, as illustrated in figure 23. To seal off the housing a graphite gasket was considered to be used over the whole surface of the splitted part. The outer geometry of the housing remained the same, but was splitted in two parts. The material of shaft, housing, turning wheel and pinion are the same as in the current design. The turning wheel was chosen to have the same design and mounting method as its predecessor. The bolts that are holding the packing box compressor in place are A320 L7 socket head cap bolts.

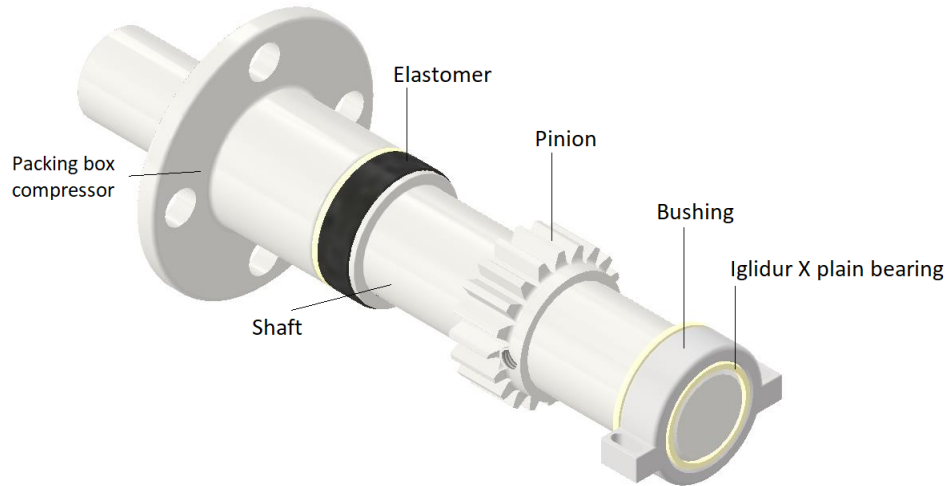


**Figure 23:** Shaft configuration made in Inventor

To achieve a sufficient sealing between the two parts a graphite gasket was considered. The desires from design review 1, which included an option for adjusting opportunities, were fulfilled by incorporating an adjustable bushing at one end, along with an Iglidur X plain bearing assembled to it, as illustrated in figure 24. By assembling the bushing with four bolts and setting it at a pre-calculated position, a higher degree of sealing ability could be achieved.

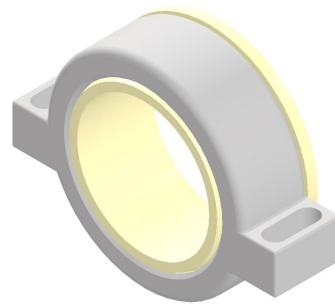


**Figure 24:** Assembly of bushing and Iglidur X plain bearing made in Inventor



---

## 5.2 Design 2

Design 2 was created with two roller bearings and a spring-energized seal. Additionally, a flange was designed to secure the single row tapered roller bearing and shaft in place, which both are of super duplex S32750, such as previous designs. To hold the pinion in place, splines were considered, but were not included in the 3D model due to time constraints and the ongoing development of the next design. The turning wheel and mounting method chosen for this design is identical to the current design. The geometry of the shaft became more complex in order to accommodate the single row tapered roller bearing and spring-energized seal in an appropriate way. While the outer housing geometry remained unchanged, the inner housing design of the housing was modified to accommodate the new shaft assembly with bearings and the spring energized seal. Figure 25 shows the assembly and the different components included.

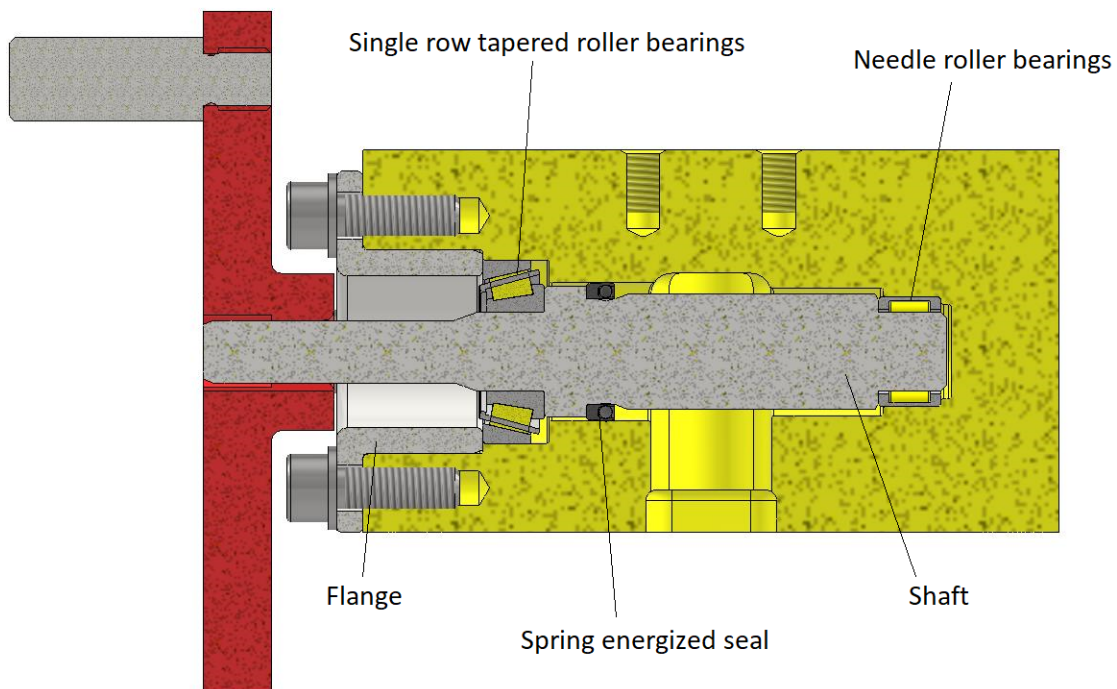


**Figure 25:** Half section view of design 2 with the different components made in Inventor

### 5.3 Design 3

After several design reviews and continuous development, the ultimate outcome is design 3, as represented in figure 26. This section showcases the results of an extensive and thorough design process, resulting in the final iteration. The complete implementation of this concept is presented, accompanied by the calculations and results that indicate the potential feasibility and efficacy of the design. This concept is designed fully, and the calculations with corresponding values will be shown here. Detailed calculations can be found in Appx. A, Appx. B, and Appx. C.

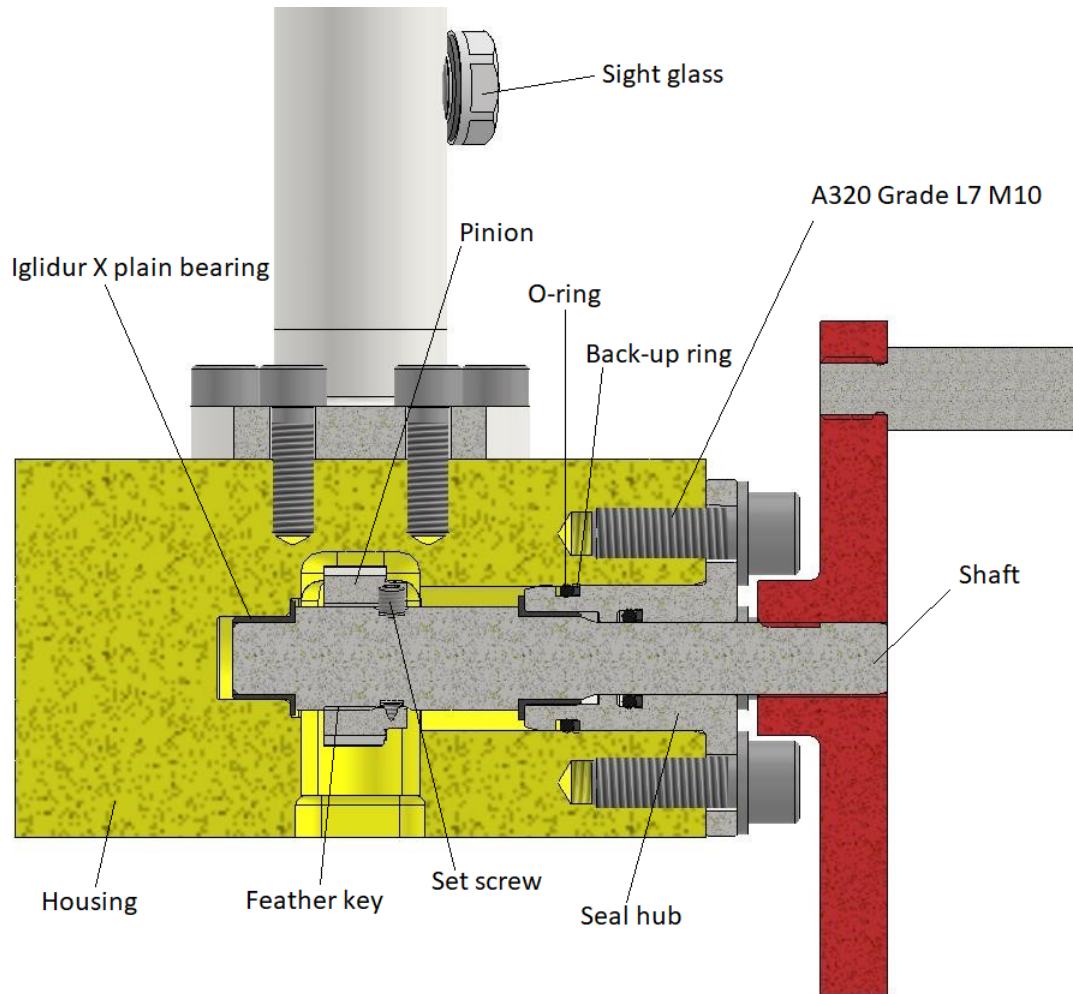


**Figure 26:** Half section view of design 3 with the different components made in Inventor

In figure 26, the different components of the design are illustrated. While the outer geometry of the housing remained unchanged, the inner part of the housing was redesigned to ensure that the new components would fit. There were no changes made to the material of the housing, which is P460 NL2 material for pressure purposes, refer to section 2.4.4 for more details. The bearings used were Iglidur X plain bearings XFM-1416-12 and XFM-1618-12, see Appx. F. To achieve optimal performance for these bearings, the material of the shaft was chosen to be Super Duplex S32750, referring to section 2.4.3 for more information on Super Duplex, with a surface finish of  $Ra\ 0.8\ \mu\text{m}$ . The surface pressure working on the flange of the bearing was found by dividing the thrust force by

the pressure area working on the flange of the bearing, the dimensions of the bearing flange can be found in Appx. F. The thrust force is calculated in Appx. B. With this value the surface pressure working on the flange was found to be:

$$P_{surface} = \frac{F_{thrust}}{A_{shaft} - A_{innerøigus}} = \frac{15271 N}{\frac{\pi \cdot 20^2 mm}{4} - \frac{\pi \cdot 16^2 mm}{4}} = 135 MPa$$

Additionally, a sight glass has been included in the rack housing to provide a constant indication of the position of the rack under operation. To eliminate potential slipping of the pinion, a feather key was added to the existing mounting with set screws. Additionally, a new seal hub was designed with glands for the O-rings and corresponding back-up rings. This seal hub is made of the same material as the shaft, super duplex S32750. The seal hub is illustrated in figure 28. The turning wheel was chosen to have the same design and mounting method as its predecessor. The following subsections will provide an overview of the results obtained for the main components.

### 5.3.1 Shaft calculations and design

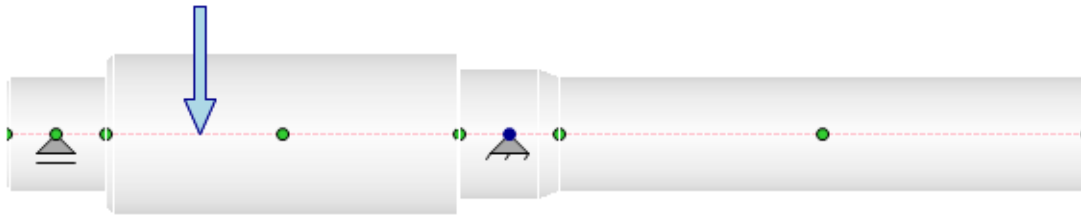


**Figure 27:** Free body diagram of shaft made in Inventor

The material selected for the shaft is Super Duplex. The analysis involved calculating the reaction forces, moments, and deflection of the shaft.

To determine the reaction forces, eqs. 34 and 35 were used. With a force of 100 N, this value is obtained by summing the mass of the rack, pinion, and the blind spade and multiplied by gravitational acceleration. The reaction forces were found to be:

- $R_a = 68.2 N$
- $R_b = 31.8 N$

Once the reaction forces were obtained, a shear force and moment diagram could be constructed. The diagrams can be found in Appx. A.

The moment diagram results were then used to plot the  $\frac{M}{EI}$  diagram. This involved pre-calculating the EI values for each section and determining the moment at the three sections. The moments were calculated by multiplying the forces in the shear force diagram by the corresponding distance x from the starting point to each action point. The calculated moments are as following (note that  $M_3$  is calculated from the opposite end for simplicity):

- $x = 6 mm, M_1 = 409.20 Nmm$
- $x = 23.5 mm, M_2 = 1602.23 Nmm$

- 
- $x = 61 \text{ mm}$ ,  $M_3 = 190 \text{ Nmm}$

Using the calculated values, the deflection of the shaft can be determined graphically using the moment-area theorem. The final result shows an upward deflection of  $2.91 \cdot 10^{-4} \text{ mm}$ . Extensive calculations are shown in Appx. A.

Furthermore, the tolerances and surface roughness for the bearings were considered. The tolerances for both bearings on the shaft were set to h9. This selection ensures proper alignment and fit between the shaft and the bearings. Additionally, the surface roughness at the seal hub section was specified as  $Ra \ 0.3 \mu\text{m}$ , providing a suitable surface finish for optimal performance and sealing. For a clearer visualization, please refer to the technical drawings provided in the Appx. E.



**Figure 28:** Mounted Iglidur X plain bearing in seal hub made in Inventor

---

### 5.3.2 Bolt calculations

The bolts chosen to fasten the seal hub were A320 Grade L7 socket head cap screws. These are manufactured to the metric size M10x1.5, refer to figure 29 for illustration. These bolts are specifically designed for bolting valves and flanges, making them a reliable choice. The calculations done for the bolts, verified that a appropriate size was selected by finding several safety factors. For extensive bolt calculations, including calculations performed using the Inventor calculation tool for bolted connections, please refer to Appx. B.



**Figure 29:** Illustration of A320 Grade L7 M10x1.5 bolt taken from Inventor

Using eq. 21, the von Mises stress was found to be:

$$\sigma_e = \sqrt{\sigma_{bolt}^2 + 3\tau_i^2} = \sqrt{578^2 \text{ MPa} + 3 \cdot 68^2 \text{ MPa}} = 590 \text{ MPa}$$

With the von Mises stress, the safety factor of yielding could be obtained:

$$n_{yielding} = \frac{R_{p0.2}}{\sigma_e} = \frac{725 \text{ MPa}}{589 \text{ MPa}} = 1.23$$

The yielding factor of safety using eq. 26 gave the result of:

$$n_p = \frac{725 \text{ MPa} \cdot 58 \text{ mm}^2}{0.52 \cdot \frac{15271 \text{ N}}{4} + 31538 \text{ N}} = 1.25$$

The load factor of safety was obtained by eq. 28:

$$n_L = \frac{725 \text{ MPa} \cdot 58 \text{ mm}^2 - 31538 \text{ N}}{0.52 \cdot \frac{15271 \text{ N}}{4}} = 5.30$$

Safety factor against joint separation was found from eq. 29:

---

$$n_0 = \frac{31538 \text{ N}}{\frac{15271 \text{ N}}{4} \cdot (1 - 0.52)} = 17.21$$

The result using the bolt load ratio from EN13445-3 standard was obtained by eq. 31 with the result:

$$\Phi_B = \frac{\frac{15271 \text{ N}}{4}}{\frac{\pi \cdot (10 \text{ mm} - \frac{3}{4} \cdot \sqrt{3} \cdot 1.5)^2}{4} \cdot 358.333 \text{ MPa}} \cdot \sqrt{1 + \left(\frac{4}{3} \cdot 3.2 \cdot 0.1\right)^2} = 0.23$$

---

### 5.3.3 O-rings and Back-up Rings

The selected O-rings for this design can be found in the Parker O-ring catalog. For static sealing, the chosen O-ring is identified by code 2-119, accompanied by the corresponding back-up ring with code 8-119. Conversely, for dynamic sealing, the designated O-ring is identified by code 2-113, paired with the corresponding back-up ring with code 8-113.

Both O-rings are made of HNBR material, refer to 2.4.8 for more information, with a hardness of shore A 70. As for the back-up ring, a scarf cut back-up ring made of PTFE was chosen for convenient installation, as it is split in the middle. For more details on O-rings and back-up rings, please refer to Appx. F. The relevant items are highlighted in red for easy identification.

The gland fill for static O-ring was determined using eq. 4:

$$\text{Gland fill} = \frac{5.39 \text{ mm}^2}{9.87 \text{ mm}^2 - 2.94 \text{ mm}^2} \cdot 100 \% = 78 \%$$

The compression was determined using eq. 8:

$$\text{Compression} = \frac{2.62 \text{ mm} - 2.1 \text{ mm}}{2.62 \text{ mm}} \cdot 100 \% = 20 \%$$

While for dynamic sealing, the gland fill and compression was calculated using eqs. 4 and 8 respectively.

$$\text{Gland fill} = \frac{5.39 \text{ mm}^2}{10.58 \text{ mm}^2 - 2.94 \text{ mm}^2} \cdot 100 \% = 70 \%$$

$$\text{Compression} = \frac{2.62 \text{ mm} - 2.25 \text{ mm}}{2.62 \text{ mm}} \cdot 100 \% = 14 \%$$

The dimensions can be found in Appx. F.

For static sealing, the recommended surface roughness is Ra  $0.4 \mu\text{m}$ , with an upper limit of  $0.8 \mu\text{m}$ , while the gland surface roughness is specified as Ra  $1.52 \mu\text{m}$ . For dynamic sealing, the recommended surface roughness for the sealing surface is Ra  $0.3 \mu\text{m}$ , as discussed in section 2.5.2. It is crucial to ensure that the surface roughness does not fall below  $0.15 \mu\text{m}$ .

The diametrical clearance gap is given by the tolerances on the shaft in the technical drawings in Appx. E. For extensive calculations, please refer to Appx. C.

---

## 6 Discussion

The following section will provide an in-depth discussion of the results of the different designs, including its issues and successful design parameters.

As discussed in section 2.2, designing or optimizing any parts of the AOGV requires careful consideration of several restrictions. To ensure compliance with industry standards, Izomax has based the design parameters on standard EN 13445 and had it validated by a notified body, DNV, for industrial use. By adhering to this standard, the new design meets the requirements for CE marking.

### 6.1 Design 1

The first design was intended to address Izomax's requirements and solve existing issues related to sealing. The concept aimed to provide easy assembly and offer the option to adjust the sealing pressure. To achieve this, an open rack and pinion housing is considered the most logical choice, which resolved some challenges with the original design but also introduced new ones. To save time, a decision was made based on appearance and experience as to whether an in-depth analysis of the design was appropriate. This decision took place in the first design review.

The most notable difference in this version is the rack and pinion housing being split into two parts. This will allow personnel to assemble the shaft and its components, such as bearings, bushings, and seals, outside the housing before installing the packing box compressor. For a visual representation, please refer to figure 23. This is intended to allow for a more precise assembly method. However, it introduces new complications due to sealing between the two splitted parts. The main issue is the uncertainty when applying a graphite gasket over a large surface area. There was concerns for uncontrolled gas leakage, which could damage the gasket itself or the housing due to high pressure. A possible way to address this is to determine the number of bolts required to achieve the highest contact pressure between the two divided parts evenly on the contact surface.

Izomax requested also a solution that would allow for an adjustable sealing system for the rack and pinion, giving mechanics the option to further increase the sealing ability in case of a leakage. The chosen solution involves an adjustable bushing at one end with a plain bearing assembled to it, please refer to figure 24 for illustration. This would give additional control of the contact pressure applied to the elastomer, which was the best-suited sealing solution for this purpose. By assembling the bushing with four bolts and setting it at a desired position, a higher degree of sealing ability could be achieved. When the packing box compressor is assembled in the rack and pinion housing, it would apply pressure to the elastomer and extruding it. Depending on the distance between the packing box compressor and the bushing, the extrusion of the elastomer would determine the sealing ability. However, higher pressure on the elastomer would eventually lead to greater friction.



---

Initially, the concept idea seemed promising as it addressed some of the current issues, such as providing an option to increase sealing ability in the field. However, after a design review with Izomax, it was decided that this design was not suitable for further development and in-depth analysis. The decision was based on the potential for uncontrolled leakage in the area between the divided parts. To improve the design, the housing should not be split to allow for better control of the leakage path and to reduce the risk of gas leaks.

## 6.2 Design 2

After the first design review and a feedback from Izomax, design 2 was created. This design went back to the one part housing system. The main characteristics in this design are the new roller bearings and the closure of one side, that eliminates one potential leakage path. This design is created with two roller bearings to improve the operation and make it easier to use by reducing friction, please refer to figure 25 for an illustration of the design. Tapered roller bearings are highly suitable for supporting combined loads, which is not especially necessary in this case, due to small radial force. Nevertheless this type of bearing is chosen considering that higher axial load would make the bearing and the shaft sit more secured. The needle roller bearing is chosen because of its relatively high axial load capacity and its small size. The spring-energized seal is used to seal off the system. With a designated place to fit the seal, its sealing ability is obtained on the condition that the shaft surface finish is in the recommended range for the seal.

This design was viewed as a feasible solution to the current issues, given its convenient and easy operation with reduced friction. However, there are some issues to consider, such as the need for high precision during assembly of the single row tapered roller bearing. Additionally, the bearing sizes are quite large, which could result in a robust but oversized system. Further research is needed to find an optimal solution for using roller bearings. Regarding the spring-energized seal it is worth noting that Izomax is hesitant about using it due to the difficulty of proper sealing.

Nevertheless, this design was considered not suitable for further development and in-depth analysis.

---

### 6.3 Design 3

After conducting 2 design reviews, design 3 was created, as illustrated in figure 26. This design was intended to address Izomax's initial requirements and weaknesses in design 1 and 2. This solution aims to achieve a proper sealing, eliminating potential leakage paths, easy assembly, more convenient and a reliable mounting of the pinion.

Like design 1 and 2, the outer geometry of the housing wasn't changed in this design, due to the limitations given by Izomax, as it must fit the existing tool. The main difference in this design compared to the current one is the closure from one side of the housing, which eliminates one potential leakage path but increases the force that the bolts have to bear, as the system is no longer balanced. The force of 15 271 N is calculated with the test pressure of 248 bar and the area of the seal hub that is mounted inside the housing.

Initially, the current M8 bolts were used to determine if they were capable of bearing the force in an unbalanced system. The calculations that are not included here, showed that the strength of the bolts was exceeded and therefore the choice was made to use M10x1.5 bolts.

From section 5.3.2, the bolts used to mount the seal hub are A320 grade L7 socket head cap screws, which are manufactured in the metric size of M10x1.5. These bolts are used due to their high mechanical properties and the common use for flanges, valves, fittings and pressure vessels. Corresponding hardened washers are selected to evenly distribute the load and to prevent the bolt from getting damages. The calculations done to verify the right choice of bolts is made in two ways. One is the approach where the stiffness of the fastener and member is considered. Shigley's frustum method is used like described in section 2.6, to find the stiffness of the clamped components. This method predicts the pressure distribution throughout the thickness of the grip, please refer to figure B1 for the dimensions found for this connection. The primary dimensions of the fastener, which are obtained from the results, is a standard procedure for determining the correct lengths of the fastener. Once the fastener length has been determined, ISO's adopted Renard series can be used to select a standard length that will minimize both cost and time. Since the unthreaded area of the bolt is small, it is assumed that the bolt is threaded throughout its entire length. This assumption does not significantly impact the calculations and yields reliable results.

The result for the stiffness constant of the joint  $C$  is the percent of the load that will be carried by the bolt. So here the parameter indicates 0.52, as calculated in Appx. B, which means that approximately half of the external tensile load is carried by the bolt and the other half is carried by the members. With this constant the safety factors of statically loaded tension joints with preload are determined. To ensure that the bolts can be reused, the recommended preload for non permanent connections is 75 % of the proof load.

With the parameters found in the results, the safety factors are determined. With a yielding factor of safety of 1.25, it is verified that the force working on the bolts will not permanently deform them. Because it is common to load a bolt close to its proof strength, the factor of safety against yielding is often not much greater than 1, as seen in this case. The load factor of bolts indicate the amount of load that a bolt can safely withstand without exceeding the proof strength. This means that the result of 5.30 from section 5 can be interpreted in the way that the load could be 5.30 times higher than it is now without causing any permanent elongation of the fastener. The last safety factor found is the safety factor against joint separation, which resulted in a high value of 17.21, indicating that there will be no separation. The stress in the bolts will reach their proof strength before the members start separating. Calculations to determine the thickness of the flange in the

---

seal hub were not conducted due to time constraints. Instead, the thickness was chosen based on the dimensions of the current system. However, further investigation is recommended, as these dimensions were originally designed for a balanced system. This might influence the calculations for the stiffness of the members, what would result in a different joint constant.

The second approach is using von Mises stress for combining tensile stress with shear stress that occurs from preloading the bolts. The von Mises stress is calculated to be 590 MPa which is less than the yield strength of the bolt with 725 MPa, as shown in Appx. B. This means that the bolt has not reached the plastic range and gives a yielding factor of safety of 1.23, which is close to the result using the first approach.

Izomax is required to use the EN 13445-3 standard to design its AOGV, which includes a bolt load ratio to determine bolt utilization in hubs. From the result the calculated bolt load ratio is 0.23, which means that the bolts are underutilized, as a normal ratio should be between 0.3 and 1. Despite this, the result confirms that the bolts are capable of withstanding the applied force.

During normal operation conditions, the rack and pinion system is calculated assuming no external resistance on the blind spade as it travels inside the AOGV body. The blind spade has a mass of 8.9 kg, while the rack and pinion are estimated to be approximately 0.4 kg and 0.1 kg, respectively. A load of 100 N is therefore used in this calculation.

The material chosen is Super Duplex, please refer to section 2.4.3 for more details. This is also the same material as the shaft from the original design. There is no reason to change the material as it is exceptional against corrosion in harsh environment and has high strength.

Since there was an incident regarding deflection where the shaft rubbed against the sealing hub in the original design, a thorough analysis is conducted to determine how much load can be exerted on the shaft. The factor that influences the allowable deflection is the small gap between the shaft and sealing hub, as indicated by the H9/f7 tolerances. Please refer to the technical drawings in Appx. E for a visual representation. However, there are many other factors that can affect the maximum allowable deflection, including the sealing ability as the O-ring surface rubs against the shaft. According to Parker's handbook, the maximum clearance gap radially is given as 25.4  $\mu\text{m}$ , which is also the worst-case scenario. However, the clearance given by the tolerances on the shaft and sealing hub is much smaller and will therefore not be an issue.

When calculating the shaft displacement, the results indicate a deflection of 2.91  $\mu\text{m}$  in the upward radial direction. Given the complexity and potential for error in manually calculating deflection for shafts of varying sizes, the iteration of different forces was not included in this analysis. Instead, the shaft analysis tool in Autodesk Inventor was utilized to perform the calculations. The results obtained from the software were then compared to the calculations presented in section 5.3.1 and further details can be found in Appx. A. It should be noted that the values derived from Autodesk Inventor, as detailed in Appx. D, were utilized to reach conclusions. Furthermore, other factors, such as the off-center concentricity of the shaft, were also taken into consideration, as discussed in section 2.5.2.

---

Initially, the shaft had 14 mm in cross-section diameter from the end exposed to the environment to the section where the pinion is mounted, which is also known as the sealing surface. This is thought as a possible issue for machining the shaft as it has no physical boundaries that divides the various tolerances on the shaft. To address the diverse tolerances on the shaft, a new bearing with an inner diameter of 16 mm is chosen. This allows for physically separated sections on the shaft and would probably be more convenient for the machinist when machining the tolerances. This may cause stress concentration on the transition between the two sections. To address this, a chamfer is implemented to smoothen out the sections.

The shaft features a h9 fitting tolerance for the bearing, enabling smooth rotation of the components. In contrast, the housing tolerance is H7. The selected bearing is an Iglidur X plain bearing with an inner diameter of 16 mm in the sealing hub and 14 mm on the blended side. These plain bearings exhibit excellent resistance to hydrocarbons, making them well-suited for applications in the oil and gas industry. To optimize their performance, the shaft's surface finish is chosen to be  $0.8 \mu\text{m}$ . Given their exceptional properties, the bearings remain unchanged from the current design.

In this configuration, the shaft exerts pressure on the flange of the Igus bearing. It is important to consider potential issues if the pressure exceeds the bearing's maximum surface pressure. The manufacturer's recommended surface pressure, provided in Appx. F, is 150 MPa. In this case, the calculated result indicates a slightly lower pressure of 135 MPa. Based on this, it can be concluded that the bearing is expected to withstand the applied pressure.

The seal hub plays a crucial role in the rack and pinion system as it securely holds the shaft in place and contains grooves for both static and dynamic sealing. Initially, the design included two O-rings in series for sealing, resulting in four grooves. However, during the design review, concerns arose regarding the potential difficulty caused by trapped gas acting as a vacuum and exerting pressure. To address this, the decision was made to remove the O-ring that was farthest from the pressure source to minimize this risk.

The glands in the sealing hub are essential for the sealing ability and are given dimensions according to Parker's handbook for both static piston sealing and dynamic rod sealing. The inside corner radius of the gland is set to be R 0.3 mm, which is recommended for O-rings. Rotary applications are not considered due to the small shaft speed (less than 1 m/s), making it easier to determine the correct dynamic sealing.

The chosen sealing method for this design are O-rings, which offer a cost-effective solution and provide excellent sealing performance, particularly in static applications. While not recommended for high-speed rotary seals, but can be assumed to be reciprocating if the shaft speed is 1 m/s or less. Thus, O-rings with back-up rings were selected for both static and dynamic sealing methods. To ensure accuracy, an O-ring calculator is used to verify the chosen O-ring and serves as an additional verification, it also prevents potential mistakes. The results are available in Appx. C. The calculated values displayed in Appx. C are used as input for the calculator, and the dimensions of the parts are presented in Appx. F.

In terms of static sealing, the initial plan was to position it in the rack and pinion housing. However, for convenience, it was later relocated to the seal hub. This adjustment allowed for the direct mounting of components on the seal hub, resulting in a more practical and robust component.

---

The material chosen for the O-rings is HNBR, which is commonly used for sealing natural gases, as discussed in section 2.5.2. A lower shore A hardness values lead to lower friction but has the potential to wear out faster, hardness between shore A 70 and A 80 is recommended, with A 70 being chosen for this application. When selecting the hardness of the O-ring, a trade-off between wear resistance, sealing ability, and friction had to be considered. This trade-off is considered fair as the price for O-rings is among the cheapest sealing method in the market, and can be easily replaced. To facilitate installation, a spliced PTFE back-up ring was chosen. PTFE is suitable for natural gases as well, and is a natural choice when selecting a material for the back-up ring.

One reason for the sealing challenges in the original design was an error in specifying the correct surface roughness. In this design, addressing this challenge and ensuring the optimal sealing performance is crucial. The surface roughness Ra in this design is determined based on guidelines provided by Parker's handbook, and will be discussed later in this section.

For the static sealing, an O-ring with code 2-119 from Parker was selected, along with corresponding back-up rings with code 8-119, these components can be obtained in Appx. F for static piston sealing. Calculations were conducted to ensure the correct gland fill and stretch were applied in the design, and the results showed that a gland fill of 78 % was appropriate, along with positive results for stretching and cross-section reduction. The compression of the O-ring cross-section is calculated to be 20 %, as calculated in Appx. C, but the actual compression may vary due to tolerance differences in the machined part. The surface roughness for the sealing surface is given according to Parker's guidelines to be Ra 0.4  $\mu m$  and gland surface roughness of Ra 1.6  $\mu m$ . It is important to avoid going below Ra 0.15  $\mu m$  to ensure sufficient surface for the lubricant to adhere to.

As for dynamic sealing, an O-ring with code 2-113 from Parker was selected, along with corresponding back-up rings with code 8-113, these components can be found in Appx. F for dynamic rod sealing. Same reasons as for static sealing, calculations are provided to indicate whether the dimensions corresponds to the guideline. The compression in cross-section area of 14 % is within the recommended range, which satisfy the criteria for proper sealing, as well does the gland fill, and reduction in cross-section area, 70 % and 0.81 % respectively also satisfying the criteria. For the surface roughness for dynamic applications the recommended sealing surface is Ra 0.3  $\mu m$ .

The obtained results appear to meet all the specified criteria. To enhance confidence in the sealing performance, an O-ring calculator was utilized to verify the calculated data, as shown in Appx. C [48]. However, it is important to note that the effectiveness of the sealing heavily relies on the quality of the components. Therefore, it is crucial to conduct pressure testing to ensure that the selected values indeed provide proper sealing.

---

The current method of mounting the pinion is with set screws and is not a reliable method, as the torque from the pinion will act only on the set screw. In design 3, the pinion from the current design is used, and is made of stainless steel. The design 3 provides an additional mounting method to secure the pinion. A standard feather key is therefore applied to secure the rotational motion without slipping and releasing the set screws from the rotational motion. This will secure the pinion from moving axial. Although splines provide longer fatigue life and can carry greater torques, the use of a feather key in this low torque system provides a reliable and cost-effective solution. Adding an adjustable solution for the pinion to provide the correct impact and increasing efficiency is a feature that would enhance the use of the system, but more research and designing would be necessary to determine the most suitable method for incorporating this feature into the system.

To determine the position of the rack with the blind spade, Izomax currently uses a turning wheel with notches, as illustrated in figure 21. However, this method is prone to inaccuracies as it relies on counting the number of revolutions of the wheel. A more reliable solution would be to add a sight glass onto the rack housing. This solution provides an indication of how to resolve the issue of a blind operation. With this type of sight glass, which can withstand great pressure, the position of the rack can always be observed, making it easier to locate its exact position during operation. However, due to insufficient research on the sight glass, this design still uses the turning wheel with notches from Izomax.

---

## 7 Conclusion

This thesis aimed to examine the existing rack and pinion system and explore other methods for enhancement. Three designs were created where design 3 fulfills the criteria for the aim of this thesis and is considered the best solution.

This design closes one side and eliminates one potential leakage path effectively. The design is robust and the original spring-energized seals are replaced by O-rings with corresponding back-up rings to withstand the high pressure in which the AOGV operates. Due to challenges with using the spring-energized seals in the current solution, the O-rings were considered as the most reliable method. Research and calculations can be viewed as sufficient for the use of O-rings in this system. The seal hub is designed to be robust and to provide space for the sealing for static applications. However, to ensure the seal hub is compliant with the EN 13445-3 standard, more research has to be done to identify the required thickness of the flange of the seal hub. This design is developed for the 2" 1500# AOGV and can in the first place only be used for this type.

This design is found to be the most sufficient in terms of being robust, functional and reliable. This design is created as an improvement to the original system and can be considered as a suggestion to Izomax. However, to validate the effectiveness and reliability of the design, it is imperative to conduct testing.

In future work, an universal external system that can fit on any AOGV could be of interest. Designing and calculating of larger components are necessary to make the system work for any sizes of the AOGV.

---

## References

- [1] IK-Group, *AOGV - Maintenance Without Cashflow Shutdown*, en-US. [Online]. Available: <https://products.ik-worldwide.com/products/isolation/aogv/> (visited on 10th Jan. 2023).
- [2] K. O. Rosén, K. Aamodt and K. Mikkelsen, ‘AOGV: New Method for Process Isolation’, Apr. 2018, D011S007R005. DOI: 10.4043/28648-MS. [Online]. Available: <https://doi.org/10.4043/28648-MS> (visited on 19th Dec. 2022).
- [3] IK-Group, *AOGV - Mechanical Isolation Tool*, en-US. [Online]. Available: <https://www.ik-worldwide.com/assets/Uploads/AOGV-Brochure-v2.pdf> (visited on 19th Jan. 2023).
- [4] ‘Unfired Pressure Vessels’, Standard EN 13445, 2021.
- [5] *Pressure equipment Directive 2014/68/EU*, 2014.
- [6] W. Sölken, *Flanges General - Pressure-temperature ratings ASTM and ASME*, 2008. [Online]. Available: [https://www.wermac.org/flanges/flanges\\_pressure-temperature-ratings\\_astm\\_asme.html](https://www.wermac.org/flanges/flanges_pressure-temperature-ratings_astm_asme.html) (visited on 31st Jan. 2023).
- [7] R. G. Budynas, J. K. Nisbett and J. E. Shigley, *Shigley’s mechanical engineering design*, eng, Eleventh edition in SI units. New York, NY: McGraw-Hill, 2021, OCLC: 1243337805, ISBN: 9789813158986.
- [8] *What Are The Teeth On A Gear Called*. [Online]. Available: <https://teethwalls.blogspot.com/2018/10/what-are-teeth-on-gear-called.html> (visited on 14th Apr. 2023).
- [9] R. C. Hibbeler, *Mechanics of materials*, eng, Tenth edition in SI units, global edition. Harlow: Pearson, 2018, ISBN: 9781292178202.
- [10] W. D. Jr. Callister and D. G. Rethwisch, *Materials Science and Engineering*, eng, 9th Edition, SI Version. John Wiley & Sons Inc, 2014, ISBN: 9781118319222.
- [11] philipfigari, *Steps to Analyzing a Material’s Properties From Its Stress/Strain Curve*, en. [Online]. Available: <https://www.instructables.com/Steps-to-Analyzing-a-Materials-Properties-from-its/> (visited on 20th Feb. 2023).
- [12] G. Formfedern, *Stress-strain diagram spring steel > Gutekunst Formfedern GmbH*, en-US, Dec. 2021. [Online]. Available: <https://info.formfedern.com/en/stress-strain-diagram-spring-steel/> (visited on 21st Feb. 2023).
- [13] Aperam, *What is Stainless Steel?*, en-US. [Online]. Available: <https://www.aperam.com/stainless/what-is-stainless-steel/> (visited on 6th Feb. 2023).
- [14] S. Steel, *EN 1.4410 / SUPER DUPLEX UNS S32750 / F53 / 2507*. [Online]. Available: <https://www.sverdrupsteel.com/products/duplex-super-duplex/alloy-1-4410-super-duplex-uns-s32750-f53-2507> (visited on 30th Jan. 2023).
- [15] E. Britannica, *Stainless steel*, en, Sep. 2022. [Online]. Available: <https://www.britannica.com/technology/stainless-steel> (visited on 6th Feb. 2023).
- [16] Gpi, *Stainless steel tanks pressure vessels EN 13445*, en-US. [Online]. Available: <https://gpi-tanks.com/stainless-steel-tanks/pressure-vessels-en-13445/> (visited on 14th Apr. 2023).
- [17] Astwood, *EN 10028 — P355 — NH — NL1 — NL2 — Supplier*, en-US, Oct. 2016. [Online]. Available: <https://masteel.co.uk/en-10028-p355-nhnl1nl2/> (visited on 14th Apr. 2023).
- [18] Astwood, *EN 10028 — P460 — NH — NL1 — NL2 — Supplier*, en-US, Oct. 2016. [Online]. Available: <https://masteel.co.uk/en-10028-p460-nhnl1nl2/> (visited on 14th Apr. 2023).



- 
- [19] S. Steel, *AISI 4140 MODIFIED / UNS G41400*, en-US. [Online]. Available: <https://www.sverdrupsteel.com/products/low-alloys/aisi-4140-modified-uns-g41400> (visited on 2nd Feb. 2023).
- [20] Robin, *Handbook: Everything You Should Know About 4140 Steel*, en-US, Jun. 2020. [Online]. Available: <https://www.rocheindustry.com/4140-steel/> (visited on 14th Apr. 2023).
- [21] BPF, *ASTM A320 Grade L7 Mechanical Properties - Boltport Fasteners*. [Online]. Available: <https://a320gradel7.com/mechanical-properties/> (visited on 14th Apr. 2023).
- [22] A. Group, *Best ASTM A320 Grade L7 Bolts Manufacturer in India - Ananka Group*, en-US, Jan. 2022. [Online]. Available: <https://hightensilenutbolts.com/astm-a320-grade-l7-bolts-manufacturer-india/> (visited on 14th Apr. 2023).
- [23] BPF, *ASTM A320 Grade L7 Socket Head Cap Screws - Boltport Fasteners*, 2020. [Online]. Available: <https://a320gradel7.com/socket-head-cap-screws/> (visited on 17th Apr. 2023).
- [24] A. Materials, *Structural Steel - S235, S275, S355 Chemical Composition, Mechanical Properties and Common Applications*, en, May 2012. [Online]. Available: <https://www.azom.com/article.aspx?ArticleID=6022> (visited on 7th Feb. 2023).
- [25] masteel, *Construction Steels — Steel Plate — Construction Industry*, en-US, Oct. 2019. [Online]. Available: <https://masteel.co.uk/construction-steels/> (visited on 7th Feb. 2023).
- [26] A. N. Gent, *Elastomer — chemical compound — Britannica*, en. [Online]. Available: <https://www.britannica.com/science/elastomer> (visited on 19th Apr. 2023).
- [27] N. Duckmanton, *What is Shore Hardness? How is Rubber Hardness measured?*, en-GB, Nov. 2019. [Online]. Available: <https://www.j-flex.com/how-is-rubber-hardness-measured-what-does-shore-hardness-mean/> (visited on 19th Apr. 2023).
- [28] Omnexus, *PTFE (Polytetrafluoroethylene) - Uses, Structure & Material Properties*, en, 2023. [Online]. Available: <https://omnexus.specialchem.com/selection-guide/polytetrafluoroethylene-ptfe-fluoropolymer> (visited on 19th Apr. 2023).
- [29] S. Elder, *The Basics of Surface Finish — GD&T Basics*, Jan. 2021. [Online]. Available: <https://www.gdandtbasics.com/basics-of-surface-finish/> (visited on 24th Feb. 2023).
- [30] *Rubber Seal Materials: Which One is Best for Your Parts? - Blog — Rubber Articles — Timco Rubber*. [Online]. Available: <https://www.timcorubber.com/blog/archive/rubber-seal-materials-which-one-is-best-for-your-parts/> (visited on 3rd Feb. 2023).
- [31] B. Figliulo, *Matching Seals to Dynamic Sealing Applications*. [Online]. Available: <https://www.powermotiontech.com/technologies/seals/article/21887824/matching-seals-to-dynamic-sealing-applications> (visited on 31st Jan. 2023).
- [32] *Dynamic Seals Information*. [Online]. Available: [https://www.globalspec.com/learnmore/mechanical\\_components/seals/dynamic\\_seals](https://www.globalspec.com/learnmore/mechanical_components/seals/dynamic_seals) (visited on 3rd Feb. 2023).
- [33] *High-performance — Spring-energised seals — James Walker*, en. [Online]. Available: <https://www.jameswalker.biz/our-solutions/our-products/engineered-thermoplastics/spring-energised-seals> (visited on 3rd Apr. 2023).
- [34] *Spring-Energized Seals — Bal Seal®*, en-US. [Online]. Available: <http://https%253A%252F%252Fwww.balseal.com%252Fseal%252F> (visited on 3rd Apr. 2023).
- [35] M. W. Brown, *Seals and sealing handbook*, 4th ed. Oxford, UK: Elsevier Advanced Technology, 1995, ISBN: 9781856172325.
-

- 
- [36] W. Huang, G. Feng, H.-L. He, J.-Z. Chen, J.-Q. Wang and Z. Zhao, ‘Development of an ultra-high-pressure rotary combined dynamic seal and experimental study on its sealing performance in deep energy mining conditions’, *Petroleum Science*, vol. 19, no. 3, pp. 1305–1321, Jun. 2022, ISSN: 1995-8226. DOI: 10.1016/j.petsci.2021.11.020. [Online]. Available: <https://www.sciencedirect.com/science/article/pii/S1995822621001540>.
- [37] ttv, ‘O- and X-rings – technical information’, Tech. Rep., May 2015. [Online]. Available: [https://www.ttv-gmbh.de/pdf/Downloads/Technische\\_Infos/ttv-Technische-Infos-O-und-X-Ringe.pdf](https://www.ttv-gmbh.de/pdf/Downloads/Technische_Infos/ttv-Technische-Infos-O-und-X-Ringe.pdf).
- [38] Parker, ‘Parker O-Ring Handbook ORD 5700’, Cleveland, Ohio, Tech. Rep., 2021. [Online]. Available: <https://www.parker.com/content/dam/Parker-com/Literature/O-Ring-Division-Literature/O-RingKitsFactSheet.pdf>.
- [39] H. G. Lemu, ‘Dimensjonering av maskinelementer’, Tech. Rep., Jan. 2020.
- [40] S. J. Temitope, ‘Condition Monitoring of bolted Joints’, Tech. Rep., Jun. 2015. [Online]. Available: <https://core.ac.uk/download/pdf/30268741.pdf>.
- [41] *Guideline for Bolted Joint Design & Analysis — Engineering Library*, 2008. [Online]. Available: <https://engineeringlibrary.org/reference/bolted-joint-design-analysis-sandia> (visited on 12th May 2023).
- [42] J. Sabhadiya, *Shafts: Definition, Types, And Application*, en-us, Oct. 2020. [Online]. Available: <https://www.engineeringchoice.com/what-is-mechanical-shaft/> (visited on 14th Apr. 2023).
- [43] NSK, *Introduction to Bearings — Basic Knowledge — Services — NSK Global*, 2022. [Online]. Available: <https://www.nsk.com/services/basicknowledge/introduction/> (visited on 14th Feb. 2023).
- [44] Igus, ‘Iglidur® X catalogue PDF cylindrical bearing with flange, mm’, Tech. Rep., 2022. [Online]. Available: [https://igus.widen.net/content/zwanhycyj4/original/03\\_EU\\_GL11\\_igl\\_03\\_temperature\\_RZ\\_screen.pdf?download=true](https://igus.widen.net/content/zwanhycyj4/original/03_EU_GL11_igl_03_temperature_RZ_screen.pdf?download=true).
- [45] *Shaft key & keyway — Key types — Keyed Joint application & benefits*, en-US. [Online]. Available: <https://engineeringproductdesign.com/knowledge-base/keys-keyways/> (visited on 15th Apr. 2023).
- [46] B. Shakya, *Feather Key And Woodruff Key - MechoMotive*, en-US, Jan. 2021. [Online]. Available: <https://mechomotive.com/feather-key-and-woodruff-key/> (visited on 15th Apr. 2023).
- [47] M. Campbell, *Collaborative Engineering 101: Types of Design Reviews*, en, May 2021. [Online]. Available: <https://www.colabsoftware.com/post/collaborative-engineering-101-design-review-types> (visited on 11th Apr. 2023).
- [48] *ERIKS O-Ring Calculator*. [Online]. Available: <https://oringcalculator.eriksgroup.com/#> (visited on 9th May 2023).

---

## Appendix

### A Shaft Calculations

This Appendix provides detailed calculations and diagrams related to the shaft calculations in section 5.3.1. It includes the determination of forces exerted by the pinion, reaction forces on the bearings, shear force and moment diagrams,  $\frac{M}{EI}$  diagram, and the calculation of the tangential deviation and length  $\delta_D$ .

To simplify the analysis, it was assumed that the pin connection is located at the center of the bearings, and the applied force on the shaft by the pinion is denoted as  $F$ , which is set to 100 N in this case.

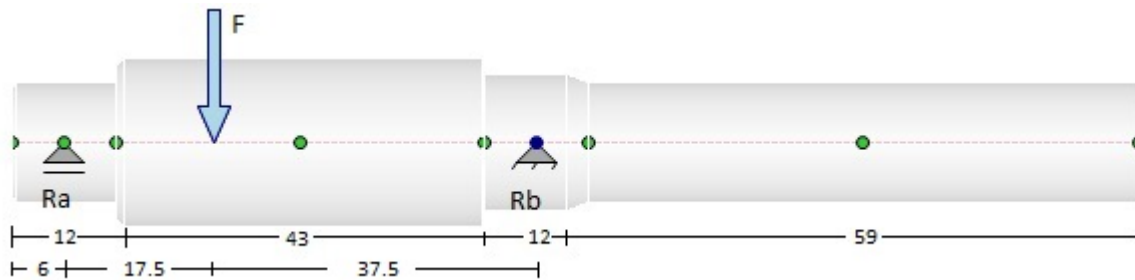


**Figure A1:** Free body diagram of the shaft with corresponding lengths made in Inventor

The Appendix begins with a free body diagram of the shaft with the corresponding lengths, as shown in the figure above. From this diagram, the following eqs. 34 and 35 can be used:

$$\sum F = 0 = R_a - 100 N + R_b$$

$$\sum M_a = 0 = 100 N \cdot 17.5 \text{ mm} - R_b \cdot 55 \text{ mm}$$

By solving these equations algebraically, the reaction forces are determined as follows:

- $R_a = 68.2 N$
- $R_b = 31.8 N$

The reaction forces serve as the basis for plotting the corresponding shear force and moment diagrams, as illustrated below.

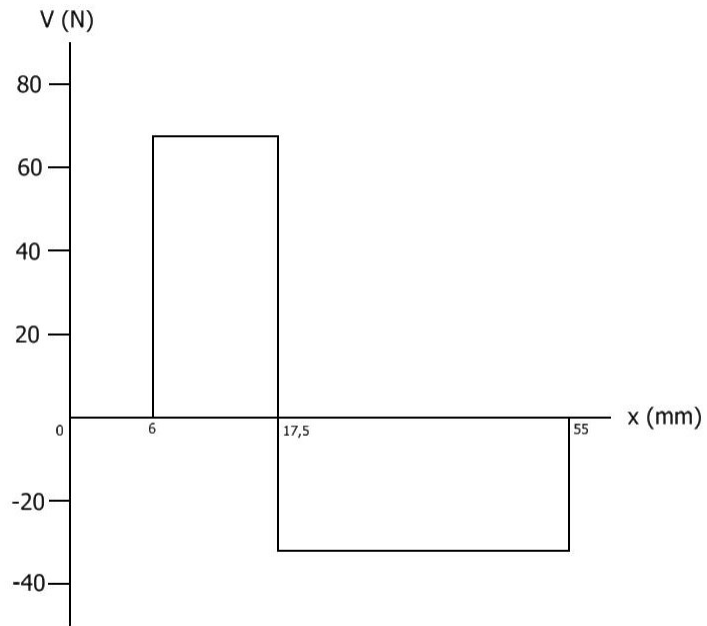


**Figure A2:** Shear force diagram made in Inventor

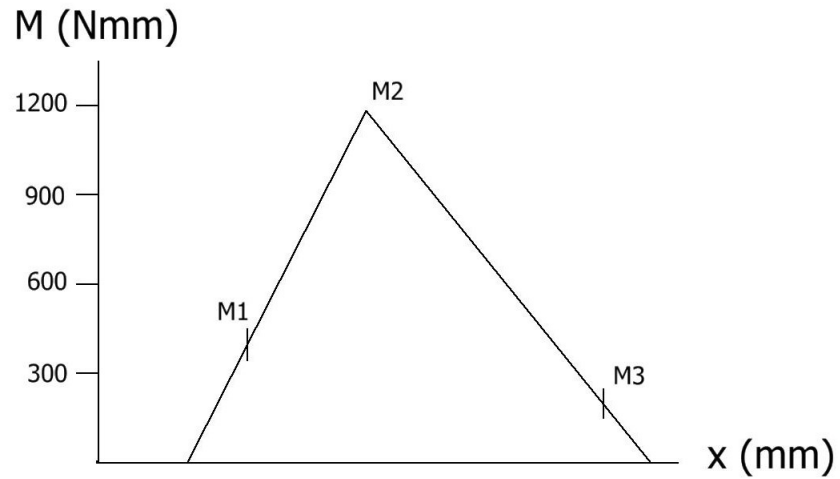


**Figure A3:** Moment diagram made in Inventor

The relevant moments obtained from figure A3 are listed below.

- $M_1 = 409.08 \text{ Nmm}$
- $M_2 = 1198.18 \text{ Nmm}$
- $M_3 = 190.00 \text{ Nmm}$

Using the pre-calculated values for the EI of each section, the  $\frac{M}{EI}$  diagram, shown below, is constructed. The  $\frac{M}{EI}$  values represent the heights in the diagram, which are then used to calculate the area of each section.

- $EI_1 = 3.77 \cdot 10^8 \text{ Nmm}^2$
- $EI_2 = 1.57 \cdot 10^9 \text{ Nmm}^2$
- $EI_3 = 6.43 \cdot 10^8 \text{ Nmm}^2$
- $EI_4 = 3.77 \cdot 10^8 \text{ Nmm}^2$

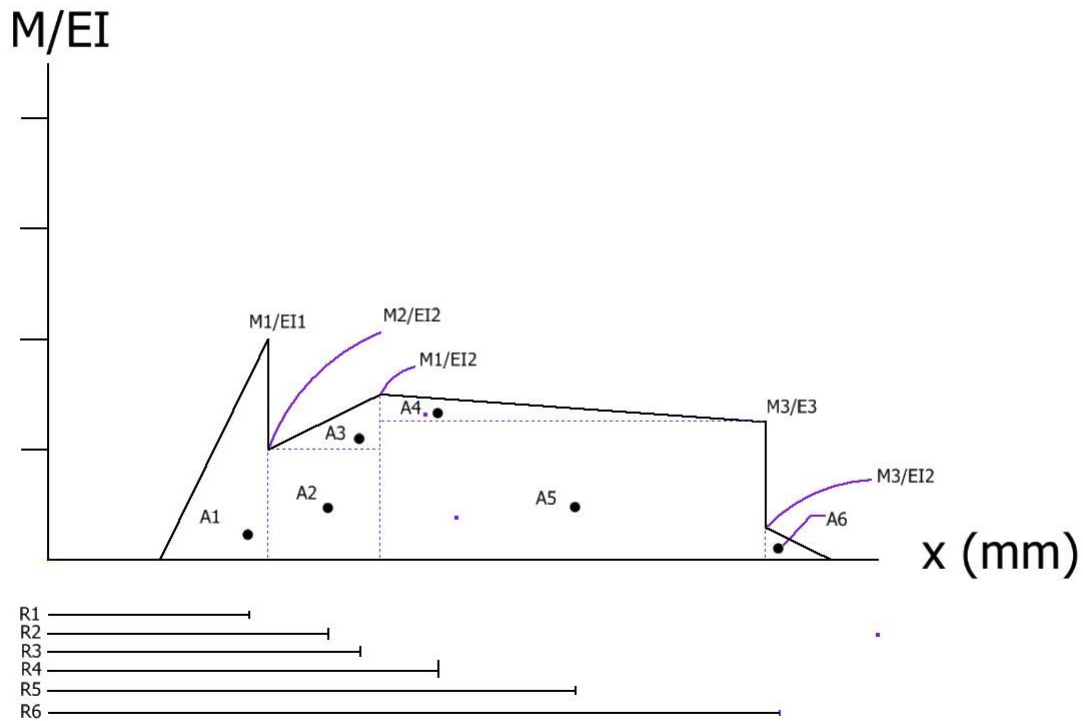


**Figure A4:**  $\frac{M}{EI}$  diagram made in Inventor

The calculated areas and their corresponding centroids are presented in table A1. The centroid values are multiplied by their respective areas and summed to obtain the total area and centroid.

- $\frac{M_1}{EI_1} = 1.09 \cdot 10^{-6} \text{ mm}^{-1}$
- $\frac{M_1}{EI_2} = 2.61 \cdot 10^{-7} \text{ mm}^{-1}$
- $\frac{M_2}{EI_2} = 7.63 \cdot 10^{-7} \text{ mm}^{-1}$
- $\frac{M_3}{EI_3} = 2.95 \cdot 10^{-7} \text{ mm}^{-1}$
- $\frac{M_3}{EI_2} = 1.21 \cdot 10^{-7} \text{ mm}^{-1}$

**Table A1:** Area and centroid in tableform

Section	$A_i$	$R_i$
1	$6.51 \cdot 10^{-6}$	8.00
2	$2.99 \cdot 10^{-6}$	17.75
3	$2.52 \cdot 10^{-7}$	19.67
4	$7.37 \cdot 10^{-6}$	34.00
5	$9.29 \cdot 10^{-6}$	39.25
6	$3.63 \cdot 10^{-7}$	57.00
$\sum A_i R_i$	$7.46 \cdot 10^{-4}$	

$$V_a = \sum A_i R_i = 7.46 \cdot 10^{-4} \text{ mm}$$

The tangential deviation line ( $V_a$ ) is determined using eq. 36 It is calculated as the sum of the products of each section's area and centroid distance from the starting point ( $x = 0$ ), as shown in figure A4.

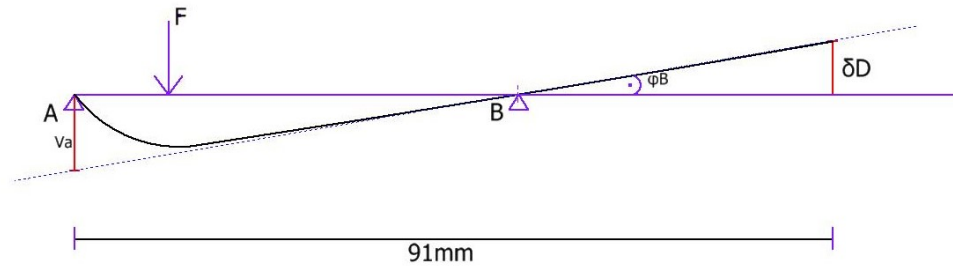


**Figure A5:** Elastic curve figure made in Inventor

---

The angle  $\phi_B$  is calculated based on the geometry of the system. It is determined by dividing the tangential deviation ( $V_a$ ) by the length ( $L_{AB}$ ) from point A to point B.

$$\phi_B = \frac{7.46 \cdot 10^{-4} \text{ mm}}{91 \text{ mm}} = 8.20 \cdot 10^{-6}$$

Finally, the length  $\delta_D$  is calculated by multiplying the angle  $\phi_B$  by the length  $L_{AB}$ . The result represents the deflection at point D.

$$\delta_D = 8.20 \cdot 10^{-6} \cdot 35.5 \text{ mm} = 2.91 \cdot 10^{-4} \text{ mm}$$

Appx. D provides a comprehensive set of calculations and diagrams that contribute to the understanding of the shaft's behavior and performance.

---

## B Bolt calculations

A320 Grade L7 manufactured to metric size M10x1.5 socket head cap screw were used to fasten the seal hub to the housing. The material used for the seal hub and the housing is Super Duplex S32750 and P460 NL2, respectively. The force acting on the bolts is a thrust force and calculated with the geometry of design 3. Refer to Appx. E for the dimensions used.

$$F_{thrust} = P_{test}A = 24.8 \text{ MPa} \cdot \frac{\pi \cdot 28^2 \text{ mm}}{4} = 15271 \text{ N}$$

The proofload  $F_p$  is found by eq. 10 and with the proof load the recommended preload  $F_i$  was found by eq. 9:

$$F_p = A_t S_p = 58 \text{ mm}^2 \cdot 725 \frac{\text{N}}{\text{mm}^2} = 42050 \text{ N}$$

$$F_i = 0.75 F_p = 0.75 \cdot 42050 \text{ N} = 31538 \text{ N}$$

The torque required to achieve the recommended preload was found by eq. 11, with a friction coefficient of  $k = 0.2$  and eq. 12 for the nominal diameter  $d_s$ :

$$M_t = k F_i d_s = 0.2 \cdot 31538 \text{ N} \cdot \sqrt{\frac{4 \cdot 58 \text{ mm}^2}{\pi}} = 54204 \text{ Nmm} = 54.21 \text{ Nm}$$

Using the following equation, the effective grip length was determined for the case of  $t_2 \geq d$ :

$$l = h + \frac{d}{2} = 8 \text{ mm} + \frac{10 \text{ mm}}{2} = 13 \text{ mm}$$

The length of the fastener and the threaded length were found using eqs. 16 and 17, respectively:

$$L > h + 1.5d > 8 \text{ mm} + 1.5 \cdot 10 \text{ mm} = 23 \text{ mm}$$

$$L_T = 2d + 6 \text{ mm} = 2 \cdot 10 \text{ mm} + 6 \text{ mm} = 26 \text{ mm}$$

By rounding up the threaded length, M10x1.5x30 was chosen by using the Ranard series to get a preferred number and a standard length of the fastener.



---

The increasing tensile force on each bolt was found by eq. 22:

$$F_b = C \cdot F_{thrust} = \frac{k_{b_{total}}}{k_{b_{total}} k_m} \cdot F_{thrust} = 0.52 \cdot \frac{15271}{4} = 1986 \text{ N}$$

With the bolt force for each bolt the bolt stress could be determined with eq. 23:

$$\sigma_{bolt} = \frac{F_i + F_b}{A_t} = \frac{31538 \text{ N} + 1986 \text{ N}}{58 \text{ mm}^2} = 578 \text{ MPa}$$

The preload stress for each bolt was found by eq. 24:

$$\sigma_i = \frac{F_i}{n \cdot A_t} = \frac{31538 \text{ N}}{4 \cdot 58 \text{ mm}^2} = 136 \text{ MPa}$$

The shear stress caused by torsion is given by eq. 25:

$$\tau_i \cong 0.5 \cdot \sigma_i = 0.5 \cdot 136 \text{ MPa} = 68 \text{ MPa}$$

Together with the above calculated parameters the von Mises eq. 21 was used to determine the equivalent stress:

$$\sigma_e = \sqrt{\sigma_{bolt}^2 + 3\tau_i^2} = \sqrt{578^2 \text{ MPa} + 3 \cdot 68^2 \text{ MPa}} = 590 \text{ MPa}$$

The fastener stiffness was identified by eq. 15 and gave the result:

$$k_{b_1} = \frac{A_t E}{l} = \frac{58 \text{ mm}^2 \cdot 200000 \text{ MPa}}{13 \text{ mm}} = 8.92 \cdot 10^5 \frac{\text{N}}{\text{mm}}$$

For the stiffness for all bolts together, the result is timed by 4:

$$k_{b_{total}} = 8.92 \cdot 10^5 \frac{\text{N}}{\text{mm}} \cdot 4 = 3.57 \cdot 10^6 \frac{\text{N}}{\text{mm}}$$

The member stiffness for every member was identified by using the frustum. Every part in the grip contain contain 1 or 2 frustums. See figure B1 for the dimensions found for each frustum with the half-apex angle of 30 °. With the dimensions and eq. 19 the individual stiffnesses where determined:

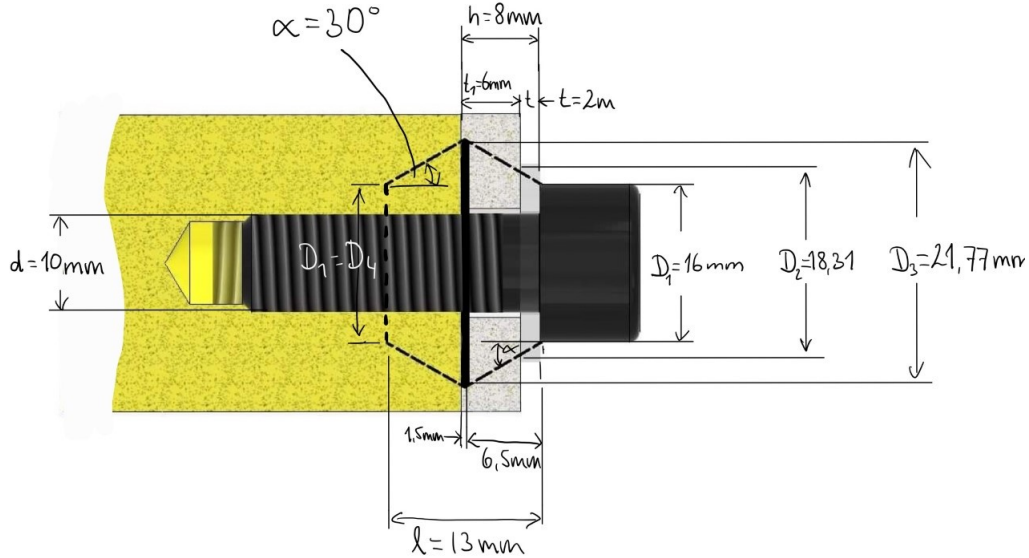


**Figure B1:** The stress frustum with dimensions made in Inventor

$$k_{m_i} = \frac{\pi E d \tan \alpha}{\ln \left( \frac{(2l \tan \alpha + D - d)(D + d)}{(2l \tan \alpha + D + d)(D - d)} \right)}$$

$$k_{m_1} = \frac{\pi \cdot 200000 \text{ MPa} \cdot 10 \text{ mm} \cdot \tan 30}{\ln \left( \frac{(2 \cdot 2 \text{ mm} \cdot \tan 30 + 16 \text{ mm} - 10 \text{ mm})(16 \text{ mm} + 10 \text{ mm})}{(2 \cdot 2 \text{ mm} \cdot \tan 30 + 16 \text{ mm} + 10 \text{ mm})(16 \text{ mm} - 10 \text{ mm})} \right)} = 1.51 \cdot 10^7 \frac{\text{N}}{\text{mm}}$$

$$k_{m_2} = \frac{\pi \cdot 200000 \text{ MPa} \cdot 10 \text{ mm} \cdot \tan 30}{\ln \left( \frac{(2 \cdot 4.5 \text{ mm} \cdot \tan 30 + 18.31 \text{ mm} - 10 \text{ mm})(18.31 \text{ mm} + 10 \text{ mm})}{(2 \cdot 4.5 \text{ mm} \cdot \tan 30 + 18.31 \text{ mm} + 10 \text{ mm})(18.31 \text{ mm} - 10 \text{ mm})} \right)} = 1.14 \cdot 10^7 \frac{\text{N}}{\text{mm}}$$

$$k_{m_3} = \frac{\pi \cdot 200000 \text{ MPa} \cdot 10 \text{ mm} \cdot \tan 30}{\ln \left( \frac{(2 \cdot 1.5 \text{ mm} \cdot \tan 30 + 21.77 \text{ mm} - 10 \text{ mm})(21.77 \text{ mm} + 10 \text{ mm})}{(2 \cdot 1.5 \text{ mm} \cdot \tan 30 + 21.77 \text{ mm} + 10 \text{ mm})(21.77 \text{ mm} - 10 \text{ mm})} \right)} = 4.31 \cdot 10^7 \frac{\text{N}}{\text{mm}}$$

$$k_{m_4} = \frac{\pi \cdot 200000 \text{ MPa} \cdot 10 \text{ mm} \cdot \tan 30}{\ln \left( \frac{(2 \cdot 5 \text{ mm} \cdot \tan 30 + 16 \text{ mm} - 10 \text{ mm})(16 \text{ mm} + 10 \text{ mm})}{(2 \cdot 5 \text{ mm} \cdot \tan 30 + 16 \text{ mm} + 10 \text{ mm})(16 \text{ mm} - 10 \text{ mm})} \right)} = 7.66 \cdot 10^6 \frac{\text{N}}{\text{mm}}$$

With the individual stiffnesses, the total spring rate was obtained by equation 18:

$$\frac{1}{k_m} = \frac{1}{k_1} + \frac{1}{k_2} + \frac{1}{k_3} + \dots + \frac{1}{k_i}$$

$$\frac{1}{k_m} = \frac{1}{1.508 \cdot 10^7 \frac{N}{mm}} + \frac{1}{1.144 \cdot 10^7 \frac{N}{mm}} + \frac{1}{4.308 \cdot 10^7 \frac{N}{mm}} + \frac{1}{7.660 \cdot 10^6 \frac{N}{mm}} = 3.25 \cdot 10^6 \frac{N}{mm}$$

To find the safety factors the stiffness constant of the joint was revealed using eq. 20:

$$C = \frac{k_b}{k_b + k_m} = \frac{3.57 \cdot 10^6 \frac{N}{mm}}{3.57 \cdot 10^6 \frac{N}{mm} + 3.25 \cdot 10^6 \frac{N}{mm}} = 0.52$$

From the results above, the safety factors were determined with using the thrust force on the seal hub of 15 271 N and number of bolts n. Using eq. 26 the yielding factor of safety was found:

$$n_p = \frac{S_p A_t}{C F_{thrust} + F_i} = \frac{725 \text{ MPa} \cdot 58 \text{ mm}^2}{0.52 \cdot \frac{15271 \text{ N}}{4} + 31538 \text{ N}} = 1.25$$

After using von Mises, eq. 21, the yielding factor of safety was found to be:

$$n_{yielding} = \frac{R_{p0.2}}{\sigma_e} = \frac{725 \text{ MPa}}{590 \text{ MPa}} = 1.23$$

The load factor of safety is obtained by eq. 28:

$$n_L = \frac{S_p A_t - F_i}{C F_{thrust}} = \frac{725 \text{ MPa} \cdot 58 \text{ mm}^2 - 31538 \text{ N}}{0.52 \cdot \frac{15271 \text{ N}}{4}} = 5.30$$

Safety factor against joint separation from eq. 29:

$$n_0 = \frac{F_i}{F_{thrust}(1 - C)} = \frac{31538 \text{ N}}{\frac{15271 \text{ N}}{4} \cdot (1 - 0.52)} = 17.21$$

By using the EN13445-3 to verify the bolt size, eq. 30 for identifying the nominal design stress for normal operating load cases was used:

$$f_d = \min\left(\frac{R_{p0.2}}{1.5}, \frac{R_m}{2.4}\right)$$

---


$$f_d = \min\left(\frac{725 \text{ MPa}}{1.5}, \frac{860 \text{ MPa}}{2.4}\right) = \min 358.33 \text{ MPa}$$

With  $f_d$  the bolt load ratio could be obtained by using eq. 31 with  $C = 4/3$  and a coefficient of friction of the threads of  $\mu = 0.1$ .

$$\Phi_B = \frac{F_B}{A_B f_d} \cdot \sqrt{1 + (C \cdot 3.2 \cdot \mu)^2}$$

$$\Phi_B = \frac{\frac{15271 \text{ N}}{4}}{\frac{\pi \cdot (10 \text{ mm} - \frac{3}{4} \cdot \sqrt{3} \cdot 1.5)^2}{4}} \cdot 358.33 \text{ MPa} \cdot \sqrt{1 + \left(\frac{4}{3} \cdot 3.2 \cdot 0.1\right)^2} = 0.23$$

---

## C Seals calculations

The calculations for compression and gland fill percentage apply for static and dynamic seals, please refer to Appx. F for product specifications.

- O-ring Parker 2-119 and 2-113
- Back-up ring 8-119 and 8-113

Calculating the compression for static sealing in cross-section area by applying eq. 8.

$$compression = \frac{2.62 \text{ mm} - 2.1 \text{ mm}}{2.62 \text{ mm}} \cdot 100 \% = 19.9 \%$$

Calculating the compression for dynamic sealing in cross-section area by applying eq. 8.

$$compression = \frac{2.62 \text{ mm} - 2.25 \text{ mm}}{2.62 \text{ mm}} \cdot 100 \% = 14 \%$$

Calculating the gland fill by using eq. 4, starting by retrieving data such as cross-section area for O-ring, back-up ring, and gland. Table for specification can be found in Appx. F for seals.

Starting with calculating the area of O-ring.

$$A_{oring} = \pi \cdot \frac{(2.62 \text{ mm})^2}{4} = 5.39 \text{ mm}^2$$

Followed by the cross-section area of back-up ring.

$$A_{backup} = 2.18 \text{ mm} \cdot 1.35 \text{ mm} = 2.94 \text{ mm}^2$$

Calculating cross-sectional area of gland in the static application.

$$A_{gland} = 4.7 \text{ mm} \cdot 2.1 \text{ mm} = 9.87 \text{ mm}^2$$

Followed by cross-sectional area of gland for dynamic application.

$$A_{gland} = 4.7 \text{ mm} \cdot 2.25 \text{ mm} = 10.58 \text{ mm}^2$$

The minimum gland fill for both applications can be found by applying eq. 4.

---

For static application the gland fill is following

$$Glandfill = \frac{5.39 \text{ mm}^2}{9.87 \text{ mm}^2 - 2.94 \text{ mm}^2} \cdot 100 \% = 77.8 \%$$

Followed by dynamic application, the gland fill is.

$$Glandfill = \frac{5.39 \text{ mm}^2}{10.58 \text{ mm}^2 - 2.94 \text{ mm}^2} \cdot 100 \% = 70 \%$$

Furthermore, calculating the stretch and reduction in cross-area section are separated for static and dynamic sealing.

Stretch in the piston sealing can be found by eq. 5.

$$S = \frac{23.8 \text{ mm} - 23.47 \text{ mm}}{23.47 \text{ mm}} \cdot 100 \% = 1.41 \%$$

Following the calculations for reduction in cross-section area can be found by applying eq. 7.

$$R = 0.56 + 0.59 \cdot 1.41 - 0.0046 \cdot 1.41^2 = 1.38 \%$$

Stretch in the rod sealing (dynamic sealing) can be found by eq. 6.

$$S = \frac{14.00 \text{ mm} - 13.94 \text{ mm}}{13.9 \text{ mm}} \cdot 100 \% = 0.43 \%$$

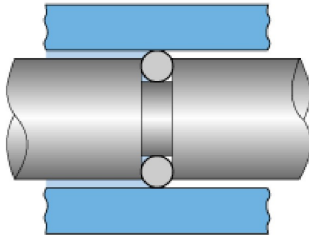
Following the calculations for reduction in cross-section area can be found by applying eq. 7.

$$R = 0.56 + 0.59 \cdot 0.43 - 0.0046 \cdot 0.43^2 = 0.81 \%$$

The gland surface roughness is set to be minimum Ra  $0.4 \mu\text{m}$  and the surface roughness for the shaft must not exceed Ra  $0.8 \mu\text{m}$ , as discussed in section 2.5.2. While clearance gap is given in table (Parker design chart 5-1) was  $\frac{1}{2}E$  which is in this case  $25.4 \mu\text{m} - 63.5 \mu\text{m}$ .

For dynamic sealing, it is used Parker O-ring 2-113 with 70 shore A hardness and corresponding spliced back-up ring 8-113 made of PTFE. This is designed based on a reciprocating application, and chosen design recommendations for rod sealing. The surface roughness for dynamic seals is set to be Ra  $0.3 \mu\text{m}$ .

A shaft calculator by Eriks [48] was used to verify both O-rings. The first figure presents the result for the static application and the second calculation was done for the dynamic application by ERIKS calculator.



Piston - groove dimensions				
material	Steel (stainless)			
free groove volume at inst (%)	20			
bore diameter (mm)	28.00	0.033	0	H8
piston diameter (mm)	28.00	-0.02	-0.041	f7
groove diameter (mm)	23.80	0	-0.052	h9
groove width (mm)	4.70	0.2	0suggestion	
radius (mm)	0.3			
inner diameter stretch at inst (%)	1.41			

Application		O-Ring			
Sealing principle	Piston	compound	NBR		
design	Design O-Ring	chemical volume swell (%)	0		
temperature (°C)	21	inner diameter (mm)	23.469085889	0.29	ISO 3601
movement	static	cross section diameter (mm)	2.68717941244	0.1	ISO 3601
pressure	over pressure				
compression (%)	20				

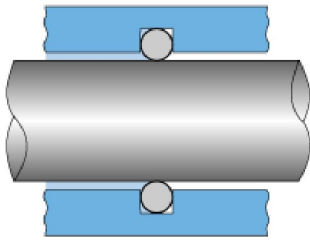
Results at Installation	min.	nom.	max.
Calculated Values at Central Position of Piston:			
O-Ring Compression (%)	14.28	20.01	24.66
Free Groove Volume (%)	36.39	41.74	49.98
O-Ring Inner Diameter Stretch (%)	- 0.05	1.41	2.68
Results at Service	min.	nom.	max.
Calculated Values at Central Position of Piston:			
O-Ring Compression (%)	14.28	20.01	24.66
Free Groove Volume (%)	36.39	41.74	49.98
O-Ring Inner Diameter Stretch (%)	- 0.05	1.41	2.68
Groove Depth incl. Gap (mm)	2.10	2.10	2.14
Sealing Gap (mm)	0.01	0.00	0.04
Calculated Values at Excentrical Position of Piston:			
O-Ring Compression (%)	12.80		25.39
Groove Depth incl. Gap (mm)	2.08		2.18
Sealing Gap (mm)	0.00		0.07

Comments
Results at Installation
Results at Service

**Disclaimer**

This information is, to the best of our knowledge, accurate and reliable to the date indicated. The above mentioned data have been obtained by tests we consider as reliable. We don't assure that the same results can be obtained in other laboratories, using different conditions by the preparation and evaluation of the samples.

**Figure C1:** Results from ERIKS calculator for O-rings for static application [48]



Rod - groove dimensions		+		-	
material	Steel (stainless)				
free groove volume at inst (%)	20				
bore diameter (mm)	14.00	0.027	0	H8	
rod diameter (mm)	14.00	-0.016	-0.034	f7	
groove diameter (mm)	18.50	0.052	0	h9	
groove width (mm)	4.70	0.2	0	0	suggestion
radius (mm)	0.3				
Max. Excentricity	0.2				
inner diameter stretch at inst (%)	1.43				

Application		O-Ring		±	
Sealing principle	Rod	compound	NBR		
design	Design O-Ring	chemical volume swell (%)	0		
temperature (°C)	21	inner diameter (mm)	13.8026224983	0.22	ISO 3601
movement		cross section diameter (mm)	2.71084337349	0.1	ISO 3601
pressure					
compression (%)	17				

Results at Installation	min.	nom.	max.
Calculated Values at Central Position of Rod:			
O-Ring Compression (%)	9.26	15.32	19.67
Free Groove Volume (%)	39.18	44.33	52.38
O-Ring Inner Diameter Stretch (%)	- 0.40	1.43	2.96

Results at Service	min.	nom.	max.
Calculated Values at Central Position of Rod:			
O-Ring Compression (%)	9.26	15.32	19.67
Free Groove Volume (%)	39.18	44.33	52.38
O-Ring Inner Diameter Stretch (%)	- 0.40	1.43	2.96
Groove Depth incl. Gap (mm)	2.26	2.25	2.29
Sealing Gap (mm)	0.01	0.00	0.03

Results at Service	min.	nom.	max.
Calculated Values at Excentrical Position of Piston:			
O-Ring Compression (%)	0.14		20.43
Groove Depth incl. Gap (mm)	2.24		2.52
Sealing Gap (mm)	0.00		0.06

Comments
Results at Installation
Results at Service

**Disclaimer**

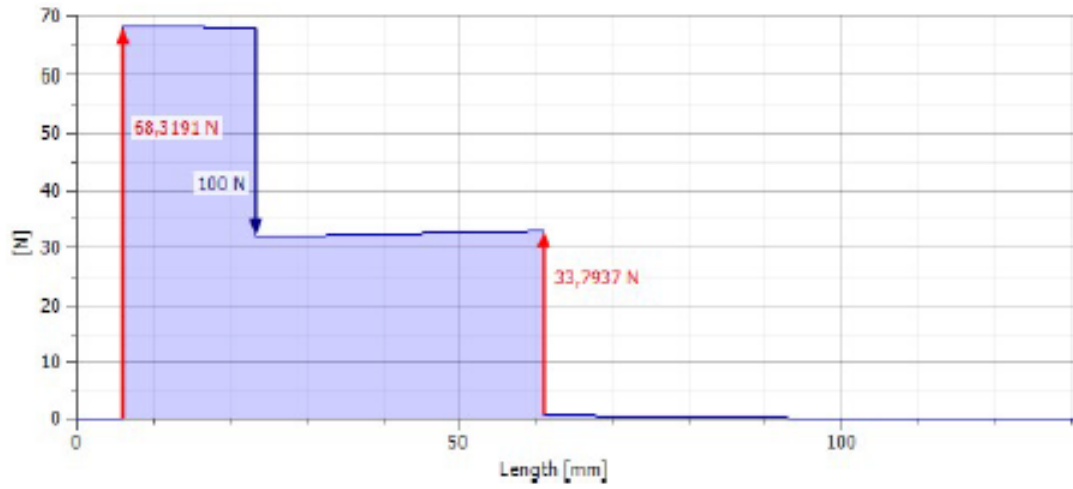
This information is, to the best of our knowledge, accurate and reliable to the date indicated. The above mentioned data have been obtained by tests we consider as reliable. We don't assure that the same results can be obtained in other laboratories, using different conditions by the preparation and evaluation of the samples.

**Figure C2:** Results from ERIKS calculator for O-rings for dynamic application [48]

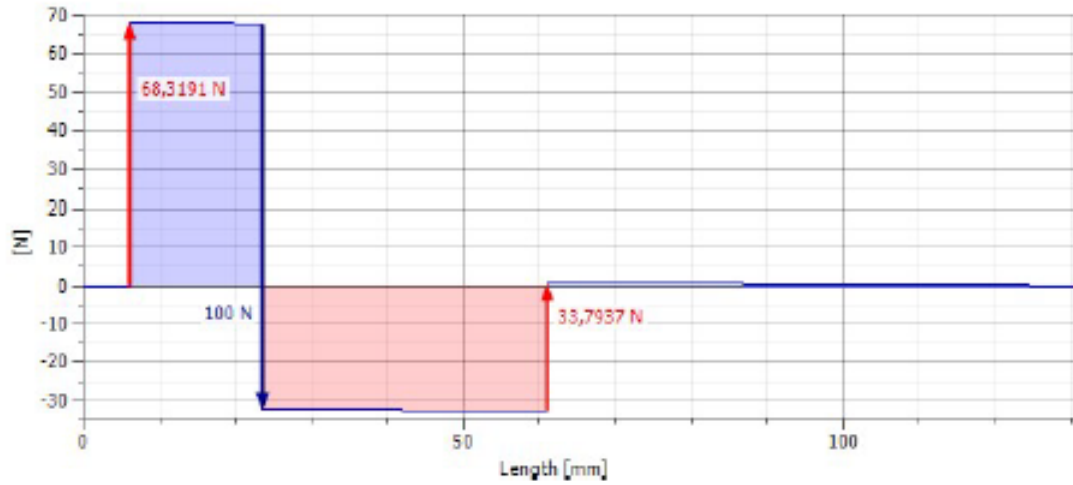




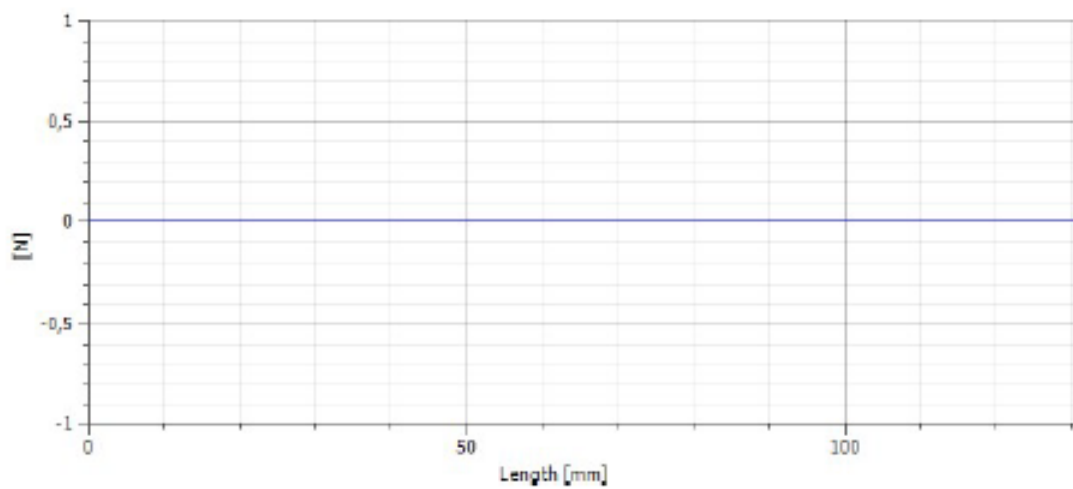
### Shear Force



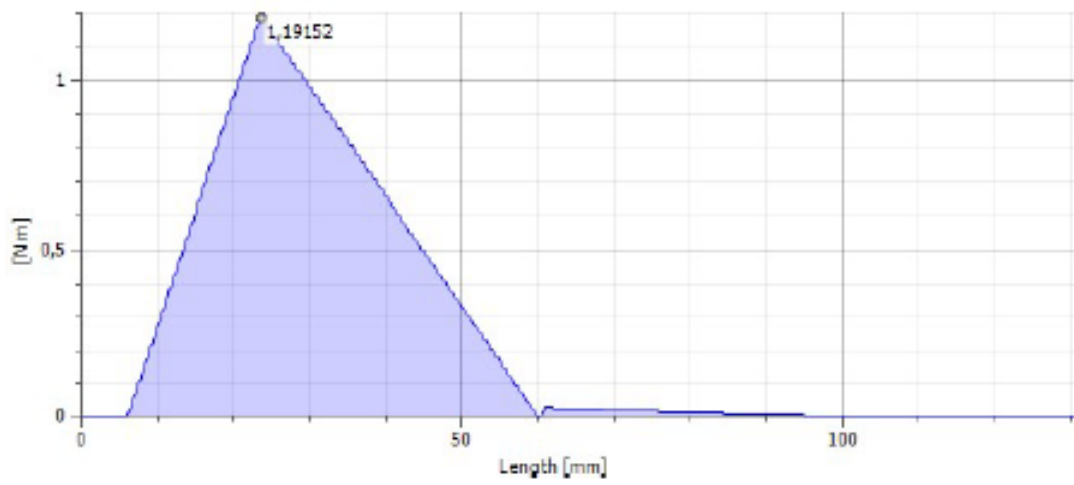
### Shear Force, YZ Plane



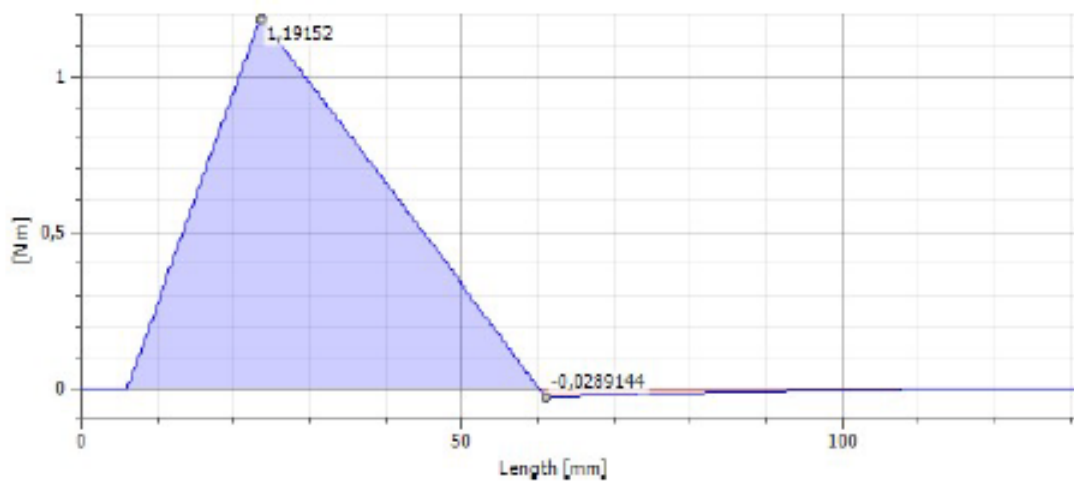
### Shear Force, XZ Plane



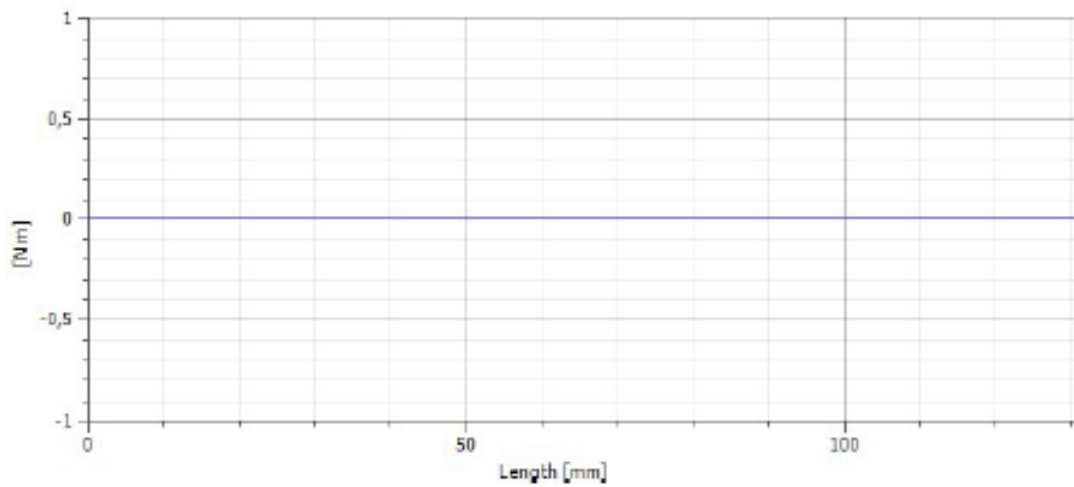
### Bending Moment



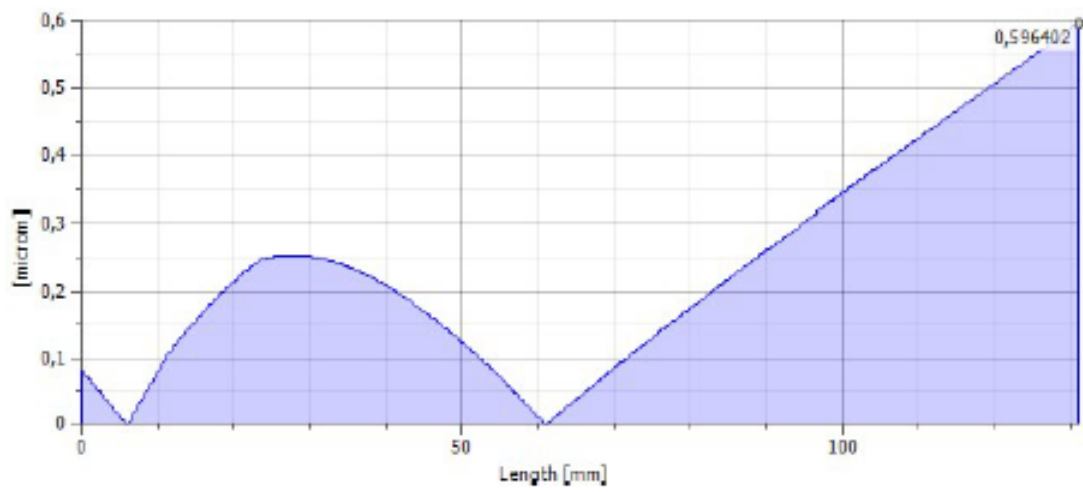
**Bending Moment, YZ Plane**



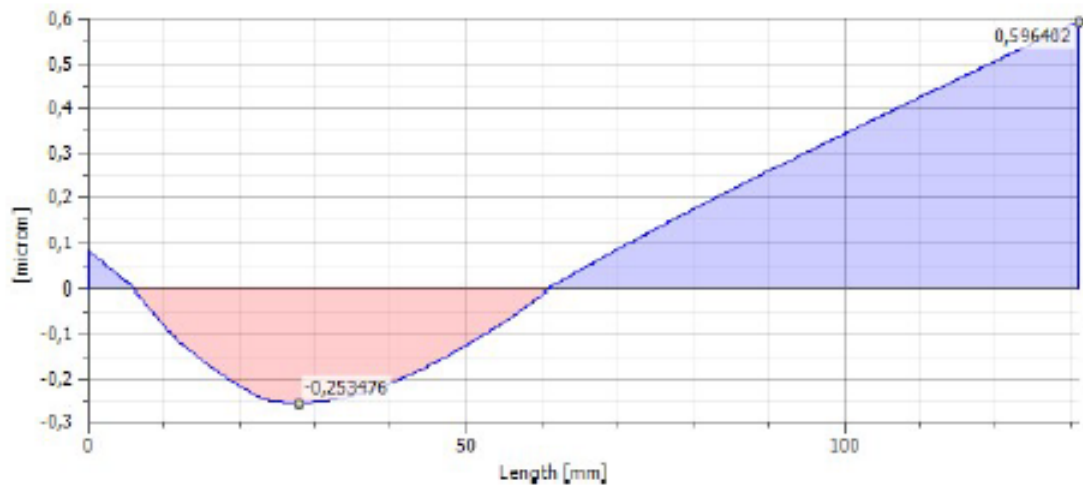
**Bending Moment, XZ Plane**



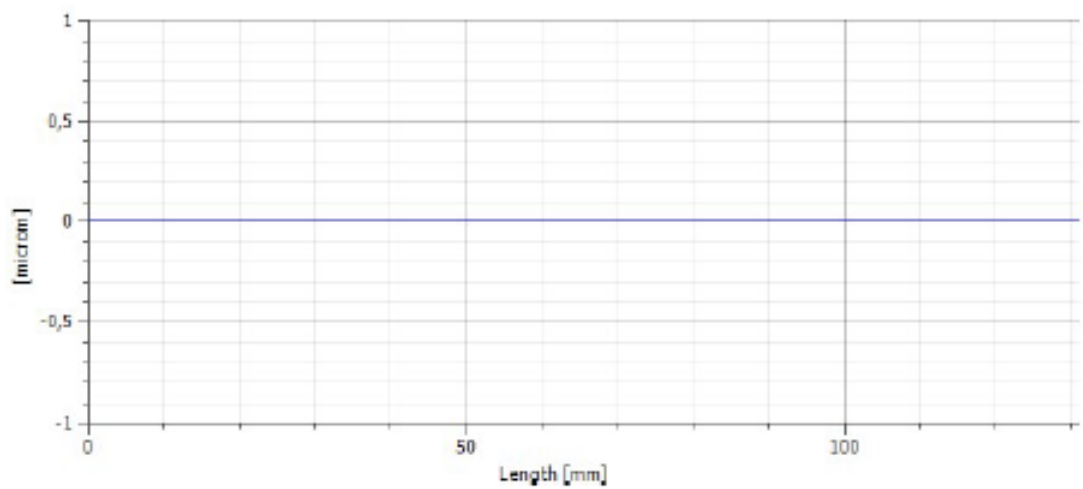
**Deflection Angle**



**Deflection, YZ Plane**



**Deflection, XZ Plane**



# Bolted Connection Component Generator (Version: 2023 (Build 270158000, 158))

03.05.2023

## Project Info (iProperties)

### Static Calculation

#### Guide

Type of Strength Calculation - Check Calculation

#### Loads

Tightness Factor	k	1,50 ul
Maximum axial Force	F <sub>a</sub>	15271 N
Force Input Factor	n	0,50 ul
Maximum tangent Force	F <sub>t</sub>	0 N
Joint Friction Factor	f	0,80 ul

#### Bolt

Bolt Number	z	4 ul
Thread Diameter	d	10,000 mm
Thread Pitch	p	1,500 mm
Mean Bolt Diameter	d <sub>s</sub>	9,026 mm
Minimum Bolt Diameter	d <sub>min</sub>	8,160 mm
Material		User material
Yield Strength	S <sub>y</sub>	725 MPa
Required Safety Factor	k <sub>s</sub>	3,00 ul
Allowable Thread Pressure	p <sub>a</sub>	200 MPa
Modulus of Elasticity	E	200000 MPa
Thread Friction Factor	f <sub>1</sub>	0,20 ul
Head Friction Factor	f <sub>2</sub>	0,80 ul

#### Material

Joint Functional Width	L	13,000 mm
Modulus of Elasticity	E	200000 MPa

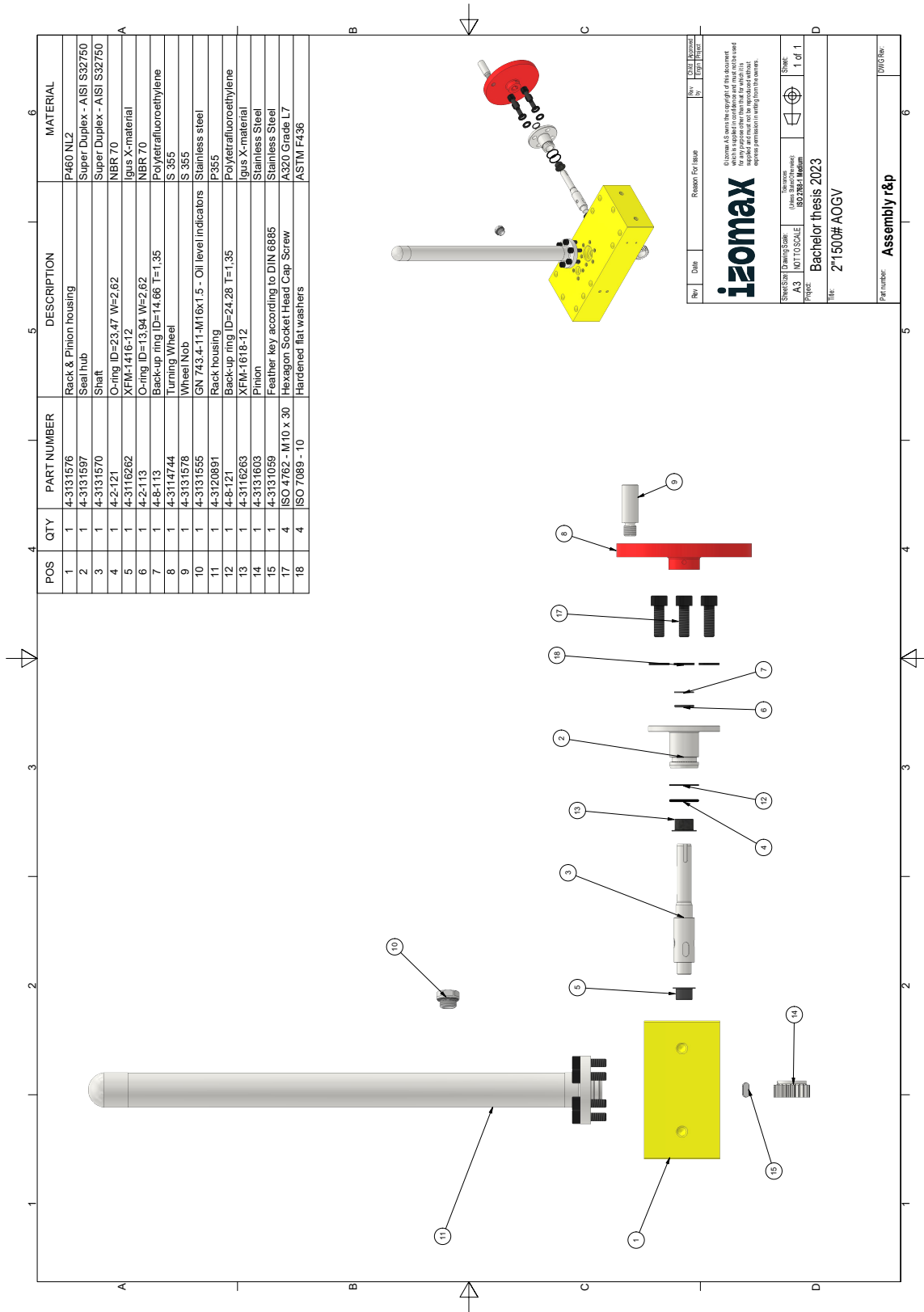
#### Results

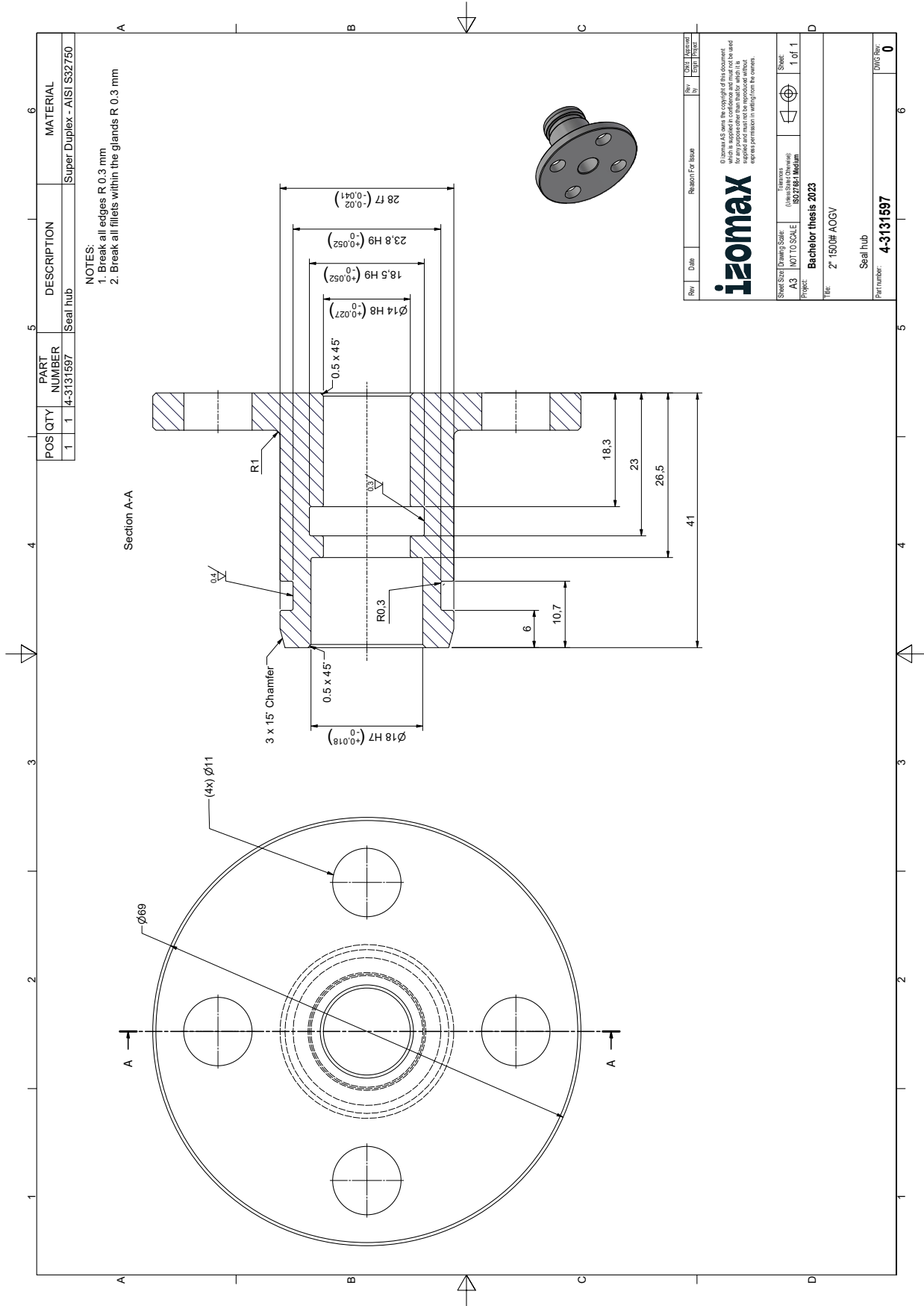
Prestress Force	F <sub>v</sub>	5270,655 N
Working Force	F <sub>max</sub>	5726,625 N
Required Tightening Moment	M <sub>u</sub>	36,454 N m
Tensile Stress	σ <sub>t</sub>	100,792 MPa
Torsional Stress	τ <sub>k</sub>	65,047 MPa
Reduced Stress	σ <sub>red</sub>	151,170 MPa
Stress from Maximum Force	σ <sub>max</sub>	109,512 MPa
Thread Pressure	p <sub>c</sub>	45,817 MPa
Strength Check		Positive

## Summary of Messages

15:01:53 Calculation: Calculation indicates design compliance!

# E Inventor drawings





POS	QTY	PART NUMBER	DESCRIPTION	MATERIAL
1	1	4-3131597	Seal hub	Super Duplex - AISI S32750

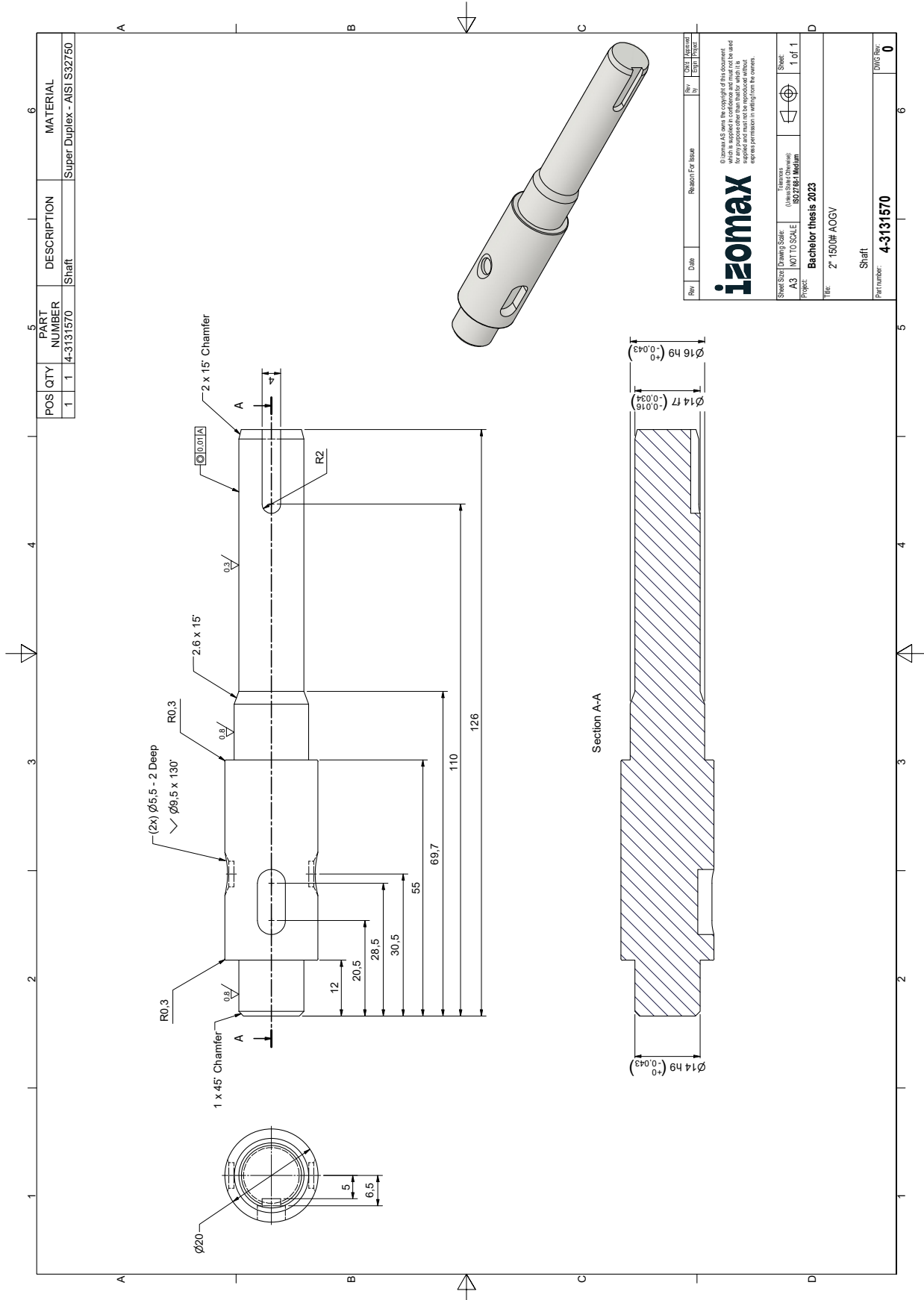
NOTES:  
 1. Break all edges R 0.3 mm  
 2. Break all fillets within the glands R 0.3 mm

Rev	Date	Reason For Issue	Rev No	DATE	APPROVED
					Design Engineer

**izomax**  
 © Izomax AS owns the copyright of this document. No part of this document may be reproduced or used for any purpose other than that for which it is supplied and must not be reproduced without explicit permission in writing from the authors.

Sheet Size	Drawing Scale	Examination (If used)	Sheet
A3	NOT TO SCALE	S077881 Medium	1 of 1

Project: **Bachelor thesis 2023**  
 Title: **2" 1500# AOGV**  
 Seal hub  
 Part number: **4-3131597**  
 DWG Rev: **0**



POS	QTY	PART NUMBER	DESCRIPTION	MATERIAL
1	1	4-3131570	Shaft	Super Duplex - AISI S32750

Rev	Date	Reason For Issue	Rev	DATE	APPROVED
					Design Engineer

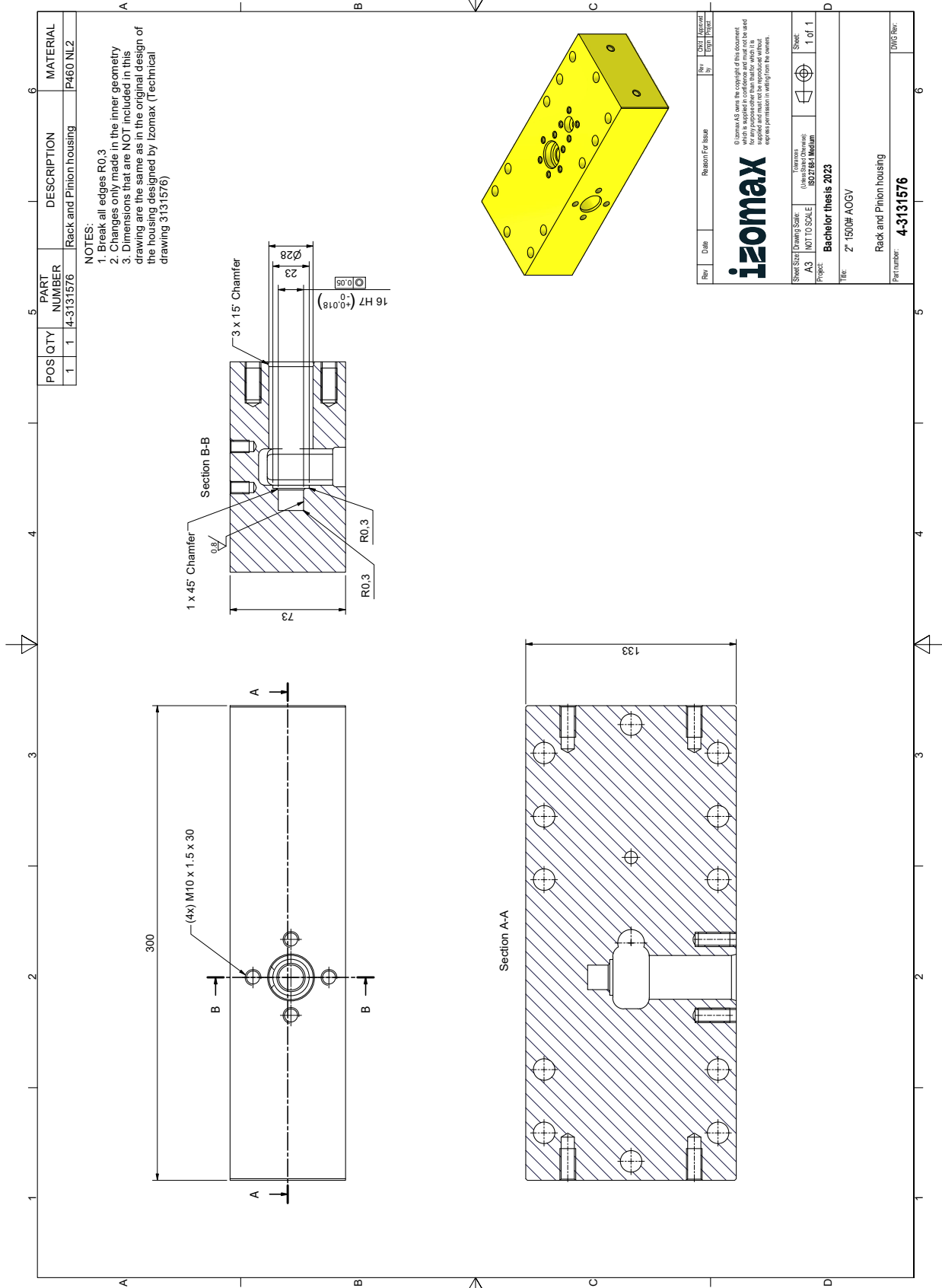
**izomax**  
 © Izomax AS owns the copyright of this document.  
 This drawing is the property of Izomax AS and is to be used  
 for any purpose other than that for which it is  
 supplied and must not be reproduced without  
 express permission in writing from the authors.

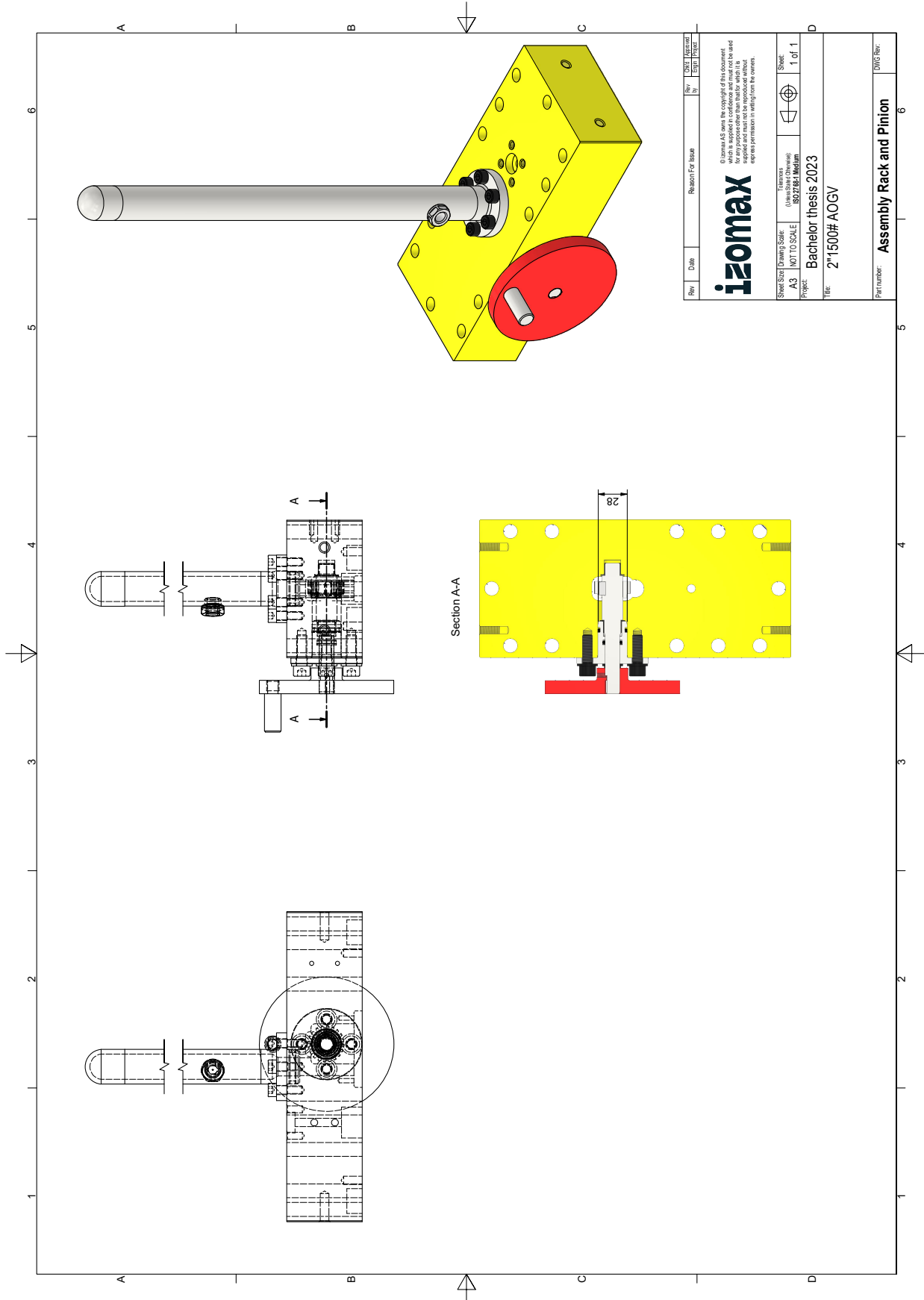
Sheet Size	Drawing Scale	Examination	Examination	Sheet
A3	NOT TO SCALE	(Izomax logo)	(Izomax logo)	1 of 1

Project: **Bachelor thesis 2023**  
 Title: **2" 1500# AOGV**

Part number:	<b>4-3131570</b>
DNIG Rev:	<b>0</b>







Rev	Date	Reason For Issue	Rev. No.	DATE	APPROVED
					Design Engineer

© izomax AS owns the copyright of this document. No part of this document may be reproduced, stored in a retrieval system, or transmitted in any form or by any means, electronic, mechanical, photocopying, recording, or by any information storage and retrieval system, without the prior written permission in writing from the author.

Sheet Size	Drawing Scale	Examination (Please mark)	Sheet
A3	NOT TO SCALE	SDZ/RSK/Mediam	1 of 1

Project: Bachelor thesis 2023  
 Title: 2\*1500# AOGV

Part number:	Assembly Rack and Pinion	DWG Rev:	6
--------------	--------------------------	----------	---

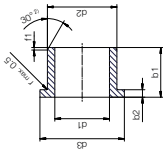


# F Standard parts

igidur® X  
+250°C  
150MPa

## Bearing technology | Plain bearing | iglidur® X

Flange bearing (form F)



<sup>a</sup> Thickness < 0.6mm: Chamfer = 20°

Chamfer in relation to d1  
 d1 [mm] Ø 1-6 | Ø 6-12 | Ø 12-30 | Ø > 30  
 f1 [mm] 0.3 | 0.5 | 0.8 | 1.2

<sup>b</sup> Dimensions according to ISO 3547-1 and special dimensions

<sup>c</sup> Order example: XFM-0304-05 – no minimum order quantity.

<sup>d</sup> X iglidur® material F Flange bearing M Metric Ø 03 Inner Ø d1 04 Outer Ø d2 05 Total length b1

d1 [mm]	Tolerance <sup>a</sup>	d2 [mm]	d3 [mm]	b1 [mm]	b2 [mm]	Part No.
2.0	+0.006	4.0	6.0	3.0	1.00	XFM-020406-03
3.0	+0.006	4.5	7.5	5.0	0.75	XFM-0304-05
4.0	+0.006	5.5	9.5	6.0	0.75	XFM-0405-04
4.0	+0.010	5.5	8.0	6.0	0.75	XFM-040508-06
5.0	+0.008	7.0	11.0	5.0	1.00	XFM-0507-05
6.0	+0.008	8.0	12.0	8.0	1.00	XFM-0608-04
6.0	+0.010	8.0	12.0	10.0	1.00	XFM-0608-10
8.0	+0.010	10.0	12.0	4.0	1.00	XFM-0810-04
8.0	+0.010	10.0	15.0	5.5	1.00	XFM-0810-05
8.0	+0.010	10.0	15.0	7.5	1.00	XFM-0810-07
8.0	+0.010	10.0	15.0	8.0	1.00	XFM-0810-08
8.0	+0.010	10.0	15.0	9.5	1.00	XFM-0810-09
8.0	+0.010	10.0	14.0	31.5	1.00	XFM-0810-4-31
9.0	+0.010	11.0	15.0	18.0	0.50	XFM-0911-18
10.0	+0.013	12.0	18.0	5.0	1.00	XFM-1012-05
10.0	+0.013	12.0	18.0	6.0	1.00	XFM-1012-06
10.0	+0.013	12.0	18.0	7.0	1.00	XFM-1012-07
10.0	+0.013	12.0	18.0	8.0	1.00	XFM-1012-08
10.0	+0.013	12.0	18.0	9.0	1.00	XFM-1012-09
10.0	+0.013	12.0	18.0	10.0	1.00	XFM-1012-10
10.0	+0.013	12.0	18.0	15.0	1.00	XFM-1012-15
10.0	+0.013	12.0	18.0	17.0	1.00	XFM-1012-17
10.0	+0.013	12.0	18.0	18.0	1.00	XFM-1012-18
10.0	+0.013	12.0	18.0	22.0	1.00	XFM-1012-22
10.0	+0.013	12.0	18.0	25.0	1.00	XFM-1012-25

<sup>a</sup> After press-fit. Testing methods, page 57

286 3D CAD, finder and service life calculation ... [www.igus.eu/x](http://www.igus.eu/x)



igidur® X  
+250°C  
150MPa

## Product range

d1 [mm]	Tolerance <sup>a</sup>	d2 [mm]	d3 [mm]	b1 [mm]	b2 [mm]	Part No.
25.0		28.0	35.0	21.0	1.50	XFM-2525-21
27.0	+0.020	30.0	38.0	20.0	1.50	XFM-2730-20
30.0	+0.020	34.0	42.0	16.0	2.00	XFM-3034-16
30.0	+0.104	34.0	42.0	26.0	2.00	XFM-3034-26
30.0		34.0	42.0	40.0	2.00	XFM-3034-40
32.0		36.0	45.0	15.0	2.00	XFM-3236-15
32.0	+0.025	36.0	45.0	26.0	2.00	XFM-3236-26
35.0	+0.125	39.0	47.0	16.0	2.00	XFM-3539-16
35.0		39.0	47.0	26.0	2.00	XFM-3539-26

<sup>a</sup> After press-fit. Testing methods, page 57

d1 [mm]	Tolerance <sup>a</sup>	d2 [mm]	d3 [mm]	b1 [mm]	b2 [mm]	Part No.
40.0		44.0	52.0	22.0	2.00	XFM-4044-22
40.0	+0.025	44.0	52.0	30.0	2.00	XFM-4044-30
40.0	+0.125	44.0	52.0	40.0	2.00	XFM-4044-40
45.0		50.0	58.0	50.0	2.00	XFM-4550-50
50.0		55.0	63.0	40.0	2.00	XFM-5055-40
60.0	+0.030	65.0	73.0	40.0	2.00	XFM-6065-40
70.0	+0.150	75.0	83.0	40.0	2.00	XFM-7075-40
75.0		80.0	88.0	50.0	2.00	XFM-7580-50

<sup>b</sup> Available from stock

<sup>c</sup> Detailed information about delivery time online.

[www.igus.eu/24](http://www.igus.eu/24)

<sup>d</sup> Online ordering

Including delivery times, prices, online tools

[www.igus.eu/x](http://www.igus.eu/x)

<sup>e</sup> Ordering note

Our prices are scaled according to order quantities, current prices can be found online.

<sup>f</sup> Discount scaling

1 - 9	50 - 99	500 - 999
10 - 24	100 - 199	1,000 - 2,499
25 - 49	200 - 499	2,500 - 4,999

No minimum order value.

No low-quantity surcharges.

Free shipping within Germany for orders above €150.



Lubrication-free made easy ... from stock ... no minimum order quantity 287

### 3 Design recommendations

#### 3.1 Static seals

##### 3.1.1 Compression and design dimensions

**Piston seal – radial compression**  
O-ring assembly in inside element

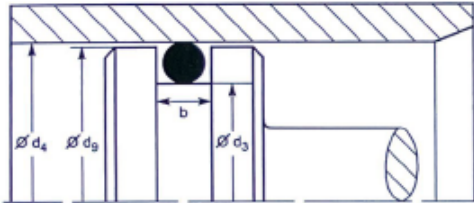


Fig. 3.1 Piston seal – radial compression

**Rod seal – radial compression**  
O-ring assembly in outside element

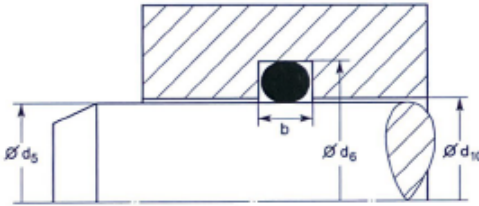


Fig. 3.2 Rod seal – radial compression

**Flange seal – axial compression**

Pressure from inside: O-ring outside diameter must be compressed

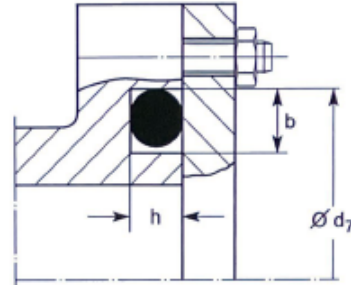


Fig. 3.3 Flange seal – axial compression

Pressure from outside: O-ring inside diameter must be stretched

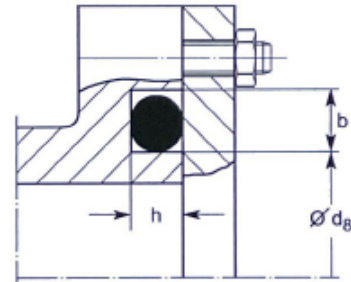
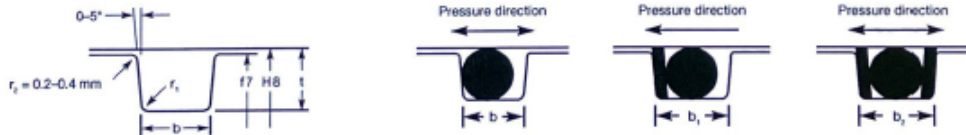


Fig. 3.4 Flange seal – axial compression



Cross-section $d_2$ [mm]	Gland depth t [mm]	Compression [mm]	Compression [%]	Groove width b without back-up ring [mm]	Groove width $b_1$ one back-up ring [mm]	Groove width $b_2$ two back-up rings [mm]	Radius $r_1$ [mm]
1.78 $\pm 0.08$	1.40	0.26 - 0.58	15 - 31	2.40 - 2.60	3.50 - 3.70	4.60 - 4.80	0.20 - 0.40
2.62 $\pm 0.09$	2.20	0.26 - 0.64	10 - 23	3.60 - 3.80	4.70 - 4.90	5.80 - 6.00	0.20 - 0.40
3.53 $\pm 0.10$	2.90	0.40 - 0.85	11 - 23	4.80 - 5.00	5.80 - 6.00	6.80 - 7.00	0.40 - 0.80
5.33 $\pm 0.13$	4.50	0.57 - 1.08	11 - 20	7.20 - 7.40	8.70 - 8.90	10.20 - 10.40	0.40 - 0.80
6.99 $\pm 0.15$	5.90	0.80 - 1.35	11 - 19	9.60 - 9.80	12.00 - 12.20	14.40 - 10.60	0.40 - 0.80

Tab. 3.1 Design dimensions for O-rings – static seal

### 3 Design recommendations

#### 3.1.2 Piston seal static

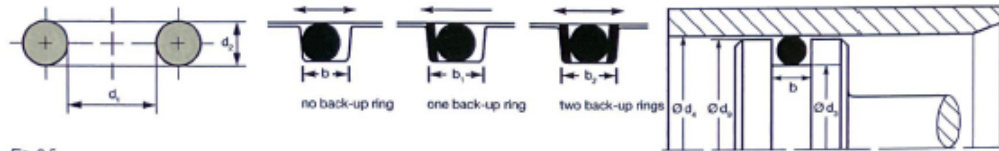


Fig. 3.5

Parker no.	d <sub>1</sub>	d <sub>2</sub>	b +0.2 0	b <sub>1</sub> +0.2 0	b <sub>2</sub> +0.2 0	d <sub>3</sub> h9	d <sub>4</sub> H8	d <sub>5</sub> f7
2-006	2.9	1.78	2.4	3.5	4.6	2.9	5.5	5.5
5-190	3.35	1.78	2.4	3.5	4.6	3.4	6	6
2-007	3.68	1.78	2.4	3.5	4.6	3.9	6.6	6.5
2-008	4.47	1.78	2.4	3.5	4.6	4.4	7	7
5-581	4.9	1.9	2.4	3.5	4.6	5	7.8	7.8
2-009	5.28	1.78	2.4	3.5	4.6	5.4	8	8
5-582	5.7	1.9	2.4	3.5	4.6	5.7	8.5	8.5
2-010	6.07	1.78	2.4	3.5	4.6	6.4	9	9
5-052	6.86	1.78	2.4	3.5	4.6	7.4	10	10
2-011	7.65	1.78	2.4	3.5	4.6	8.4	11	11
5-612	8.74	1.78	2.4	3.5	4.6	8.9	11.5	11.5
2-012	9.25	1.78	2.4	3.5	4.6	9.4	12	12
5-212	9.75	1.78	2.4	3.5	4.6	10.4	13	13
2-013	10.82	1.78	2.4	3.5	4.6	10.9	13.5	13.5
5-613	11.1	1.78	2.4	3.5	4.6	11.4	14	14
2-014	12.42	1.78	2.4	3.5	4.6	12.4	15	15
6-129	13.29	1.78	2.4	3.5	4.6	13.4	16	16
2-016	15.6	1.78	2.4	3.5	4.6	15.4	18	18
2-017	17.17	1.78	2.4	3.5	4.6	17.4	20	20
2-018	18.77	1.78	2.4	3.5	4.6	18.4	21	21
2-019	20.35	1.78	2.4	3.5	4.6	20.4	23	23
2-020	21.95	1.78	2.4	3.5	4.6	22.4	25	25
2-021	23.52	1.78	2.4	3.5	4.6	23.4	26	26
2-022	25.12	1.78	2.4	3.5	4.6	25.4	28	28
2-023	26.7	1.78	2.4	3.5	4.6	27.4	30	30
2-024	28.3	1.78	2.4	3.5	4.6	29.4	32	32
2-025	29.87	1.78	2.4	3.5	4.6	30.4	33	33
2-026	31.47	1.78	2.4	3.5	4.6	32.4	35	35
2-027	33.05	1.78	2.4	3.5	4.6	33.4	36	36
2-028	34.65	1.78	2.4	3.5	4.6	35.4	38	38
6-154	36.3	1.78	2.4	3.5	4.6	37.4	40	40
2-030	41	1.78	2.4	3.5	4.6	42.4	45	45
2-031	44.17	1.78	2.4	3.5	4.6	45.4	48	48
2-032	47.35	1.78	2.4	3.5	4.6	47.4	50	50
2-033	50.52	1.78	2.4	3.5	4.6	52.4	55	55
2-034	53.7	1.78	2.4	3.5	4.6	55.4	58	58
2-035	56.87	1.78	2.4	3.5	4.6	57.4	60	60
2-036	60.08	1.78	2.4	3.5	4.6	60.4	63	63
2-037	63.22	1.78	2.4	3.5	4.6	65.4	68	68
2-038	66.4	1.78	2.4	3.5	4.6	67.4	70	70
2-039	69.57	1.78	2.4	3.5	4.6	69.4	72	72
2-040	72.75	1.78	2.4	3.5	4.6	75.4	78	78
2-041	75.92	1.78	2.4	3.5	4.6	77.4	80	80
2-042	82.27	1.78	2.4	3.5	4.6	82.4	85	85
2-043	88.62	1.78	2.4	3.5	4.6	89.4	92	92
2-044	94.97	1.78	2.4	3.5	4.6	97.4	100	100
2-045	101.32	1.78	2.4	3.5	4.6	102.4	105	105
2-046	107.67	1.78	2.4	3.5	4.6	107.4	110	110
2-047	114.02	1.78	2.4	3.5	4.6	117.4	120	120
2-048	120.37	1.78	2.4	3.5	4.6	122.4	125	125
2-049	126.72	1.78	2.4	3.5	4.6	127.4	130	130
2-050	133.07	1.78	2.4	3.5	4.6	135.4	138	138
2-110	9.19	2.62	3.6	4.7	5.8	9.3	13.5	13.5
5-614	9.93	2.62	3.6	4.7	5.8	9.8	14	14
2-111	10.77	2.62	3.6	4.7	5.8	10.8	15	15
5-615	11.91	2.62	3.6	4.7	5.8	11.8	16	16
2-112	12.37	2.62	3.6	4.7	5.8	12.8	17	17
5-616	13.11	2.62	3.6	4.7	5.8	13.3	17.5	17.5
2-113	13.94	2.62	3.6	4.7	5.8	14	18	18
5-239	14.48	2.69	3.6	4.7	5.8	14.6	19	19
5-243	15.34	2.62	3.6	4.7	5.8	15.8	20	20
2-114	15.54	2.62	3.6	4.7	5.8	16.8	21	21
2-115	17.12	2.62	3.6	4.7	5.8	17.8	22	22
5-256	17.96	2.62	3.6	4.7	5.8	18.8	23	23
2-116	18.72	2.62	3.6	4.7	5.8	19.8	24	24
2-117	203.29	2.62	3.6	4.7	5.8	20.8	25	25
2-118	21.89	2.62	3.6	4.7	5.8	21.8	26	26
2-119	23.47	2.62	3.6	4.7	5.8	23.8	28	28
2-120	25.07	2.62	3.6	4.7	5.8	25.8	30	30
2-121	26.64	2.62	3.6	4.7	5.8	27.8	32	32
2-122	28.24	2.62	3.6	4.7	5.8	28.8	33	33
2-123	29.82	2.62	3.6	4.7	5.8	30.8	35	35
2-124	31.42	2.62	3.6	4.7	5.8	31.8	36	36
2-125	32.99	2.62	3.6	4.7	5.8	33.8	38	38
2-126	34.59	2.62	3.6	4.7	5.8	35.8	40	40
2-127	36.17	2.62	3.6	4.7	5.8	36.8	41	41

### 3 Design recommendations

#### 3.2 Dynamic seals

For dynamic seals, our recommendations refer to the diameter range and are dependent upon the cross-section thickness. The dynamic application of O-rings over 250 mm diameter is not recommended.

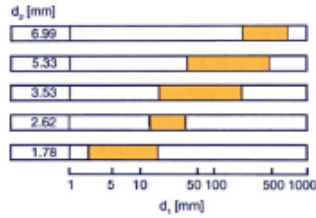


Fig. 3.8 Recommended inside diameter range  $d$ , for O-rings vary according to cross-section  $d_2$

#### 3.2.1 Hydraulic – compression and design dimensions

##### Piston seal – radial compression

O-ring assembly in inside element

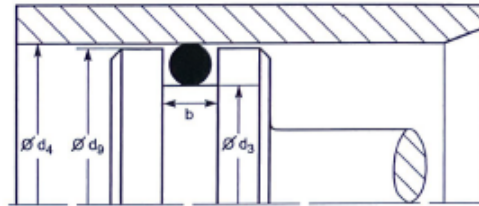


Fig. 3.9 Piston seal – radial compression

##### Rod seal – radial compression

O-ring assembly in outside element

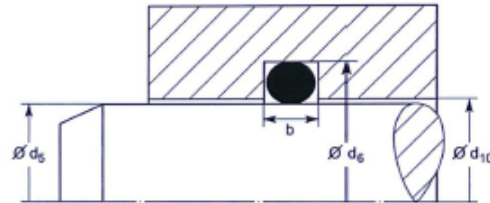
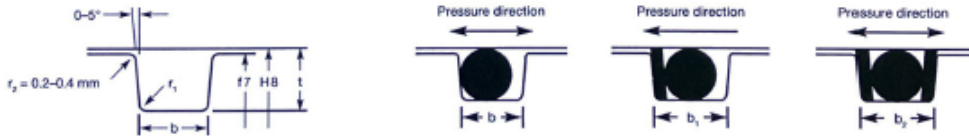


Fig. 3.10 Rod seal – radial compression



Cross-section $d_2$ [mm]	Gland depth $t$ [mm]	Compression [mm]	Compression [%]	Groove width $b$ without back-up ring [mm]	Groove width $b_1$ one back-up ring [mm]	Groove width $b_2$ two back-up rings [mm]	Radius $r_1$ [mm]
1.78 $\pm 0.04$	1.45	0.16 - 0.45	9 - 25	2.40 - 2.60	3.50 - 3.70	4.60 - 4.80	0.20 - 0.40
2.62 $\pm 0.06$	2.20	0.26 - 0.64	10 - 23	3.60 - 3.80	4.70 - 4.90	5.80 - 6.00	0.20 - 0.40
3.53 $\pm 0.10$	3.05	0.27 - 0.70	8 - 19	4.80 - 5.00	5.80 - 6.00	6.80 - 7.00	0.40 - 0.80
5.33 $\pm 0.13$	4.65	0.37 - 0.93	7 - 17	7.20 - 7.40	8.70 - 8.90	10.20 - 10.40	0.40 - 0.80
6.99 $\pm 0.15$	6.20	0.50 - 1.05	7 - 15	9.60 - 9.80	12.00 - 12.20	14.40 - 14.60	0.40 - 0.80

Tab. 3.5

### 3 Design recommendations

#### 3.2.6 Pneumatic – rod seal dynamic

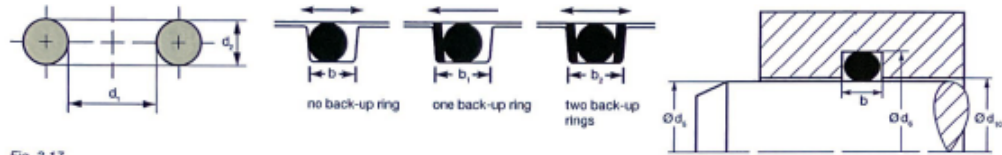


Fig. 3.17

Parker no.	d <sub>1</sub>	d <sub>2</sub>	b +0.2 0	b <sub>3</sub> +0.2 0	d <sub>5</sub> f7	d <sub>6</sub> H9	d <sub>10</sub> H8	Parker no.	d <sub>1</sub>	d <sub>2</sub>	b +0.2 0	b <sub>3</sub> +0.2 0	d <sub>5</sub> f7	d <sub>6</sub> H9	d <sub>10</sub> H8
2-006	2.9	1.78	2.4	2	3	5.9	3	2-122	28.24	2.62	3.6	3	28	32.5	28
2-007	3.68	1.78	2.4	2	3.5	6.4	3.5	2-123	29.82	2.62	3.6	3	30	34.5	30
6-166	3.9	1.8	2.4	2	4	6.9	4	2-124	31.42	2.62	3.6	3	32	36.5	32
2-008	4.47	1.78	2.4	2	4.5	7.4	4.5	2-125	32.99	2.62	3.6	3	33	37.5	33
5-581	4.9	1.9	2.4	2	5	8.1	5	2-126	34.55	2.62	3.6	3	35	39.5	35
2-009	5.28	1.78	2.4	2	5.5	8.4	5.5	2-127	36.17	2.62	3.6	3	36	40.5	36
2-010	6.07	1.78	2.4	2	6	8.9	6	2-128	37.77	2.62	3.6	3	38	42.5	38
5-052	6.86	1.78	2.4	2	7	9.9	7	2-210	18.64	3.53	4.8	4	19	25.1	19
2-011	7.65	1.78	2.4	2	7.5	10.4	7.5	5-595	19.8	3.6	4.8	4	20	26.2	20
5-585	8	1.88	2.4	2	8	11.1	8	2-211	20.22	3.53	4.8	4	20	26.1	20
5-612	8.74	1.78	2.4	2	9	11.9	9	2-212	21.82	3.53	4.8	4	22	28.1	22
2-012	9.25	1.78	2.4	2	9.5	12.4	9.5	2-213	23.39	3.53	4.8	4	24	30.1	24
5-212	9.75	1.78	2.4	2	10	12.9	10	2-214	24.99	3.53	4.8	4	25	31.1	25
2-013	10.82	1.78	2.4	2	11	13.9	11	5-618	25.81	3.53	4.8	4	26	32.1	26
6-366	11.89	1.78	2.4	2	12	14.9	12	2-215	26.57	3.53	4.8	4	27	33.1	27
2-014	12.42	1.78	2.4	2	12.5	15.4	12.5	2-216	28.17	3.53	4.8	4	28	34.1	28
2-015	14	1.78	2.4	2	14	16.9	14	2-217	29.74	3.53	4.8	4	30	36.1	30
6-085	15	1.8	2.4	2	15	17.9	15	2-218	31.34	3.53	4.8	4	32	38.1	32
2-016	15.6	1.78	2.4	2	16	18.9	16	2-219	32.92	3.53	4.8	4	33	39.1	33
2-017	17.17	1.78	2.4	2	17	19.9	17	2-220	34.52	3.53	4.8	4	35	41.1	35
2-110	9.19	2.62	3.6	3	9.5	14	9.5	2-221	36.09	3.53	4.8	4	36	42.1	36
5-614	9.93	2.62	3.6	3	10	14.5	10	2-222	37.69	3.53	4.8	4	38	44.1	38
2-111	10.77	2.62	3.6	3	11	15.5	11	5-321	39.6	3.53	4.8	4	40	46.1	40
5-615	11.91	2.62	3.6	3	12	16.5	12	2-223	40.87	3.53	4.8	4	41	47.1	41
2-112	12.37	2.62	3.6	3	12.5	17	12.5	2-224	44.04	3.53	4.8	4	44	50.1	44
5-616	13.11	2.62	3.6	3	13	17.5	13	5-035	45.36	3.53	4.8	4	45	51.1	45
2-113	13.94	2.62	3.6	3	14	18.5	14	2-225	47.22	3.53	4.8	4	47	53.1	47
5-239	14.48	2.69	3.6	3	14.5	19	14.5	5-701	49.2	3.53	4.8	4	49	55.1	49
2-114	15.54	2.62	3.6	3	15.5	20	15.5	2-226	50.39	3.53	4.8	4	50	56.1	50
5-617	15.88	2.62	3.6	3	16	20.5	16	2-227	53.57	3.53	4.8	4	54	60.1	54
2-115	17.12	2.62	3.6	3	17	21.5	17	2-228	56.74	3.53	4.8	4	56	62.1	56
5-256	17.96	2.62	3.6	3	18	22.5	18	2-229	59.92	3.53	4.8	4	60	66.1	60
2-116	18.76	2.62	3.6	3	19	23.5	19	2-230	63.09	3.53	4.8	4	63	69.1	63
2-117	20.29	2.62	3.6	3	20	24.5	20	2-231	66.27	3.53	4.8	4	66	72.1	66
2-118	21.89	2.62	3.6	3	22	26.5	22	2-232	69.44	3.53	4.8	4	70	76.1	70
2-119	23.47	2.62	3.6	3	24	28.5	24	2-233	72.62	3.53	4.8	4	73	79.1	73
2-120	25.07	2.62	3.6	3	25	29.5	25	2-234	75.79	3.53	4.8	4	76	82.1	76
2-121	26.64	2.62	3.6	3	27	31.5	27	2-235	78.97	3.53	4.8	4	80	86.1	80



Other dimensions			
Parker no.	R [mm]	T [mm]	A [mm]
004-050	2.21	1.24	1.14
102-178	3.28	1.35	1.14
201-284	4.42	1.27	1.02
309-395	6.65	1.93	1.52
425-475	8.74	2.97	2.44

Tab. 4.15

Back-up ring Dimension	W [mm]	Groove width b <sub>1</sub> one back-up ring [mm]	Groove width b <sub>2</sub> two back-up rings [mm]
8-006 - 8-050	1.35	3.5 - 3.7	4.6 - 4.8
8-102 - 8-178	2.18	4.7 - 4.9	5.8 - 6.0
8-201 - 8-284	3.00	5.8 - 6.0	6.8 - 7.0
8-309 - 8-395	4.65	8.7 - 8.9	10.2 - 10.4
8-425 - 8-475	5.99	12.0 - 12.2	14.4 - 14.6

Tab. 4.12 Modified groove widths are necessary when using Parbak® back-up rings

#### 4 O-rings and Parbak® back-up rings

Parker no.	M [mm]	W <sup>0.08</sup> [mm]	Parker no.	M [mm]	W <sup>0.08</sup> [mm]
8-102	1.96	2.18	8-150	73.48	2.18
8-103	2.77	2.18	8-151	76.66	2.18
8-104	3.56	2.18	8-152	83.01	2.18
8-105	4.34	2.18	8-153	89.36	2.18
8-106	5.13	2.18	8-154	95.71	2.18
8-107	5.94	2.18	8-155	102.06	2.18
8-108	6.73	2.18	8-156	108.41	2.18
8-109	8.31	2.18	8-157	114.76	2.18
8-110	9.91	2.18	8-158	121.11	2.18
8-111	11.48	2.18	8-159	127.46	2.18
8-112	13.08	2.18	8-160	133.81	2.18
8-113	14.66	2.18	8-161	140.16	2.18
8-114	16.26	2.18	8-162	146.51	2.18
8-115	17.83	2.18	8-163	152.86	2.18
8-116	19.43	2.18	8-164	159.21	2.18
8-117	21.11	2.18	8-165	165.56	2.18
8-118	22.68	2.18	8-166	171.91	2.18
8-119	24.26	2.18	8-167	178.26	2.18
8-120	25.86	2.18	8-168	184.61	2.18
8-121	27.46	2.18	8-169	190.96	2.18
8-122	29.03	2.18	8-170	197.31	2.18
8-123	30.63	2.18	8-171	203.66	2.18
8-124	32.21	2.18	8-172	210.01	2.18
8-125	33.81	2.18	8-173	216.36	2.18
8-126	35.38	2.18	8-174	222.71	2.18
8-127	36.98	2.18	8-175	229.06	2.18
8-128	38.56	2.18	8-176	235.41	2.18
8-129	40.16	2.18	8-177	241.76	2.18
8-130	41.73	2.18	8-178	248.11	2.18
8-131	43.33	2.18			
8-132	44.91	2.18			
8-133	46.51	2.18			
8-134	48.08	2.18			
8-135	49.68	2.18			
8-136	51.26	2.18			
8-137	52.86	2.18			
8-138	54.43	2.18			
8-139	56.03	2.18			
8-140	57.61	2.18			
8-141	59.21	2.18			
8-142	60.78	2.18			
8-143	62.38	2.18			
8-144	63.96	2.18			
8-145	65.56	2.18			
8-146	67.13	2.18			
8-147	68.73	2.18			
8-148	70.31	2.18			
8-149	71.91	2.18			